IDENTIFYING ICEBERG PRODUCTION PROCESSES, DRIFT PATTERNS, AND COEXISTENCE WITH SHIPS IN THE EASTERN CANADIAN ARCTIC

ABIGAIL DALTON

A thesis submitted in partial fulfillment of the requirements for the

Doctorate in Philosophy degree in Geography

Department of Geography, Environment, and Geomatics

Faculty of Arts

University of Ottawa

Abstract

Tidewater glaciers drain a significant proportion of the Greenland Ice Sheet and ice masses of the Canadian Arctic and provide the primary source of icebergs in Canadian waters. However, there remains uncertainty surrounding the processes controlling ice discharge from Canadian Arctic glaciers, the drift paths of icebergs in Canadian waters, and the proximity of icebergs to shipping in the region. This thesis quantifies the processes controlling glacier dynamics from four primary glacier basins on the Prince of Wales (POW) Icefield and using a multi-year dataset of iceberg drift tracks, identifies drift patterns and proximity to ships throughout the eastern Canadian Arctic.

On the POW Icefield between 2009 and 2019, Cadogan and Ekblaw glaciers underwent multiyear acceleration and deceleration limited to their lower parts, consistent with characteristics of "pulse-type" glaciers. Trinity and Wykeham glaciers underwent repeating multiyear periods of velocity acceleration between 2009 and 2019 which coincided with significant thinning at their termini. As of 2017, Trinity and Wykeham were each within ~10 m of flotation over their lowermost 4 km. These findings suggest that Trinity and Wykeham glaciers have transitioned to a flow type dominated by dynamic thinning, which is strongly influenced by subglacial topography and may be susceptible to instability of the glacier front and large-scale collapse. Given that both glaciers are grounded below sea level for ~40 km up-glacier from their termini, this process could lead to significant increases in acceleration, retreat, and solid ice discharge.

Using a multi-year dataset (2011-2019) of in-situ iceberg drift locations, it was found that icebergs consistently drifted southeast along the east coast of Baffin Island, controlled by a combination of local conditions including short-term wind events, ocean surface currents and semi-diurnal tidal oscillations. A test of the assumption that icebergs drift at 2% of the wind speed indicates that this rule does not apply for the majority of icebergs in this study, which typically exceeded 2% of the wind speed, particularly at low values. The highest median iceberg drift speeds occurred during the winter and spring, reaching up to 2.3 m s^{-1} in Nares Strait. Icebergs in this study commonly became grounded near eastern Coburg Island and along the SE coast of Baffin Island, where mean residence time exceeded 180 days in all seasons.

Through an analysis of a comprehensive database of ship tracks derived from AIS (automatic identification system) data in combination with a subset of iceberg drift locations derived from in-situ satellite trackers and the Canadian Ice Island Drift, Deterioration, and Detection Database

(CI2D3), areas of iceberg-ship coexistence throughout Baffin Bay were identified between 2012 and 2019. The regions that saw the largest increases in iceberg-ship coexistence were along the east coast of Baffin Island and east of Bylot Island for dry bulk vessels, and northward into Smith Sound for passenger vessels. As passenger vessels commonly have little ice strengthening, this could pose an elevated hazard to vessels operating in these regions.

The results of this study provide a comprehensive examination of the factors controlling glacier terminus dynamics and stability on SE Ellesmere Island, and the drift paths of icebergs once calved. This provides insights into the life cycle of icebergs in Canadian waters, how they may change in a warming climate, and the hazards that they may pose for shipping, particularly given the rapid recent increase in ship transits across the Canadian Arctic.

Preface

Thesis Format

This doctoral thesis is written in article format and consists of three manuscripts (Chapters 2, 3, and 4). Chapter 1 provides the Introduction, including an outline of the literature motivating the work in this thesis. Chapter 2 provides a regional overview of the processes driving ice discharge from the four major tidewater glaciers on the POW Icefield, using and expanding upon velocity data from Van Wychen et al. (2016), 3D tomography data, optical and SAR satellite imagery, and DEM differencing. Chapter 3 uses a dataset of iceberg drift tracks collected between 2011 and 2019 to provide the most comprehensive assessment to date of icebergs in Canadian waters, and to help fill the knowledge gap surrounding the drift patterns that icebergs follow once they calve from Canadian Arctic glaciers. Chapter 4 assesses iceberg-ship coexistence in Canadian waters using a comprehensive database of ship tracks derived from AIS data to create maps for regions that have high iceberg and shipping traffic. Chapter 5 synthesizes the findings of these articles, presenting key findings and discussing areas for future research. All references can be found at the end of each respective chapter.

The first manuscript (Chapter 2) has been published and therefore reflects the stylistic requirements for the Journal of Geophysical Research Earth Surface. The other two (Chapters 3 and 4) will be submitted to peer-reviewed journals with the following proposed titles and authorship:

1. **Dalton, A**., Van Wychen, W., Copland, L., Gray, L. and Burgess, D. 2022. Seasonal and multiyear flow variability on the Prince of Wales Icefield, Ellesmere Island, 2009-2019. Journal of Geophysical Research Earth Surface, 127(4), e2021JF006501.

2. **Dalton, A**., Garbo, A., Copland, L., Van Wychen, W., Mueller, D., and Tivy, A. (In preparation). Long-term field tracking of icebergs in the eastern Canadian Arctic.

3. **Dalton, A**., Copland, L., Van Wychen, W., Cook, A., Dawson, J., Garbo, A., Mueller, D., and Tivy, A. (In preparation). Coexistence of icebergs and ships in the eastern Canadian Arctic: 2012-2019.

Author Contributions

I am the primary author for each chapter and am responsible for the research methodology, satellite image processing, fieldwork and data collection, data analysis, and manuscript writing, with guidance and input from my co-supervisors, Luke Copland and Wesley Van Wychen. Specific contributions of co-authors to the individual manuscripts are as follows:

1. Laurence Gray provided the MATLAB speckle-tracking algorithm to derive surface velocities. Laurence Gray also provided Cryosat-2 altimetry data and assisted with data access and processing. David Burgess provided access to the Radarsat-2 data through a project agreement with Natural Resources Canada and the Canadian Space Agency. All co-authors contributed to the final manuscript with revisions including three anonymous reviewers and editor Dr. Sergienko from the Journal of Geophysical Research Earth Surface.

2. Adam Garbo and Luke Copland contributed to data collection in the field, and iceberg beacon development, construction, and deployment. Adam Garbo contributed substantially to analysis and processing of iceberg drift tracks. Adrienne Tivy provided access to iceberg tracking beacons through Environment and Climate Change Canada. Derek Mueller and Adrienne Tivy contributed to initial project planning and reviewing and editing the final manuscript.

3. Adam Garbo, Luke Copland, and Alison Cook contributed to data collection in the field. Jackie Dawson provided access to AIS ship track data through MEOPAR. Alison Cook and Jackie Dawson helped with data acquisition and initial project planning. Derek Mueller assisted with analysis of ice island data. All co-authors contributed to the final manuscript.

Table of Contents

List of Tables

List of Figures

Acknowledgements

I would first like to thank my supervisors, Dr. Luke Copland and Dr. Wesley Van Wychen. I could not have asked for better mentors throughout my graduate career. Your guidance has made me a better writer and researcher, and prepared me well for life beyond academia. Luke, the countless opportunities you have provided me over the last eight years have been truly life changing. I could have never imagined the things I would accomplish or places I would travel. Wes, thank you for taking me on as your first student and continually encouraging me to prioritize my personal well-being above academic pursuits.

Thank you to the various organizations that funded this research through grants and scholarships. Support for this project was provided by the Natural Sciences and Engineering Research Council of Canada, Ontario Graduate Scholarship, Canada Foundation for Innovation, Ontario Research Fund, ArcticNet Network of Centres of Excellence Canada, University of Ottawa, Northern Scientific Training Program, Transport Canada, Royal Canadian Geographical Society, Society of Naval Architects and Marine Engineers (Arctic Section), and Polar Knowledge Canada. Travel to conferences and attendance of courses was also generously supported by the RemoteEx project of the Norwegian Centre for International Cooperation in Higher Education (SIU), the International Glaciological Society, and the International Arctic Science Committee.

Fieldwork for this research was made not only possible but immensely enjoyable thanks to the help of Adam Garbo, Alison Cook, Jill Rajewicz, and Claire Bernard-Grand'Maison. I am especially appreciative of the CCGS Amundsen crew and members of the Canadian Coast Guard, in particular helicopter pilots Dick Morissette and Guillaume Carpentier, for their support during four seasons of fieldwork. I will always be grateful for my time spent aboard the Amundsen and the many adventures I had exploring glaciers and icebergs around the Canadian Arctic.

I would like to acknowledge all members, past and present, of the Laboratory for Cryospheric Research at the University of Ottawa and the Glaciology Group at the University of Waterloo. Although most of our time together was virtual, I appreciate your friendship and valuable feedback over the past few years and look forward to future collaborations. I also wish to thank my committee members, Dr. David Burgess, Dr. Jackie Dawson, Dr. Anders Knudby, and external examiner Dr. Rocky Taylor, for their time and contributions to the final version of this thesis.

Finally, completing this PhD would not have been possible without the support of my family and friends. To my family, especially my parents, Chris and Debra Dalton, thank you for always encouraging my curiosity and accepting the takeover of several rooms in your house over the last three years. Writing my PhD during a global pandemic was challenging in many ways and I am so grateful I was able to do it at home surrounded by family. To Patrick, thank you for years of patience through this project and reassurance when I needed it most that I could make it to the end.

Chapter 1: Introduction

Between 2000 and 2020, all Arctic regions have lost glacier ice mass (Hugonnet et al., 2021; Wouters et al., 2019; Jakob & Gourmelen, 2023). Since 2003, long-term ice mass loss from Greenland and the Canadian Arctic Archipelago (CAA; Figure 1-1) has increased, including an acceleration of glacier surface thinning (Harig & Simons, 2016; Hugonnet et al., 2021) and widespread terminus retreat (Kochtitzky and Copland, 2022). A warming Arctic climate has led to a long-term increase in ice discharge from tidewater glaciers, although adjacent marine terminating glaciers can respond differently to common oceanic and atmospheric forcing, highlighting the importance of studying individual smaller glaciers and ice caps (Mouginot et al., 2019).

Retreat of marine terminating glaciers on western Greenland over the past ~20 years has been driven in part by increases in ocean temperature to depths of ~500 m and submarine melting to depths of ~200 m (Chauché et al., 2014). Ice discharge is defined as the mass or volumetric flux of ice through a glacier cross section generally located near to the terminus (Cogley et al., 2011). In Greenland, Enderlin et al. (2014) found that despite observed widespread acceleration for 178 outlet glaciers, ~50% of all discharge from the ice sheet is controlled by four glaciers, including Jakobshavn Isbrae (West Greenland). Following the collapse of a floating ice tongue between 1998 and 2003, Jakobshavn Isbrae underwent a rapid increase in velocity and significant retreat up to the grounding line ~12 km up-glacier from the terminus (Joughin et al., 2004; 2008). Since 2016, Jakobshavn Isbrae has been slowly advancing into shallower depths and re-thickening as ocean temperatures have cooled in Disko Bay by nearly 2°C between 2016 and 2018 (Khazendar et al., 2019; Joughin et al., 2020). A similar velocity increase coupled with dramatic retreat was observed in Alaska on the Columbia Glacier between the 1970s and 1990s, indicating a relationship between calving and terminus stretching rate (Van der Veen, 1996). The thinning of marine-terminating glaciers can lead to increased buoyancy and enhanced flow near the terminus, furthering mass loss through iceberg calving (Carr et al., 2013; James et al., 2014; Catania et al., 2019). Similar to Greenland, three glaciers in the CAA (Trinity, Wykeham, and Belcher glaciers) were responsible for ~60% of all ice discharge for 2015-2020 (Van Wychen et al., 2021). Due to a lack of long-term observational data of glacier velocity, surface elevations and ice discharge, there is currently insufficient evidence to determine whether similar trends exist in glacier dynamics in the CAA.

Figure 1-1: Map of main study area including inset map showing location of the main iceberg producing glaciers on the Prince of Wales Icefield, SE Ellesmere Island. Glacier outlines: Randolph Glacier Inventory (RGI) version 6.0 (RGI Consortium, 2017)

A significant impact of the loss of Arctic land ice is its contribution to global sea level rise. The Greenland Ice Sheet is currently the largest contributor to global sea level rise in the Arctic, with a total of 13.7 ± 1.1 mm since 1972 (Mouginot et al., 2019). Mass balance estimates for the Greenland Ice Sheet show that mass loss increased from 187 ± 17 Gt a^{-1} in 2000–2010, to 286 ± 20 Gt a^{-1} in 2010–2018 (Mouginot et al, 2019). Over these periods, surface melting has been the primary contributor to total mass loss. Between 2010 and 2018, the Greenland Ice Sheet lost 160 ± 26 Gt a^{-1} to surface mass balance (SMB) and 126 ± 9 Gt a^{-1} to ice discharge, compared to 98 ± 16 Gt a^{-1} to SMB and 87 ± 8 Gt a^{-1} to ice discharge from 2000-2010. However, mass loss through glacier dynamics (i.e., iceberg discharge at the terminus) has increased continuously between 1972, highlighting the important role it plays in the total mass budget (Mouginot et al., 2019).

1.1 Changes to Canadian Arctic glaciers and ice caps

The CAA contains the largest area of glacier ice when excluding the ice sheets (~150,000 km^2) (Lenaerts, 2013; Sharp et al., 2014). Outside of the Greenland Ice Sheet, the northern Canadian Arctic Archipelago (CAA) contains about 40% of the marine terminating glaciers in the northern hemisphere (Kochtitzky et al., 2022) and is one of the largest Arctic contributors to global sea level rise is the CAA, which has contributed 3.2 ± 0.7 mm since 1971, ~14% of total Arctic glacier and Greenland Ice Sheet contributions (Box et al., 2018). From 1996 to 2015, glaciers in the northern CAA have lost mass at a rate of 28.2 ± 11.5 Gt a^{-1}, compared to 22.0 ± 4.5 Gt a^{-1} for the southern CAA (Noël et al., 2018). Annual surface mass balance measurements in the CAA began in the 1950s at four glaciers: White Glacier (Axel Heiberg Island), Meighen Ice Cap, Melville Ice Cap and Sverdrup Glacier (Devon Island) and, up until 2003, annual mass balances were slightly negative. On Meighen Ice Cap, mass loss between 2005 and 2016 was at a rate five times greater than the 1960-2004 average as a result of changes in summer air temperature, increased surface melt and lengthening of the melt season (Sharp et al., 2011; Mortimer et al., 2016; Noël et al., 2018; Burgess & Danielson, 2022).

In the Queen Elizabeth Islands (QEI) of the Canadian Arctic, surface velocities are relatively low, typically <10 m a^{-1} in the interior of ice caps and icefields (Van Wychen et al., 2014). Land-terminating glaciers typically range in velocity from ~20-50 m a^{-1} along their main trunks, increasing to <75 m a^{-1} at the terminus, while tidewater glaciers typically range from ~30-90 m a^{-1} along the main trunk, increasing to <300 m a^{-1} at the terminus (Millan et al., 2017; Sánchez-Gámez

& Navarro, 2017; Van Wychen et al., 2021). Since 2000, only two glaciers in the QEI, Trinity and Wykeham glaciers of the Prince of Wales (POW) Icefield, have consistently accelerated. As of 2020, Trinity and Wykeham contributed ~50% of total ice discharge from tidewater glaciers in the QEI (1.60 Gt a^{-1}), compared to ~22% (0.55 Gt a^{-1}) in 2000 (Van Wychen et al., 2021). Velocity increase of Trinity Glacier coincided with terminus retreat of ~6.1 km between 1959 and 2016, with about half of the retreat occurring since approximately 2003 (Mair et al., 2009; Van Wychen et al., 2014; 2016). Between 1959 and 2015, 94% of all marine-terminating glaciers in the QEI underwent terminus retreat (Cook et al., 2019; White & Copland, 2019). In addition to terminus retreat and an acceleration in velocity, the combined termini of Trinity and Wykeham glaciers have undergone an increase in surface thinning from ~4 m a^{-1} to ~6 m a^{-1} between 2000 and 2016 (Van Wychen et al., 2016; Harcourt et al., 2020).

1.2 Knowledge gaps in terms of iceberg production and drift in the Canadian Arctic

Iceberg production into Baffin Bay primarily occurs from the calving of marine-terminating glaciers in West Greenland and the eastern Canadian High Arctic (Mouginot et al., 2019; Van Wychen et al., 2021; Kochtitzky et al., 2022). These icebergs typically drift in a counter-clockwise direction around Baffin Bay, before drifting southwards along the east coast of Canada, driven by wind and ocean currents (Valeur et al., 1996; Tang et al., 2004; Münchow et al., 2015). Most iceberg calving results from crevasses caused by longitudinal strain or a decrease in ice thickness (Benn & Evans, 2010; Amundson et al., 2010). Between 2005 and 2014, total mass loss from the QEI averaged 33.0 ± 3.0 Gt a^{-1}, ~90% of which was dominated by surface mass balance (i.e., surface melt) (Millan et al., 2017). Frontal ablation from the northern CAA, which is dominated by iceberg production, but also includes subaerial frontal melting, sublimation, and subaqueous frontal melting, was responsible for a total of 4.28 ± 1.18 Gt a^{-1} from 2010-2020 compared to 4.14 ± 1.11 Gt a^{-1} from 2000-2010 (Kochtitzky et al., 2022). Marine-terminating glaciers on West Greenland discharged on average ~76 Gt a^{-1} of ice from 2010-2018 (Mouginot et al., 2019), with Jakobshavn Isbrae alone discharging ~38 Gt in 2017 (Mankoff et al., 2019), indicating that Greenland is the source of ~95% of icebergs in Baffin Bay.

Data from the Canadian Arctic on iceberg drift is limited, although previous studies using satellite-tracked icebergs have shown patterns such as intrusions into Lancaster Sound while following the southward-flowing Baffin Island Current, and large-scale looping off the southeastern coast of

Bylot Island (Marko et al., 1982). Winds are an important driver of iceberg drift because of their influence on iceberg/ice island freeboard and surrounding pack ice (Van Wychen & Copland, 2017; Andersson et al., 2018). In a study conducted by Larsen et al. (2015) which tracked ten icebergs in Melville Bay (near Northwest Greenland), icebergs with large surface areas moved at the highest speeds, with greatest drift occurring during strong wind events. When sea ice is present, wind is the dominant force that steers iceberg motion. The presence of sea ice can also hinder iceberg drift, especially if the sea ice is landfast (e.g., frozen to shore or a glacier terminus). In the eastern Canadian Arctic, icebergs can often become frozen in sea ice as they follow the Baffin Island Current (BIC) which flows close to the coast of eastern Baffin Island (Marko et al., 1982). The icebergs remain static within the sea ice pack until the sea ice is free to move again (Tang et al., 2004).

The area between Baffin Bay and the Grand Banks of Newfoundland is commonly referred to as "Iceberg Alley". Icebergs within Iceberg Alley have been monitored since 1913, one year after the sinking of the RMS Titanic following an iceberg collision on April 14, 1912. The International Ice Patrol (IIP) works in conjunction with the Canadian Ice Service (CIS) to monitor iceberg presence in the North Atlantic Ocean and provide iceberg warnings and charts to those navigating. The IIP monitors this region from February to July each year, and the CIS from August to January. Icebergs are mainly monitored via reconnaissance flights, but can also be tracked using optical (e.g., Scheick et al., 2019) and synthetic aperture radar (SAR) sensors (e.g., Frost et al., 2016). This poses several challenges based on satellite image resolution (both temporal and spatial), and the difficulty to differentiate between icebergs, waves and ships in certain types of imagery. The operational model used for iceberg drift by the CIS has undergone limited testing in the Canadian Arctic and relies on in-situ observations for verification which are currently scarce (Kubat et al., 2005; Garbo, 2022; Turnbull et al., 2022).

1.3 Shipping in the Canadian Arctic

Shipping in the CAA is dependent on environmental factors such as sea ice conditions and the length of the open water season. It is also controlled by demand, as shipping in the CAA is primarily destinational, and vessels which navigate this region are there for a purpose such as resource extraction, community resupply, or tourism (Stephenson et al., 2015). The Northwest Passage (NWP) is a sea route that runs through the CAA, connecting the North Atlantic to the

Pacific Ocean. It has been identified as a potential future transportation route to connect regions such as Japan with eastern North America as sea ice extent decreases in the Arctic (Dawson et al., 2018; 2022).

From 1990-2015, shipping traffic in the CAA nearly tripled, but most of the change occurred after 2007 (Dawson et al., 2018). For example, between 1990 and 2007, Arctic shipping remained relatively constant, before experiencing a dramatic increase in vessel traffic and change in vessel type after 2007, coinciding with a (then) record low minimum sea ice extent. Since 1990, the total distance travelled by vessels in the CAA has also increased. The greatest increase has been observed in Hudson Strait, where many mines are located (up to ~550 km a^{-1}), followed by the Beaufort Sea (up to ~450 km a^{-1}), and Baffin Bay (up to ~350 km a^{-1}) (Pizzolato et al., 2016). Between 1990 and 2015 there was also a shift in vessel type visiting the CAA. Prior to 2007, shipping traffic in the Arctic was dominated by cargo ships and government research vessels. From 2006-2015, there has been an increase in the number of pleasure crafts and passenger ships navigating northern areas including the Northwest Passage as the tourism demand increases and sea ice conditions change (Dawson et al., 2018). This allows for vessels that are poorly ice-strengthened to navigate Arctic waters where essentially no real-time monitoring of icebergs currently exists (Pizzolato et al., 2016; Dawson et al., 2018, 2022).

Many communities in northern Canada are inaccessible by road and therefore rely heavily on service and supplies via shipping (Dawson et al., 2018; 2022). Fluctuations in shipping traffic are also dependent on economic demands such as the opening and closing of mines (Pizzolato et al., 2016; Dawson et al., 2022). For example, between 1990 and 2015, shipping traffic decreased within the NWP with the closure of the Nanisivik mine on northern Baffin Island and the Polaris mine on Cornwallis Island. Communities on Baffin Island (e.g., Pond Inlet, Clyde River) have seen an increase in shipping traffic between 1990 and 2015 as they have become more popular destinations for passenger ships and tourism (Dawson et al., 2018). As sea ice extent continues to decrease as a result of warming air and ocean temperatures, the possibility of increased shipping traffic as the Arctic becomes a more popular destination has been posited (Bourbonnais & Lasserre, 2015; Guy & Lasserre, 2016; Mudryk et al., 2021). Increased open water areas in the eastern CAA may allow for access to previously inaccessible areas (Mudryk et al., 2021). However, the sea ice conditions within the CAA are highly variable and models are unable to

predict how a changing climate will impact shipping in the future (Haas & Howell, 2015; Howell & Brady, 2019).

1.4 Objectives

Previous work on tidewater glacier dynamics in the Canadian Arctic has mainly focused on quantifying surface velocities and ice fluxes to the ocean, but few studies have completed in-depth investigations of the processes controlling ice flux dynamics and iceberg production from specific glaciers. In addition, there is a significant gap in our knowledge of the processes controlling iceberg drift once they have calved, and the hazards they may pose to shipping within this region.

This thesis focuses on the following central research objectives:

1. Determine the processes controlling glacier flow from the four primary sources of iceberg flux from the POW Icefield to Baffin Bay from 2009-2019. Winter surface velocities combined with terminus retreat rates, ice thickness, surface elevation, and terminus buoyancy are used to determine whether glacier geometry is contributing to destabilizing changes in the largest glacier basin (Trinity and Wykeham) in the CAA.
2. Provide an in-depth analysis of iceberg characteristics and drift through Canadian waters, using a combination of field and remote sensing methods. A 9-year record of iceberg drift tracks through Baffin Bay is combined with bathymetry, ocean current, wind current, and sea ice conditions to characterize iceberg behaviour in Baffin Bay and describe the forces driving iceberg drift patterns.
3. Identify iceberg prevalence along primary shipping routes in the eastern Canadian Arctic. Known ship tracks derived from AIS data and a multi-year dataset of known iceberg drift tracks are used to establish areas of overlap between icebergs and ships throughout the eastern Canadian Arctic. This is used to identify patterns in iceberg-ship proximity based on vessel type and along primary shipping routes.

Based on the above, this thesis provides an exploration of iceberg production and drift in the eastern Canadian Arctic (Figure 1-1), from source to sink. This research significantly improves our understanding of glacier processes on the POW Icefield and is pertinent for understanding the drift paths and life cycle of icebergs through Canadian waters and for improving safety for Arctic navigation.

References

Amundson, J. M., Fahnestock, M., Truffer, M., Brown, J., Lüthi, M. P. and Motyka, R. J. (2010) Ice mélange dynamics and implications for terminus stability, Jakobshavn Isbræ, Greenland. *Journal of Geophysical Research*, 115(F1), 1-12.

Benn, D.I., Evans, D.J.A. (2010) Glaciers and Glaciation. 2nd edition. Hodder Education, London.

Bourbonnais, P., & Lasserre, F. (2015). Winter shipping in the Canadian Arctic: Toward year-round traffic? *Polar Geography*, 38(1), 70–88. https://doi.org/10.1080/1088937X.2015.1006298

Box, J. E., Colgan, W. T., Wouters, B., Burgess, D. O., O'Neel, S., Thomson, L. I., & Mernild, S. H. (2018). Global sea-level contribution from Arctic land ice: 1971–2017. *Environmental Research Letters*, 13(12), 125012. https://doi.org/10.1088/1748-9326/aaf2ed

Burgess, D. O., & Danielson, B. D. (2022). Meighen Ice Cap: Changes in geometry, mass, and climatic response since 1959. *Canadian Journal of Earth Sciences*, 59(11), 884–896. https://doi.org/10.1139/cjes-2021-0126

Carr, J. R., Stokes, C. R., & Vieli, A. (2013). Recent progress in understanding marine-terminating Arctic outlet glacier response to climatic and oceanic forcing: Twenty years of rapid change. *Progress in Physical Geography: Earth and Environment*, 37(4), 436–467. https://doi.org/10.1177/0309133313483163

Catania, G. A., Stearns, L. A., Sutherland, D. A., Fried, M. J., Bartholomaus, T. C., Morlighem, M., Shroyer, E., & Nash, J. (2018). Geometric Controls on Tidewater Glacier Retreat in Central Western Greenland. *Journal of Geophysical Research: Earth Surface*, 123(8), 2024–2038. https://doi.org/10.1029/2017JF004499

Chauché, N., Hubbard, A., Gascard, J.-C., Box, J. E., Bates, R., Koppes, M., Sole, A., Christoffersen, P., & Patton, H. (2014). Ice–ocean interaction and calving front morphology at two west Greenland tidewater outlet glaciers. *The Cryosphere*, 8(4), 1457–1468. https://doi.org/10.5194/tc-8-1457-2014

Cogley, J. G., Hock, R., Rasmussen, L. A., Arendt, A. A., Bauder, A., Braithwaite, R. J., Jansson, P., Kaser, G., Möller, M., Nicholson, L., & Zemp, M. (2011). Glossary of glacier mass balance and related terms. https://doi.org/10.5167/UZH-53475

Crawford, A., Crocker, G., Mueller, D., Desjardins, L., Saper, R., & Carrieres, T. (2018). The Canadian Ice Island Drift, Deterioration and Detection (CI2D3) Database. *Journal of Glaciology*, 64(245), 517–521. https://doi.org/10.1017/jog.2018.36

Dawson, J., Cook, A., Holloway, J., & Copland, L. (2022). Analysis of Changing Levels of Ice Strengthening (Ice Class) among Vessels Operating in the Canadian Arctic over the Past 30 Years. *Arctic*. https://doi.org/10.14430/arctic75553

Enderlin, E. M., Howat, I. M., Jeong, S., Noh, M., Van Angelen, J. H., & Van Den Broeke, M. R. (2014). An improved mass budget for the Greenland ice sheet. *Geophysical Research Letters*, 41(3), 866–872. https://doi.org/10.1002/2013GL059010

Frost, A., Ressel, R., & Lehner, S. (2016). Automated Iceberg Detection Using High-Resolution X-Band SAR Images. *Canadian Journal of Remote Sensing*, 42(4), 354–366. https://doi.org/10.1080/07038992.2016.1177451

Garbo, A. (2022) Validation of the North American Ice Service Iceberg Drift Model. *MSc thesis, University of Ottawa*. http://dx.doi.org/10.20381/ruor-27682.

Guy, E., & Lasserre, F. (2016). Commercial shipping in the Arctic: New perspectives, challenges and regulations. *Polar Record*, 52(3), 294–304. https://doi.org/10.1017/S0032247415001011

Haas, C., & Howell, S. E. L. (2015). Ice thickness in the Northwest Passage. *Geophysical Research Letters*, 42(18), 7673–7680. https://doi.org/10.1002/2015GL065704

Harcourt, W. D., Palmer, S. J., Mansell, D. T., Le Brocq, A., Bartlett, O., Gourmelen, N., Tepes, P., Dowdeswell, J. A., Blankenship, D. D., & Young, D. A. (2020). Subglacial controls on dynamic thinning at Trinity-Wykeham Glacier, Prince of Wales Ice Field, Canadian Arctic. *International Journal of Remote Sensing*, 41(3), 1191–1213. https://doi.org/10.1080/01431161.2019.1658238

Harig, C., & Simons, F. J. (2016). Ice mass loss in Greenland, the Gulf of Alaska, and the Canadian Archipelago: Seasonal cycles and decadal trends. *Geophysical Research Letters*, 43(7), 3150–3159. https://doi.org/10.1002/2016GL067759

Howell, S. E. L., & Brady, M. (2019). The Dynamic Response of Sea Ice to Warming in the Canadian Arctic Archipelago. *Geophysical Research Letters*, 46(22), 13119–13125. https://doi.org/10.1029/2019GL085116

Hugonnet, R., McNabb, R., Berthier, E., Menounos, B., Nuth, C., Girod, L., Farinotti, D., Huss, M., Dussaillant, I., Brun, F., & Kääb, A. (2021). Accelerated global glacier mass loss in the early twenty-first century. *Nature*, 592(7856), 726–731.

Jakob, L., & Gourmelen, N. (2023). Glacier Mass Loss Between 2010 and 2020 Dominated by Atmospheric Forcing. *Geophysical Research Letters*, 50(8), e2023GL102954. https://doi.org/10.1029/2023GL102954

James, T. D., Murray, T., Selmes, N., Scharrer, K., & O'Leary, M. (2014). Buoyant flexure and basal crevassing in dynamic mass loss at Helheim Glacier. *Nature Geoscience*, 7(8), 593–596. https://doi.org/10.1038/ngeo2204

Joughin, I., Abdalati, W., & Fahnestock, M. (2004). Large fluctuations in speed on Greenland's Jakobshavn Isbræ glacier. *Nature*, 432(7017), 608–610. https://doi.org/10.1038/nature03130

Joughin, I., Howat, I., Alley, R. B., Ekstrom, G., Fahnestock, M., Moon, T., Nettles, M., Truffer, M., & Tsai, V. C. (2008). Ice-front variation and tidewater behavior on Helheim and Kangerdlugssuaq Glaciers, Greenland. *Journal of Geophysical Research*, 113(F1), F01004. https://doi.org/10.1029/2007JF000837

Joughin, I., Howat, I. M., Fahnestock, M., Smith, B., Krabill, W., Alley, R. B., Stern, H., & Truffer, M. (2008). Continued evolution of Jakobshavn Isbrae following its rapid speedup. *Journal of Geophysical Research*, 113(F4), F04006. https://doi.org/10.1029/2008JF001023

Joughin, I., Shean, D. E., Smith, B. E., & Floricioiu, D. (2020). A decade of variability on Jakobshavn Isbræ: Ocean temperatures pace speed through influence on mélange rigidity. *The Cryosphere*, 14(1), 211–227. https://doi.org/10.5194/tc-14-211-2020

Khazendar, A., Fenty, I. G., Carroll, D., Gardner, A., Lee, C. M., Fukumori, I., Wang, O., Zhang, H., Seroussi, H., Moller, D., Noël, B. P. Y., Van Den Broeke, M. R., Dinardo, S., & Willis, J. (2019). Interruption of two decades of Jakobshavn Isbrae acceleration and thinning as regional ocean cools. *Nature Geoscience*, 12(4), 277–283. https://doi.org/10.1038/s41561-019-0329-3

Kochtitzky, W., & Copland, L. (2022). Retreat of Northern Hemisphere Marine-Terminating Glaciers, 2000–2020. *Geophysical Research Letters*, 49(3). https://doi.org/10.1029/2021GL096501

Kochtitzky, W., Copland, L., Van Wychen, W., Hugonnet, R., Hock, R., Dowdeswell, J. A., Benham, T., Strozzi, T., Glazovsky, A., Lavrentiev, I., Rounce, D. R., Millan, R., Cook, A., Dalton, A., Jiskoot, H., Cooley, J., Jania, J., & Navarro, F. (2022). The unquantified mass loss of Northern Hemisphere marine-terminating glaciers from 2000–2020. *Nature Communications*, 13(1), 5835. https://doi.org/10.1038/s41467-022-33231-x

Kubat, I., Sayed, M., Savage, S. B., & Carrieres, T. (2005). An operational model of iceberg drift. International Journal of Offshore and Polar Engineering, 15(2), 125–131.

Larsen, P.-H., Hansen, M. O., Buus-Hinkler, J., Krane, K. H., & Sønderskov, C. (2015). Field tracking (GPS) of ten icebergs in eastern Baffin Bay, offshore Upernavik, northwest Greenland. *Journal of Glaciology*, 61(227), 421–437. https://doi.org/10.3189/2015JoG14J216

Lenaerts, J. T. M., Van Angelen, J. H., Van Den Broeke, M. R., Gardner, A. S., Wouters, B., & Van Meijgaard, E. (2013). Irreversible mass loss of Canadian Arctic Archipelago glaciers: CAA GLACIER MASS LOSS. *Geophysical Research Letters*, 40(5), 870–874. https://doi.org/10.1002/grl.50214

Mair, D., Burgess, D., Sharp, M., Dowdeswell, J. A., Benham, T., Marshall, S., & Cawkwell, F. (2009). Mass balance of the Prince of Wales Icefield, Ellesmere Island, Nunavut, Canada. *Journal of Geophysical Research*, 114(F2), F02011. https://doi.org/10.1029/2008JF001082

Mankoff, K. D., Solgaard, A., Colgan, W., Ahlstrøm, A. P., Khan, S. A., & Fausto, R. S. (2020). Greenland Ice Sheet solid ice discharge from 1986 through March 2020. *Earth System Science Data*, 12(2), 1367–1383. https://doi.org/10.5194/essd-12-1367-2020

Millan, R., Mouginot, J., & Rignot, E. (2017). Mass budget of the glaciers and ice caps of the Queen Elizabeth Islands, Canada, from 1991 to 2015. *Environmental Research Letters*, 12(2), 024016. https://doi.org/10.1088/1748-9326/aa5b04

Mortimer, C. A., Sharp, M., & Wouters, B. (2016). Glacier surface temperatures in the Canadian High Arctic, 2000–15. *Journal of Glaciology*, 62(235), 963–975. https://doi.org/10.1017/jog.2016.80

Mouginot, J., Rignot, E., Bjørk, A. A., Van Den Broeke, M., Millan, R., Morlighem, M., Noël, B., Scheuchl, B., & Wood, M. (2019). Forty-six years of Greenland Ice Sheet mass balance from 1972 to 2018. *Proceedings of the National Academy of Sciences*, 116(19), 9239–9244. https://doi.org/10.1073/pnas.1904242116

Münchow, A., Falkner, K. K., & Melling, H. (2015). Baffin Island and West Greenland Current Systems in northern Baffin Bay. *Progress in Oceanography*, 132, 305–317. https://doi.org/10.1016/j.pocean.2014.04.001

Noël, Brice P Y. (2017). Average surface mass balance (SMB) components at 1 km for the Canadian Arctic Archipelago (1958-1995 and 1996-2015), links to RACMO2.3 model results in NetCDF format (p. 20 data points) [Text/tab-separated-values]. PANGAEA. https://doi.org/10.1594/PANGAEA.881315

Pizzolato, L., Howell, S. E. L., Dawson, J., Laliberté, F., & Copland, L. (2016). The influence of declining sea ice on shipping activity in the Canadian Arctic: Sea Ice and Shipping, Canadian Arctic. *Geophysical Research Letters*, 43(23), 12,146-12,154. https://doi.org/10.1002/2016GL071489

Sánchez-Gámez, P., & Navarro, F. (2017). Glacier Surface Velocity Retrieval Using D-InSAR and Offset Tracking Techniques Applied to Ascending and Descending Passes of Sentinel-1 Data for Southern Ellesmere Ice Caps, Canadian Arctic. *Remote Sensing*, 9(5), 442. https://doi.org/10.3390/rs9050442

Scheick, J., Enderlin, E. M., & Hamilton, G. (2019). Semi-automated open water iceberg detection from Landsat applied to Disko Bay, West Greenland. *Journal of Glaciology*, 65(251), 468–480. https://doi.org/10.1017/jog.2019.23

Sharp, M., Burgess, D. O., Cawkwell, F., Copland, L., Davis, J. A., Dowdeswell, E. K., Dowdeswell, J. A., Gardner, A. S., Mair, D., Wang, L., Williamson, S. N., Wolken, G. J., & Wyatt, F. (2014). Remote sensing of recent glacier changes in the Canadian Arctic. In J. S. Kargel, G. J. Leonard, M. P. Bishop, A. Kääb, & B. H. Raup (Eds.), Global Land Ice Measurements from Space (pp. 205–228). Springer Berlin Heidelberg. https://doi.org/10.1007/978-3-540-79818-7_9

Sharp, M., Burgess, D. O., Cogley, J. G., Ecclestone, M., Labine, C., & Wolken, G. J. (2011). Extreme melt on Canada's Arctic ice caps in the 21st century: Extreme Melt on Canada's Arctic Ice Caps. *Geophysical Research Letters*, 38(11), n/a-n/a. https://doi.org/10.1029/2011GL047381

Stephenson, S. R., & Smith, L. C. (2015). Influence of climate model variability on projected Arctic shipping futures. *Earth's Future*, 3(11), 331–343. https://doi.org/10.1002/2015EF000317

Tang, C. C. L., Ross, C. K., Yao, T., Petrie, B., DeTracey, B. M., & Dunlap, E. (2004). The circulation, water masses and sea-ice of Baffin Bay. *Progress in Oceanography*, 63(4), 183–228. https://doi.org/10.1016/j.pocean.2004.09.005

Turnbull, I. D., King, T., & Ralph, F. (2022). Iceberg Drift Simulations Using Inferred, Measured, and Ocean Model Currents. International Journal of Offshore and Polar Engineering, 32(2), 176–185. https://doi.org/10.17736/ijope.2022.jc856

Valeur, H. H., Hansen, C., Hansen, K. Q., Rasmussen, L., & Thingvad, N. (1996). Weather, sea and ice conditions in eastern Baffin Bay, offshore northwest Greenland: A review. Mineral Resources Administration for Greenland, 96–12, 37.

Van Der Veen, C. J. (1996). Tidewater calving. *Journal of Glaciology*, 42(141), 375–385. https://doi.org/10.3189/S0022143000004226

Van Wychen, W., Burgess, D. O., Gray, L., Copland, L., Sharp, M., Dowdeswell, J. A., & Benham, T. J. (2014). Glacier velocities and dynamic ice discharge from the Queen Elizabeth Islands, Nunavut, Canada. *Geophysical Research Letters*, 41(2), 484–490. https://doi.org/10.1002/2013GL058558

Van Wychen, W., Davis, J., Burgess, D. O., Copland, L., Gray, L., Sharp, M., & Mortimer, C. (2016). Characterizing interannual variability of glacier dynamics and dynamic discharge (1999-2015) for the ice masses of Ellesmere and Axel Heiberg Islands, Nunavut, Canada: Glacier Dynamics of the Canadian Arctic. *Journal of Geophysical Research: Earth Surface*, 121(1), 39–63. https://doi.org/10.1002/2015JF003708

Van Wychen, W., & Copland, L. (2017). Ice Island Drift Mechanisms in the Canadian High Arctic. In L. Copland & D. Mueller (Eds.), Arctic Ice Shelves and Ice Islands (pp. 287–316). Springer Netherlands. https://doi.org/10.1007/978-94-024-1101-0_11

Van Wychen, W., Burgess, D., Kochtitzky, W., Nikolic, N., Copland, L., & Gray, L. (2021). RADARSAT-2 Derived Glacier Velocities and Dynamic Discharge Estimates for the Canadian High Arctic: 2015–2020. *Canadian Journal of Remote Sensing*, 46(6), 695–714. https://doi.org/10.1080/07038992.2020.1859359

Wouters, B., Gardner, A. S., & Moholdt, G. (2019). Global Glacier Mass Loss during the GRACE Satellite Mission (2002-2016). *Frontiers in Earth Science*, 7, 96. https://doi.org/10.3389/feart.2019.00096

Chapter 2: Seasonal and Multi-year Flow Variability on the Prince of Wales Icefield, Ellesmere Island: 2009-2019

2.1 Introduction

Between 2000 and 2019, total glacier mass loss from the Queen Elizabeth Islands (QEI; Devon, Axel Heiberg, and Ellesmere Islands) averaged 30.6 Gt a^{-1}, with a mean surface elevation change of -0.35 m a^{-1} (Hugonnet et al., 2021). Within the QEI as a whole, mass loss is dominated by surface mass balance, which is mainly controlled by surface melt and runoff (Koerner, 2005; Millan et al., 2017; Noël et al., 2018). However, at individual glacier basins, frontal ablation can be an important component of mass loss (Cook et al., 2019; Van Wychen et al., 2021). Previous work on the dynamics of tidewater glaciers in the Canadian Arctic Archipelago (CAA) has primarily focused on quantifying and characterising inter-annual surface velocities and ice fluxes to the ocean (Williamson et al., 2008; Van Wychen et al., 2014; Van Wychen et al., 2016; Millan et al., 2017; Van Wychen et al., 2021), but less research has been undertaken on the physical processes controlling variability in glacier flow.

Between 1959 and 2015, 94% of all glaciers in the QEI underwent terminus retreat, with a region-wide acceleration in retreat since ~2000 (Cook et al., 2019). The acceleration in terminus retreat corresponded with increasingly negative surface mass balance towards the present day, which Cook et al. (2019) primarily attributed to increased surface air temperatures. Over the last two decades, Trinity, Wykeham, Ekblaw, and Cadogan glaciers have retreated and been identified as the primary sources of ice flux from Prince of Wales (POW) Icefield, accounting for ~83% of total ice discharge (Dalton et al., 2019; Van Wychen et al., 2021). In addition to this, since 2000, Trinity and Wykeham have been the only two glaciers in the QEI to have consistently accelerated (Van Wychen et al., 2016; Van Wychen et al., 2021). Van Wychen et al. (2016) found that these glaciers had thinned by ~3-5 m a^{-1} over their termini between 2008 and 2014 and were grounded below sea level for much of their length, potentially making them prone to continued acceleration and mass loss. Similarly, Harcourt et al. (2020) found that both Trinity and Wykeham glaciers have been thinning at a rate of ~4-6m a^{-1} between 2003 and 2016 in their near-terminus region, and suggest that since ~2003 they have transitioned from being fully grounded to partially floating, providing more evidence that they may be transitioning to a period of continued acceleration, retreat, and overall mass loss. The acceleration and retreat of glaciers on the POW Icefield (Cook et al., 2019; Van Wychen et al., 2021) has also resulted in increased iceberg production (Dalton et al., 2019;

Van Wychen et al., 2021), which may pose a risk to shipping routes and offshore oil exploration and lead to enhanced mass loss.

Previous studies have suggested that a relationship exists between glacier calving, rapid thinning, and velocity increase which can lead to dramatic retreat and dynamic thinning like that observed at Columbia Glacier, Alaska, since the 1980s (Van der Veen, 1996; Rasmussen et al., 2011; Vijay & Braun, 2017) and Sermeq Kujalleq (also called Jakobshavn Isbrae) since the late 1990s (Thomas et al., 2003; Joughin et al., 2004; Nick et al., 2009). Due to a lack of long-term observational data of glacier velocity, surface elevation change, and ice discharge, there has previously been insufficient evidence to determine whether similar trends exist in glacier dynamics in the CAA. To address this, here we use a dense record of winter surface velocities, annual velocity composites, basal topography, and surface elevation changes from the past decade to quantify the dynamics and changes of the four main tidewater outlet glaciers of POW Icefield: Trinity, Wykeham, Cadogan, and Ekblaw. Collectively, this enables us to:

(i) identify new seasonal and inter-annual patterns of glacier flow, and better detail the evolution of surface ice motion;

(ii) provide updated estimates of changes in glacier surface elevation, and;

(iii) determine whether glacier geometry (i.e. thickness and bed elevation) is contributing to destabilizing changes in the largest glacier basin (Trinity and Wykeham) in the CAA.

2.2 Study Site

The POW Icefield on SE Ellesmere Island covers an area of ~19,000 km^2, of which 66% is drained by tidewater glaciers flowing primarily eastwards into Baffin Bay (Sharp et al., 2014). The western margin of the POW Icefield is primarily drained by land-terminating glaciers. The Pikialasorsuaq (also called the North Water Polynya), located in Smith Sound, provides a major source of moisture for the eastern side of the icefield (Koerner, 1979).

Similar to other ice masses in the QEI, recent negative mass balance on the POW Icefield is dominated by increases in surface melt as a result of increases in summer air temperature and lengthening of the melt season (Sharp et al., 2011; Mortimer et al., 2016; Millan et al., 2017).

While overall solid ice discharge for the QEI has decreased since 2000 due to the slowdown of most glaciers, it has become an important contributor to mass loss due to acceleration of the Trinity and Wykeham outlet glaciers (Millan et al., 2017). As of 2020, Trinity and Wykeham contributed ~50% of total ice discharge from tidewater glaciers in the QEI (1.60 Gt a^{-1}), compared to ~22% (0.55 Gt a^{-1}) in 2000 (Van Wychen et al., 2021).

Cadogan Glacier is a tidewater glacier located at the head of Cadogan Inlet on the eastern POW Icefield (78.23°N, 76.94°W; Figure 2-1). It is ~65 km long and ~5 km wide at the terminus, and is grounded below sea level for ~50 km up-glacier from its front. Cadogan is characterised by multi-year phases of acceleration and deceleration in its near-terminus region, and has been identified as a primary source of ice discharge from the POW Icefield (Dalton et al., 2019; Van Wychen et al., 2021).

Ekblaw Glacier is located at the head of Baird Inlet on the eastern POW Icefield (78.51°N, 76.71°W; Figure 2-1), is ~60 km long and ~3 km wide at the terminus, and is grounded below sea level for ~35 km up-glacier from its front. Ekblaw Glacier was identified by Van Wychen et al. (2016) as "pulse type", which means that it is characterised by multi-year phases of acceleration and deceleration in the lowermost portion of the glacier, which have been linked to underlying bedrock topography.

Situated at the head of Talbot Inlet on SE Ellesmere Island, Trinity and Wykeham glaciers are large tidewater outlet glaciers that drain the SE POW Icefield (Figure 2-1). Trinity Glacier (77.97°N, 78.57°W) is ~60 km long and ~6 km wide at its terminus. Wykeham Glacier (77.89°N, 78.61°W) is ~50 km long and ~9 km wide at its terminus. Until about 2003, Trinity, Wykeham, and Talbot glaciers had a combined terminus, but a terminus retreat of ~3-4 km for Trinity Glacier and ~1 km for Wykeham Glacier since ~2003 has resulted in their separation (Mair et al., 2009).

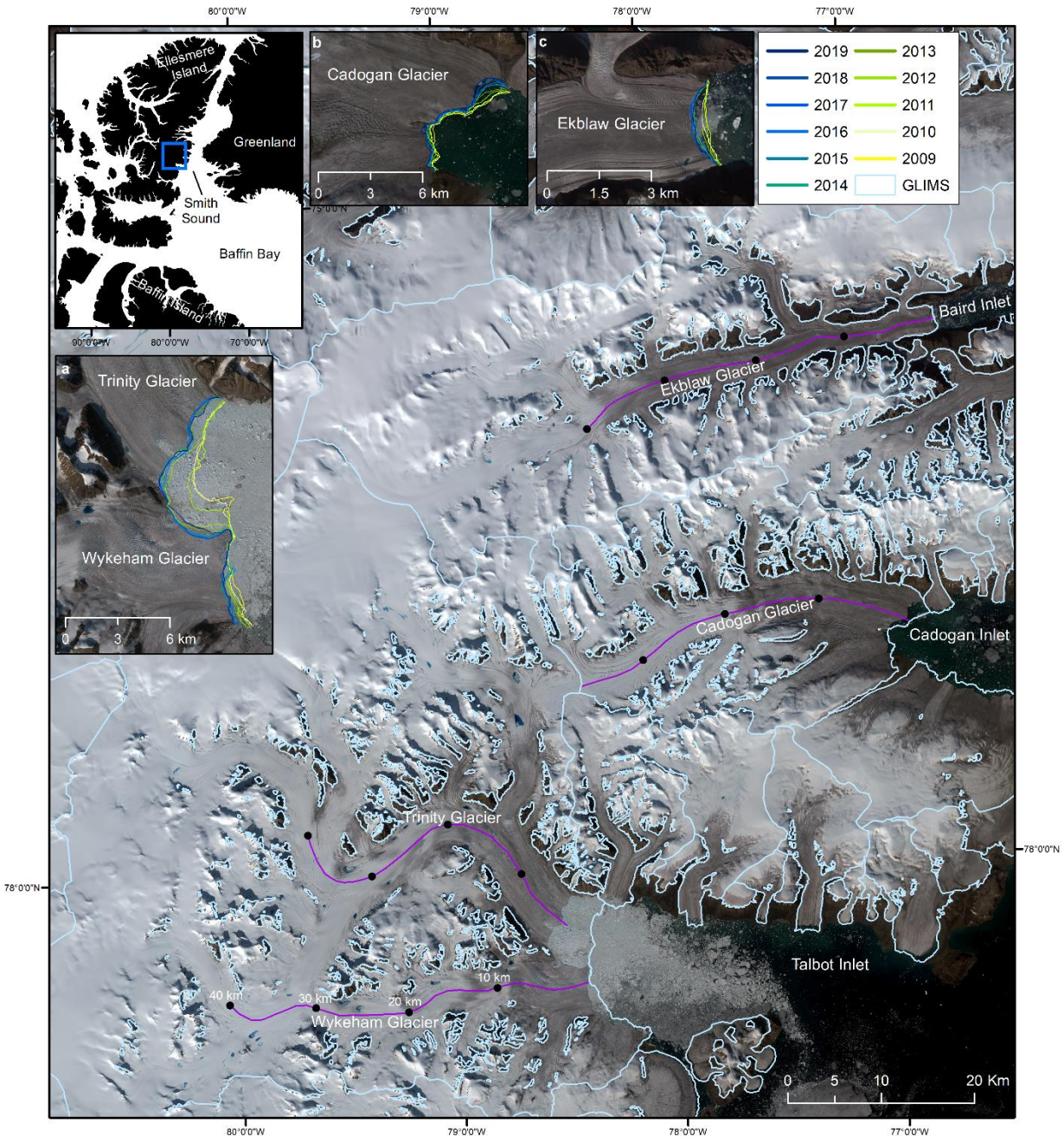

Figure 2-1: Location of the main iceberg producing glaciers from the Prince of Wales Icefield on SE Ellesmere Island. Purple lines show location of centrelines where measurements were extracted for this study, with black dots at 10 km intervals up-glacier from each terminus. Inset maps show terminus retreat between 2009 and 2019 for: a) Trinity and Wykeham glaciers, b) Cadogan Glacier, and c) Ekblaw Glacier. Base image: Sentinel-2B, August 16/17, 2019, European Space Agency.

2.3 Methods and Data

2.3.1 Glacier Velocities

2.3.1.1 Radarsat-2 Speckle-Tracking

We used a total of 167 Radarsat-2 Synthetic Aperture Radar (SAR) scene pairs collected between 2009 and 2019 through partnerships with Natural Resources Canada (NRCan), and Environment and Climate Change Canada (ECCC), to derive surface velocities of glaciers across the POW Icefield (Table 2-1). Radarsat-2 has a 24-day repeat orbital cycle and acquisitions for this project were obtained in fine and fine-wide beam mode with maximum spatial resolution of 8 m during mid to late-winter (approximately December-March), when glacier surface conditions typically remain relatively stable in the study area (i.e. minimal snowfall or surface melt). We apply a speckle tracking algorithm written in MATLAB to determine glacier surface displacement, which uses a cross-correlation algorithm on co-registered pairs of SAR images and spatial window size of 500 m x 500 m (Gray & Short, 2004; Van Wychen et al., 2012). This method uses two Radarsat-2 scenes with nearly identical imaging geometry as inputs, and requires the time span between image acquisitions be long enough that motion occurs which can be detected, but short enough to ensure that surface coherence is maintained. The 24-day orbital repeat of the Radarsat-2 system has been shown to be a good temporal window that balances these needs (Van Wychen et al., 2021). This method has previously proven to be an effective way to monitor surface ice velocity in the CAA, with errors quantified as 0.01-0.03 m d^{-1} for 24-day separated image pairs, based on comparisons with areas of known zero motion (e.g. along ice divides and bedrock outcrops) and near-simultaneous dGPS measurements (Short & Gray, 2005; Van Wychen et al., 2012; 2014; 2016; 2021).

Errors in co-registration and cross-correlation by the speckle tracking algorithm were addressed using manual filtering methods outlined by Van Wychen et al. (2012). Speckle tracking displacement results were imported into ESRI ArcGIS 10.7.1 and erroneous values manually removed using the following criteria: i) motion should be faster near the glacier centreline than near the side walls; ii) flow direction should generally follow surrounding topography (e.g. valley walls) and run parallel to surface flow features (e.g. medial moraines); and iii) flow vectors should be consistent over short distances.

Table 2-1: Summary of Radarsat-2 imagery used in this study to derive winter glacier velocities. *Averaged image pairs.

Winter	Beam Mode	Image 1	Image 2	Segment
2009	F21F	2009/01/02	2009/01/26	S1
	F6F	2009/01/04	2009/01/28	S1
	F1F	*2009-01-05	2009/01/29	S1
	F2	*2009-01-05	2009/01/29	S1
	F5F	*2009-01-06	2009/01/30	S1
	F23	*2009-01-06	2009/01/30	S1
	F4F	2009/01/25	2009/02/18	S1
	F3	*2009-01-26	2009/02/19	S1
	F21F	*2009-01-26	2009/02/19	S1
	F6F	2009/01/28	2009/02/21	S1
	F1F	*2009-01-29	2009/02/22	S1
	F2	*2009-01-29	2009/02/22	S1
	F5F	*2009-01-30	2009/02/23	S1
	F23	*2009-01-30	2009/02/23	S1
	F22	2009/02/18	2009/03/14	S1
	F3N	2009/02/19	2009/03/15	S1
	F3	2009/02/19	2009/03/15	S1
	F2	2009/02/22	2009/03/18	S1
	F5F	*2009-02-23	2009/03/19	S1
	F23	*2009-02-23	2009/03/19	S1
	F2	2009/03/01	2009/03/25	S1
	F22	2009/03/14	2009/04/07	S1
	F3	2009/03/15	2009/04/08	S1
	F2	2009/03/18	2009/04/11	S1
	F23	2009/03/19	2009/04/12	S1
	F4F	*2009-04-07	2009/05/01	S1
	F22	*2009-04-07	2009/05/01	S1
	F21F	2009/04/08	2009/05/02	S1
	F2	2009/04/11	2009/05/05	S1
2010	F6F	2009/12/30	2010/01/23	S1
	F1F	2009/12/31	2010/01/24	S1
	F22	2010/01/20	2010/02/13	S1
	F21F	2010/01/21	2010/02/14	S1
	F1F	2010/01/24	2010/02/17	S1
	F5F	*2010-01-25	2010/02/18	S1
	F23	*2010-01-25	2010/02/18	S1
	F22	2010/02/13	2010/03/09	S1
	F21F	2010/02/14	2010/03/10	S1
	F23	2010/02/18	2010/03/14	S1
	F6N	2010/02/25	2010/03/21	S1
	F6N	2010/02/25	2010/03/21	S1
	F6N	2010/02/25	2010/03/21	S2
	F6N	2010/02/25	2010/03/21	S3
	F3N	2010/03/03	2010/03/27	S1
	F22	2010/03/09	2010/04/02	S1
	F21F	2010/03/10	2010/04/03	S1
	F6F	2010/03/12	2010/04/05	S1
	F23	2010/03/14	2010/04/07	S1
	F21F	2010/04/03	2010/04/27	S1
	F6F	2010/04/05	2010/04/29	S1
	F1F	2010/04/06	2010/04/30	S1

	F23	2010/04/07	2010/05/01	S1
	F3	*2010-04-27	2010/05/21	S1
	F21F	*2010-04-27	2010/05/21	S1
	F23	2010/05/01	2010/05/25	S1
2011	F3	2011/01/16	2011/02/09	S1
	F1F	2011/01/19	2011/02/12	S1
	F5F	2011/01/20	2011/02/13	S1
	F4N	2011/01/26	2011/02/19	S1
	F4N	2011/01/26	2011/02/19	S2
	F4N	2011/01/26	2011/02/19	S3
	F1	2011/01/29	2011/02/22	S1
	F1	2011/01/29	2011/02/22	S2
	F1	2011/01/29	2011/02/22	S3
	F1	2011/01/29	2011/02/22	S4
	F1	2011/01/29	2011/02/22	S5
	F23F	2011/02/01	2011/02/25	S1
	F23F	2011/02/01	2011/02/25	S1
	F23F	2011/02/01	2011/02/25	S2
	F23F	2011/02/01	2011/02/25	S3
	F23F	2011/02/01	2011/02/25	S4
	F23F	2011/02/01	2011/02/25	S5
	F1F	2011/02/02	2011/02/26	S1
	F1F	2011/02/02	2011/02/27	S2
	F22	2011/02/08	2011/03/04	S1
	F3	*2011-02-09	2011/03/05	S1
	F21F	*2011-02-09	2011/03/05	S1
	F1F	2011/02/12	2011/03/08	S1
	F5F	2011/02/13	2011/03/09	S1
	F1	2011/02/22	2011/03/18	S1
	F23F	2011/02/25	2011/03/21	S1
	F22	2011/03/04	2011/03/28	S1
	F3	2011/03/05	2011/03/29	S1
	F1F	2011/03/08	2011/04/01	S1
	F5F	2011/03/09	2011/04/02	S1
	F22	2011/03/28	2011/04/21	S1
	F3	2011/03/29	2011/04/22	S1
	F5F	2011/04/02	2011/04/26	S1
	F21F	2011/04/22	2011/05/16	S1
	F5F	2011/04/26	2011/05/20	S1
2012	F22	2012/01/10	2012/02/03	S1
	F6F	2012/01/13	2012/02/06	S1
	F22	2012/02/03	2012/02/27	S1
	F5F	2012/02/08	2012/03/03	S1
	F22	2012/02/27	2012/03/22	S1
	F21F	2012/02/28	2012/03/23	S1
	F5F	2012/03/03	2012/03/27	S1
	F0W3	2012/03/16	2012/04/09	S3
	F0W3	2012/03/16	2012/04/09	S4
	F21F	2012/03/23	2012/04/16	S1
	F1F	2012/03/26	2012/04/19	S1
	F5F	*2012-03-27	2012/04/20	S1
	F23	*2012-03-27	2012/04/20	S1
	F0W3	2012/04/09	2012/05/03	S3
	F0W3	2012/04/09	2012/05/03	S4
	F3	*2012-04-16	2012/05/10	S1
	F21F	*2012-04-16	2012/05/10	S1

	F23	2012/04/20	2012/05/14	S1
2013	F0W3	2013/01/05	2013/01/29	S2
	F0W3	2013/01/05	2013/01/29	S3
	F0W3	2013/01/05	2013/01/29	S4
	F0W3	2013/01/29	2013/02/22	S2
	F0W3	2013/01/29	2013/02/22	S3
	F0W3	2013/01/29	2013/02/22	S4
	F0W3	2013/02/22	2013/03/18	S2
	F0W3	2013/02/22	2013/03/18	S3
	F0W3	2013/02/22	2013/03/18	S4
2014	F0W3	2013/12/07	2013/12/31	S2
	F0W3	2013/12/07	2013/12/31	S3
	F0W3	2013/12/07	2013/12/31	S4
	F0W3	2013/12/31	2014/01/24	S2
	F0W3	2013/12/31	2014/01/24	S3
	F0W3	2013/12/31	2014/01/24	S4
	F0W3	2014/01/24	2014/02/17	S2
	F0W3	2014/01/24	2014/02/17	S3
	F0W3	2014/01/24	2014/02/17	S4
	F0W3	2014/02/17	2014/03/13	S2
	F0W3	2014/02/17	2014/03/13	S3
	F0W3	2014/02/17	2014/03/13	S4
2015	F0W3	2014/12/02	2014/12/26	S2
	F0W3	2014/12/02	2014/12/26	S3
	F0W3	2014/12/26	2015/01/19	S2
	F0W3	2014/12/26	2015/01/19	S3
	F0W3	2015/01/19	2015/02/12	S2
	F0W3	2015/01/19	2015/02/12	S3
	F0W3	2015/02/12	2015/03/08	S2
	F0W3	2015/02/12	2015/03/08	S3
2016	F0W3	2015/12/21	2016/01/14	S2
	F0W3	2015/12/21	2016/01/14	S3
	F0W3	2016/01/14	2016/02/07	S2
	F0W3	2016/01/14	2016/02/07	S3
	F0W1	2016/01/15	2016/02/08	S3
	F0W1	2016/01/15	2016/02/08	S4
	F0W3	2016/02/07	2016/03/02	S2
	F0W3	2016/02/07	2016/03/02	S3
	F0W1	2016/02/08	2016/03/03	S3
	F0W1	2016/02/08	2016/03/03	S4
	F0W3	2016/03/02	2016/03/26	S2
	F0W3	2016/03/02	2016/03/26	S3
	F0W3	2016/03/26	2016/04/19	S2
2017	F0W3	2016/11/21	2016/12/15	S2
	F0W3	2016/11/21	2016/12/15	S3
	F0W3	2016/12/15	2017/01/08	S2
	F0W3	2016/12/15	2017/01/08	S3
	F0W3	2017/01/08	2017/02/01	S2
	F0W3	2017/01/08	2017/02/01	S3
	F0W3	2017/02/01	2017/02/25	S2
	F0W3	2017/02/01	2017/02/25	S3
	F0W3	2017/02/25	2017/03/21	S2
	F0W3	2017/02/25	2017/03/21	S3
	F0W3	2017/03/21	2017/04/14	S2
	F0W3	2017/03/21	2017/04/14	S3
2018	F0W3	2017/11/16	2017/12/10	S1

	F0W3	2017/11/16	2017/12/10	S2
	F0W3	2017/12/10	2018/01/03	S1
	F0W3	2017/12/10	2018/01/03	S2
	F0W3	2018/01/03	2018/01/27	S1
	F0W3	2018/01/03	2018/01/27	S2
	F0W3	2018/01/27	2018/02/20	S1
	F0W3	2018/01/27	2018/02/20	S2
	F0W3	2018/02/20	2018/03/16	S1
	F0W3	2018/02/20	2018/03/16	S2
2019	F0W3	2018/12/05	2018/12/29	S2
	F0W3	2018/12/05	2018/12/29	S3
	F0W3	2018/12/29	2019/01/22	S2
	F0W3	2018/12/29	2019/01/22	S3
	F0W3	2019/01/22	2019/02/15	S2
	F0W3	2019/01/22	2019/02/15	S3

The filtered scenes were resampled to 100 m resolution using the inverse distance weighting tool in ArcGIS to provide continuous velocity results over the whole glacier surface and clipped to the Randolph Glacier Inventory (RGI 6.0) extents for the POW Icefield. In 12 instances where multiple acquisitions were made of the same area during the same time period, we computed the mean velocity of overlapping areas to derive the final velocity value. To determine variability from 2009-2019, velocities were extracted along centrelines and cross-sections for Trinity, Wykeham, Cadogan, and Ekblaw glaciers (Figure 2-1). Glacier centrelines and cross-sections were drawn manually using cloud-free Landsat-8 imagery (acquired August 9, 2019) bounded by RGI6.0 glacier basin extents, with velocity measurements extracted in 100 m intervals.

2.3.1.2 ITS_LIVE Annual Composites

Annual ice surface velocities were derived from composites of Inter-mission Time Series of Land Ice Velocity and Elevation (ITS_LIVE) imagery. This velocity data is generated using the auto-RIFT algorithm (Gardner et al., 2018) and is provided by the NASA MEaSUREs ITS_LIVE project (Gardner et al., 2019; https://its-live.jpl.nasa.gov/). ITS_LIVE uses feature-tracking of optical Landsat image pairs with cloud cover ≤60% to identify glacier displacement. Annual composites of 240 m spatial resolution are created using the error-weighted average of all image pair velocities, where the centre-date falls within a given calendar year. Annual composites, which will be referred to as "annual" in this paper, include temporal midpoints which vary within and between years. Unlike speckle tracking of SAR imagery, optical feature tracking includes velocities obtained from imagery collected during the summer. The dates of the imagery used to create the ITS_LIVE annual composites are unknown, and likely vary between years, so may contain an unquantifiable bias towards summer velocities. Annual composites therefore likely incorporate seasonal summer speed-ups facilitated by basal sliding resulting from surface meltwater reaching the bed (Burgess et al., 2005), which are assumed to be not present in the winter SAR acquisitions.

For this study we used ITS_LIVE annual composites of the Canadian Arctic from 2009 to 2018 for comparison with speckle-tracking derived winter velocities. Velocities were manually inspected and filtered based on the above criteria for speckle-tracking. Velocities were extracted along the same centrelines drawn for the Radarsat-2 speckle-tracking results at 100 m intervals. Error values provided with the ITS_LIVE annual composites indicate average errors over our

period of interest of 0.02, 0.01, 0.03, and 0.03 m d^{-1} for Ekblaw, Cadogan, Wykeham, and Trinity, respectively (Gardner et al., 2019; https://its-live.jpl.nasa.gov/).

2.3.2 Surface Elevation

2.3.2.1 CryoSat

We downloaded annual CryoSat-2 baseline-D intermediate level 1b (L1b) SARIn altimetry data collected between 2010 and 2020 from the ESA ftp site (ftp://science-pds.cryosat.esa.int/) for Trinity and Wykeham glaciers. Processing of the L1b data to terrain height and height change was completed using the methods described in Gray et al. (2015, 2019). Swath mode processing (Gray et al., 2013; Gourmelen et al., 2019) was used for this area and provided many more height estimates than the approach that estimates the height of the 'point-of-closest approach' (POCA). The returned waveform from one along-track position includes the initial leading edge, which can be used to identify one POCA value, and then delayed returns from adjacent footprints in the cross-track direction. Swath processing uses these delayed returns to provide the additional height estimates used in this study. In many situations with a cross-track slope, the dominant delayed returns are from the area beneath the sub-satellite track at incidence angles less than that subtended to the POCA. In the along-track direction the swath-processed footprint size is ~350 m but the across-track footprint size depends on the cross-track slope and is typically ~100 m. Random errors are reduced through averaging and the standard error of the mean for the swath mode height changes depends on the number and quality of points.

The low elevation ablation zone of many glaciers, like Trinity and Wykeham, are in valleys with adjacent mountains. Returns from these mountains can compromise the shape of the waveform such that there is not a clear leading edge and any POCA estimate may be suspect. However, particularly in July and August there can be strong delayed returns from the glacier surface that can be swath mode processed to obtain surface heights (Gray, 2021). Values with power > -150 dB and coherence > 0.9 were selected to minimize the possible contribution from any unwanted range-ambiguous region. The interferometric phase was then used to geocode the returns. All the swath mode results were binned for the summer period each year (approximately June to September) into three discrete elevation bands. For Trinity and Wykeham glaciers, the elevation bands used were 0-300 m, 300-550 m, and 550-800 m relative to the WGS84 ellipsoid. Then a search was done for footprints in each summer with small separation (< 400 m horizontally) from

those in another summer, and the average height change from pairs for each elevation band and for each pair of summers was calculated. Local slope correction was used to refine the height change as described in Gray et al., (2015) and Gray (2021).

2.3.2.2 ASTER DEM Differencing

We used results produced by Hugonnet et al. (2021) to estimate changes in surface elevation for 2010-2014 and 2015-2019 for the POW Icefield, downloaded from the Theia web portal (http://maps.theia-land.fr; https://doi.org/10.6096/13). Hugonnet et al. (2021) used Advanced Spaceborne Thermal Emission and Reflection Radiometer (ASTER) satellite imagery to produce digital elevation models (DEMs) and ArcticDEM data to perform DEM differencing. ASTER DEMs were co-registered to the TanDEM-X global DEM and bias-corrected to create 100 m resolution DEMs of the region. Differencing between earlier and later DEMs was then undertaken to represent a reduction in elevation over time as a negative value, and an increase in elevation as a positive value. Resulting DEMs were validated by Hugonnet et al. (2021) using ICESat and NASA IceBridge measurements accessed through the National Snow and Ice Data Center (NSIDC) of glacier surface elevations collected between 2003 and 2019. This method provided error estimates in mean elevation change rate in Arctic Canada North (which encompasses the entire QEI) of 0.05 m a^{-1} for 2010-2014 and 0.06 m a^{-1} for 2015-2019 (Hugonnet et al., 2021).

2.3.2.3 ArcticDEM

The ArcticDEM was constructed using stereo optical satellite imagery acquired by the DigitalGlobe constellation (WorldView-1, 2, and 3) between 2008 and 2017 (Porter et al., 2018), and is available as a mosaic and as individual ‘strip files’. ArcticDEM strip files are between 16-18 km in width and 110-120 km in length and are referenced to the WGS84 ellipsoid. For this study, we resampled both 2 m resolution DEM strip files and mosaic files to 20 m resolution to allow for removal of small-scale noise and efficient processing. We used the mosaic product to derive centreline surface elevations (Appendix A) and for calculations of elevation change resulting from dynamic thinning. We used annual averages of 54 strip files covering the Trinity and Wykeham glacier basins from 2012 to 2017 to identify changes in surface elevation and calculate flotation (Table 2-2).

Table 2-2**:** Summary of ArcticDEM products used in this study. Sensor identifies DigitalGlobe WorldView satellite that collected the stereo-pair image (e.g. WV01, Worldview-1).

Strip Files						**Mosaic Files**	
Date	**Sensor**	**Segment**	**Date**	**Sensor**	**Segment**	**100km x 100km Tile**	**50km x 50km Sub-Tile**
2012-06-30	WV01	seg1	2015-03-10	WV01	seg2	29_32	2_2
2013-04-21	WV01	seg1	2015-03-12	WV01	seg1	29_33	1_2
2014-07-05	WV02	seg1	2015-03-12	WV01	seg1	29_33	2_2
2015-07-14	WV03	seg1	2015-07-11	WV01	seg1	29_34	1_2
2016-09-16	WV01	seg1	2015-07-11	WV01	seg2	29_34	2_2
2017-03-20	WV01	seg1	2015-06-03	WV02	seg1	30_32	2_1
2012-07-23	WV01	seg1	2015-03-10	WV02	seg4	30_32	2_2
2012-07-04	WV01	seg1	2015-03-23	WV02	seg1	30_33	1_1
2012-07-23	WV01	seg1	2015-05-01	WV02	seg2	30_33	1_2
2012-06-19	WV01	seg1	2015-06-03	WV03	seg1	30_33	2_1
2012-08-02	WV01	seg1	2015-09-22	WV03	seg1	30_33	2_2
2012-08-20	WV02	seg1	2015-03-13	WV03	seg1	30_34	1_1
2012-07-23	WV01	seg3	2015-03-21	WV03	seg1	30_34	1_2
2012-07-16	WV01	seg1	2016-04-19	WV01	seg1	30_34	2_1
2012-05-03	WV01	seg1	2016-04-06	WV01	seg1	30_34	2_2
2012-05-03	WV01	seg2	2016-04-19	WV01	seg1	31_32	2_1
2013-04-12	WV02	seg4	2016-06-05	WV02	seg2	31_33	1_1
2013-05-06	WV02	seg1	2016-09-16	WV02	seg1	31_33	2_1
2013-08-23	WV02	seg1	2016-03-23	WV02	seg1	31_34	1_1
2013-04-12	WV02	seg4	2016-08-12	WV03	seg1	31_34	2_1
2013-05-24	WV01	seg1	2016-09-16	WV01	seg1		
2013-08-13	WV01	seg1	2016-05-05	WV01	seg1		
2013-08-11	WV01	seg1	2017-04-08	WV01	seg1		
2014-04-21	WV02	seg1	2017-04-22	WV02	seg1		
2014-04-15	WV02	seg1	2017-04-12	WV02	seg1		
2015-06-13	W1W1	seg6	2017-03-13	WV02	seg1		
2015-06-13	W1W1	seg7	2017-03-10	WV03	seg1		

2.3.3 Bed Elevation

Bed topography data were created using airborne radar measurements from the Centre for Remote Sensing of Ice Sheet (CReSIS) Multichannel Coherent Data Depth Sounder (MCoRDS) operating at a frequency range of 180-210 MHz (CReSIS, 2016). The radar was flown on a P-3 aircraft as part of NASA Operation IceBridge over the POW Icefield in April/May 2014 using a ~5 km wide swath over Trinity and Wykeham glaciers and ~2.5 km swath over Cadogan and Ekblaw glaciers, and downloaded from the University of Kansas CReSIS data portal (https://data.cresis.ku.edu/). This technique produces an image of the bed topography using nadir-derived ice thicknesses subtracted from surface topography (Paden et al., 2010; Jezek et al., 2013). Tomography requires a good signal-to-noise ratio in order to obtain reliable off-nadir returns (Paden et al., 2010; Wu et al., 2011; Jezek et al., 2013). Medrzycka et al. (2019) used this dataset to extract bed elevation for Good Friday Bay Glacier on Axel Heiberg Island to better understand the topographic controls on glacier motion. Previous studies have found ice thickness uncertainty to be within 10-20 m using this method (Paden et al., 2010; Wu et al., 2011; Jezek et al., 2013).

Tomography data over Trinity and Wykeham glaciers was collected along four overlapping swaths that ran parallel to the centreline of both glaciers and one swath that ran perpendicular to flow along the terminus. Erroneous data in off-nadir areas of overlapping swath returns were manually filtered out based on the criteria: (1) where swaths overlap, data is removed from the swath farthest from nadir position; and (2) values should be consistent over short distances (Moore & Paden, Personal Communication, May 14, 2021; Paden et al., 2010). We resampled the 3D tomography data to 100 m resolution to reduce noise without significantly impacting the results. These 3D tomographic bed elevation measurements are consistent with those presented by Harcourt et al. (2020) which combined Operation Ice Bridge (OIB) and Canadian Arctic Geophysical Exploration (CAGE) flights ice thickness measurements in order to derive subglacial topography beneath Trinity and Wykeham glaciers.

2.3.4 Flotation Calculation

To determine how close the termini of Trinity and Wykeham glaciers were to flotation between 2012 and 2017, we compared the ratio of ice thickness to water depth to compute H_b, the thickness of ice in excess of flotation, based on the equation presented in Cuffey & Paterson (2010):

$$H_b = H_M - \frac{\rho_w}{\rho_i} H_w \quad (1)$$

where H_M is total ice thickness, ρ_w is the density of water (1000 kg m^{-3}, taking into consideration the input of freshwater at the near terminus area), ρ_i is the density of glacier ice (900 kg m^{-3}, taking into consideration crevasses and firn; Cuffey & Paterson, 2010; Cogley et al., 2011), and H_w is water depth (or distance between sea level and glacier bed, where glacier ice is present). In areas where H_b approaches 0, or is negative, flotation would likely occur (Cuffey & Paterson, 2010).

2.4 Results

2.4.1 Ekblaw & Cadogan Glaciers

Ekblaw Glacier underwent multi-year variations in velocity over the study period (2009-2019). Between 2013 and 2016, there was a clear deceleration where peak velocities decreased from ~1 m d^{-1} to ~0.5 m d^{-1} (Figure 2-2a). This overall deceleration was also observed to extend ~40 km up-glacier, compared to years when flow was faster. The highest velocities for Ekblaw Glacier for all time periods are concentrated in the near terminus area, 1-2 km from the glacier front. During periods of faster flow near the terminus (e.g., 2009 to 2012), higher velocities (>0.3 m d^{-1}) extended nearly the entire length of the glacier trunk, spanning the portion of the glacier which is grounded below sea level (~0-40 km from the terminus; Figure 2-3a, Appendix A).

When comparing the Ekblaw winter velocities with annual averages, velocity patterns outside of the winter season follow the same multi-year periods of variability (Figure 2-2b). The highest velocities observed throughout the year on Ekblaw Glacier are concentrated in the near-terminus area and only during periods of faster flow (e.g. 2009-2012 and 2016-2019) do they extend beyond ~12 km up-glacier from the terminus.

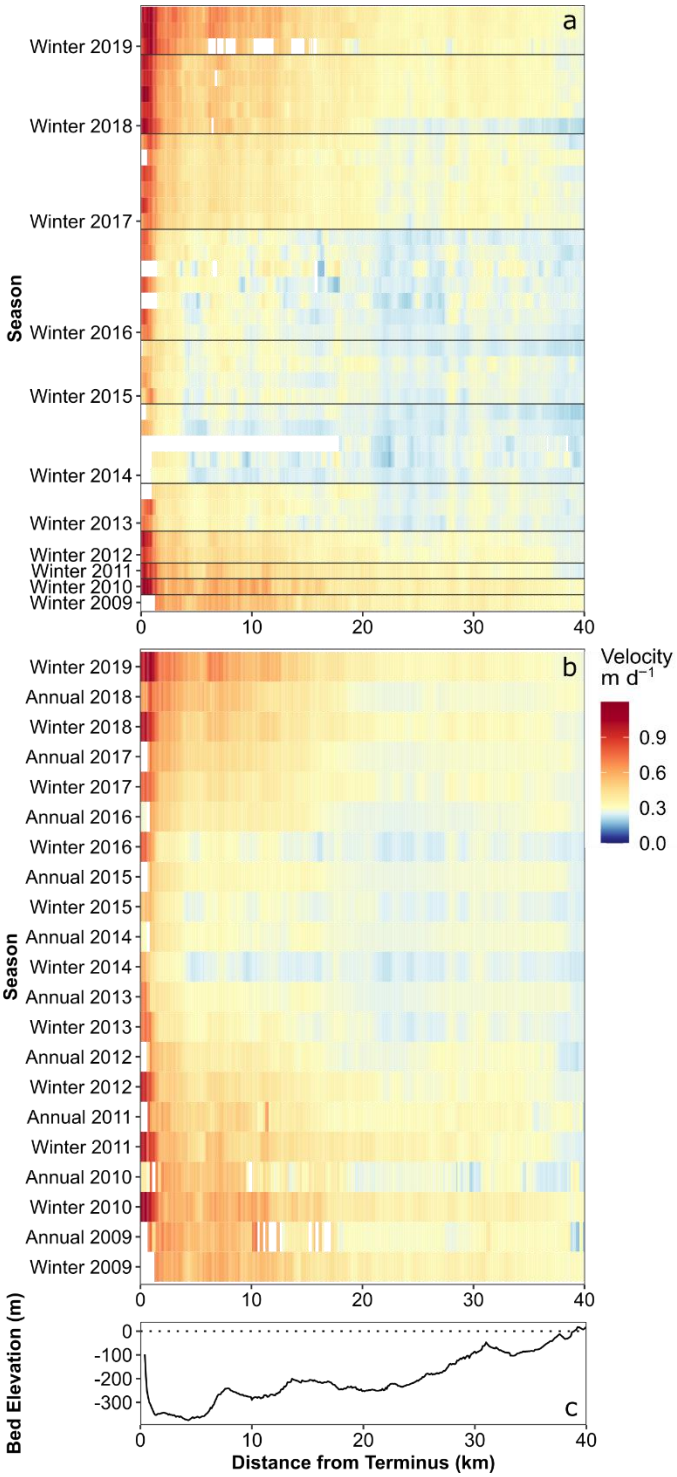

Figure 2-2: For the centreline of Ekblaw Glacier: a) Radarsat-2 speckle-tracking derived winter velocities, 2009-2019, b) Comparison between average Radarsat-2 derived winter velocities and ITS_LIVE feature-tracking derived annual velocity composites, 2009-2019, c) NASA 3D tomography derived bed elevations along the glacier centreline shown in Figure 1.

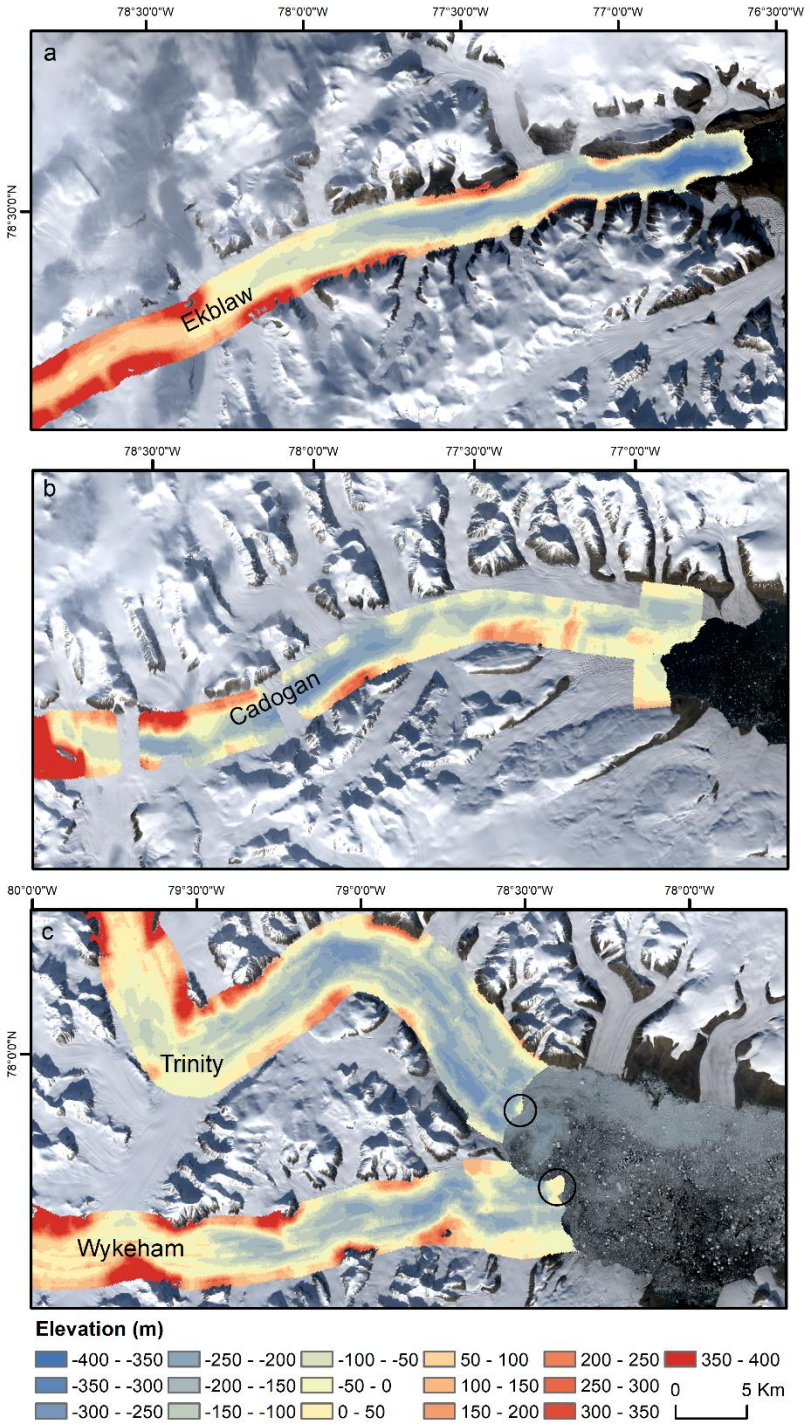

Figure 2-3: NASA 3D tomography derived bed elevations for: a) Ekblaw, b) Cadogan, and c) Trinity and Wykeham glaciers. NASA IceBridge flight data acquired on May 6, 2014. Location of probable pinning points for Trinity and Wykeham are denoted by black circles. Base image: Landsat-8 August 29, 2014, USGS/NASA Landsat.

The greatest changes in surface elevation for Ekblaw Glacier (Figure 2-4) were located in the region up to ~6 km up-glacier from the terminus, with little difference in the rate of change between the 2010-2014 and 2015-2019 periods. Surface thinning along the main glacier trunk typically ranged from ~0.3-1.6 m a^{-1}, with areas at the glacier front exceeding 2 m a^{-1}.

Similar to Ekblaw, Cadogan Glacier underwent a clear multi-year velocity decrease from 2010 to 2017, followed immediately by an increase from 2017 to 2019 (Figure 2-5a). Peak velocities for Cadogan Glacier reached ~0.5 m d^{-1} and were found within the lowermost 10 km, with the fastest flow occurring at the terminus. During periods of multiyear velocity increase, higher flow rates extended ~20 km up-glacier from the terminus. Cadogan Glacier is grounded below sea level for >40 km up-glacier from its terminus, and fastest flow corresponds with a shallow trough (50-100 m below sea level) in the lowermost 10 km (Figure 2-3b, 2-5c, Appendix A).

In comparison with annual velocity composites, winter velocities for Cadogan Glacier were lower than the annual average for all years in the study (Figure 2-5b). Consistent with the winter results, there were clear multi-year repeating periods in velocity including a deceleration from 2009 to 2012, followed by limited velocity variability from 2012 to 2017, and an acceleration from 2017 to 2019. The highest velocities were observed in the lowermost 10 km of the glacier and ice motion did not exceed ~0.1 m d^{-1} beyond 20 km up-glacier from the terminus. Velocities up-glacier of this point were generally low (0-0.1 m d^{-1}) and did not vary significantly throughout the study period.

Highest rates of surface thinning for Cadogan Glacier (Figure 2-4) were concentrated in the lowermost ~10 km of the glacier between 2010 and 2019. Average thinning rates for 2010-2014 ranged between ~0.5 and 2 m a^{-1} and extend into the accumulation area. This average surface thinning rate continued during 2015-2019, but was concentrated in the lowermost ~5 km of the glacier, located in the near terminus region, with areas of surface height increase observed in areas of higher elevation (Figure 2-4b).

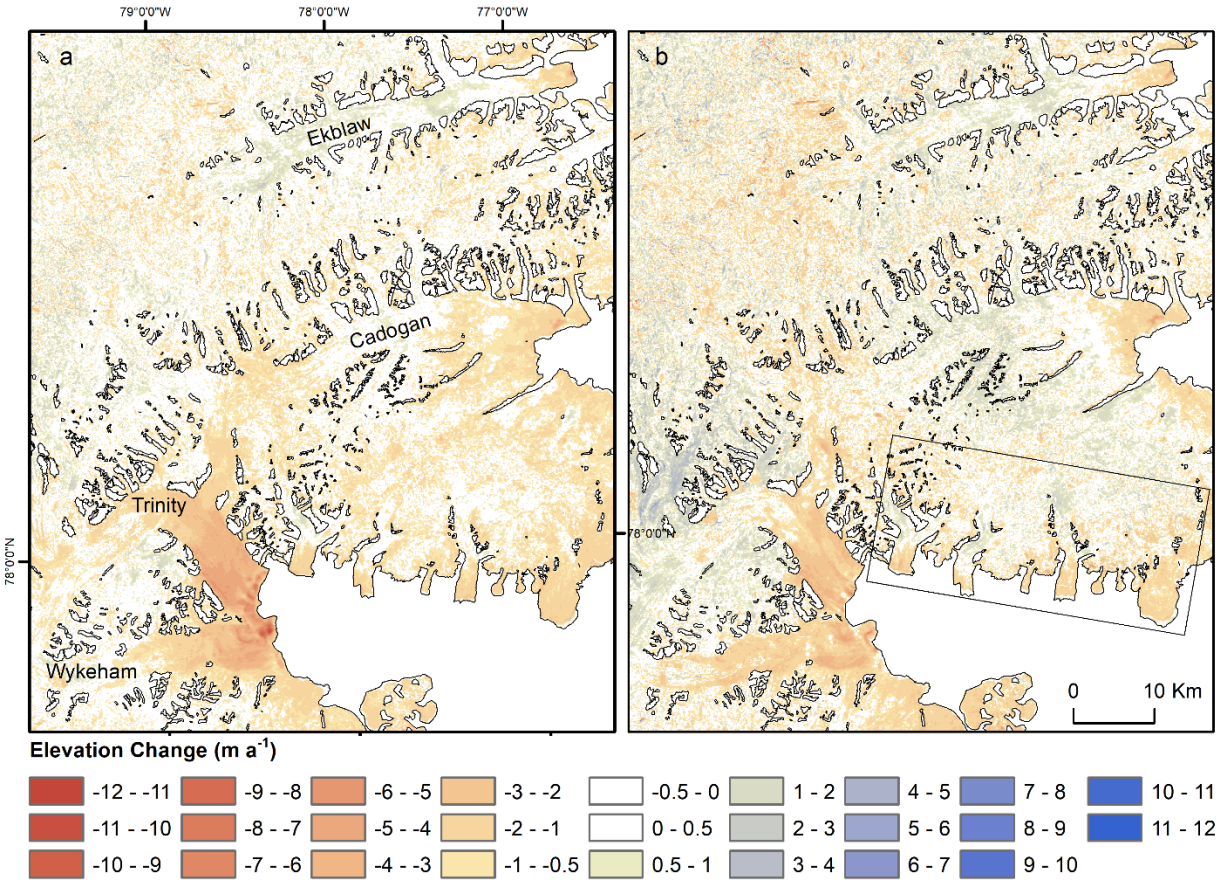

Figure 2-4: Surface elevation changes on the POW Icefield for: a) 2010-2014, and b) 2015-2019, from http://maps.theia-land.fr (Hugonnet et al., 2021). Location of glaciers used to correct dynamic thinning values for surface mass balance in Figure 12 outlined by black box in part A. Base image: Landsat-8, August 9, 2019, USGS/NASA Landsat.

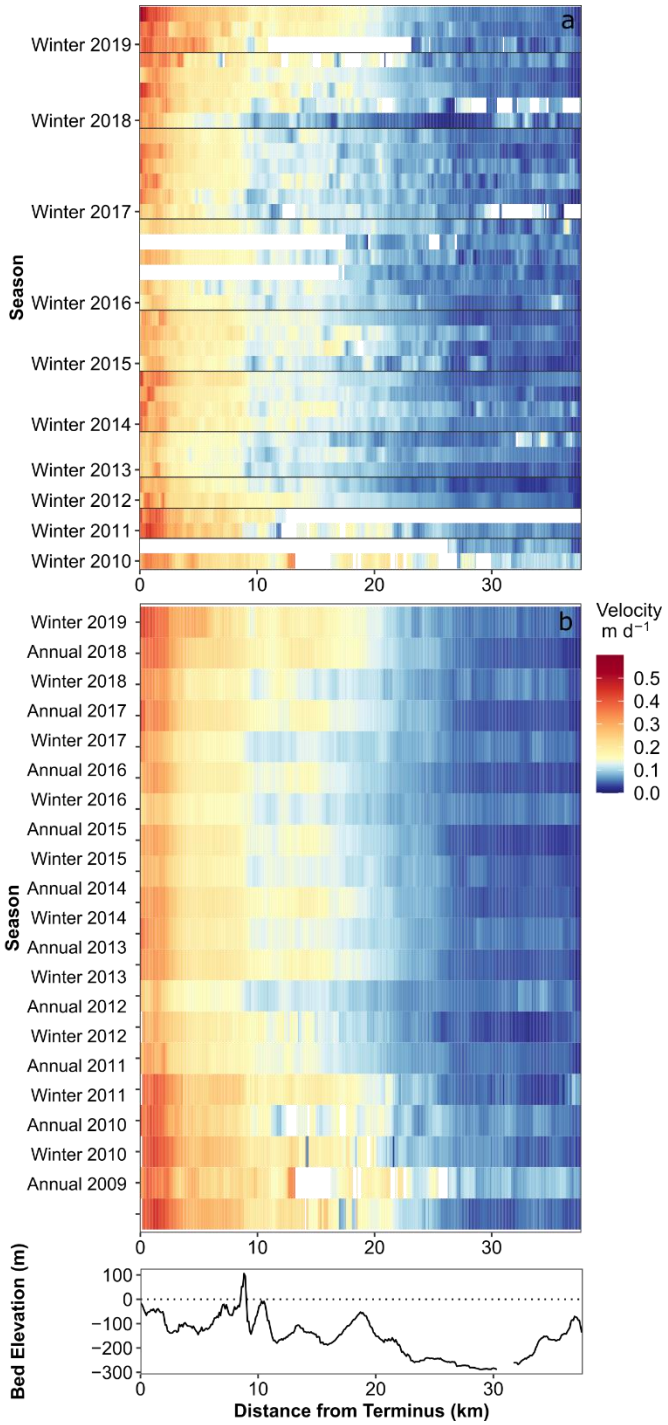

Figure 2-5: For the centreline of Cadogan Glacier: a) Radarsat-2 speckle-tracking derived winter velocities, 2009-2019, b) Comparison between average Radarsat-2 derived winter velocities and ITS_LIVE feature-tracking derived annual velocity composites, 2009-2019, c) NASA 3D tomography derived bed elevations along the glacier centreline shown in Figure 1.

2.4.2 Trinity & Wykeham Glaciers

Between 2009 and 2019, both Trinity and Wykeham glaciers underwent an overall acceleration. Beginning with Wykeham Glacier, there was a doubling of surface velocity from ~1 m d^{-1} in 2009 to ~2 m d^{-1} in 2019 in the lowermost 20 km (Figure 2-6a). In all years, the highest velocities were concentrated in the lowermost 5-10 km of the glacier, the same region which underwent some of the greatest percent increase between 2009 and 2019 (Figure 2-7). Between 2009 and 2015, there was an increase in ice motion in this region from ~1 m d^{-1} to ~1.8 m d^{-1}, followed by a brief decrease in 2017 to ~1.4 m d^{-1}, and subsequent increase to >2 m d^{-1} by 2019. Prior to 2015 we did not observe motion faster than ~0.5 m d^{-1} in the area >5 km up-glacier from the terminus. However, since 2015, there has been a clear increase in velocity in the area ~5-15 km up-glacier from the terminus, from ~0.4 m d^{-1} in 2015 to 1 m d^{-1} by 2019. The centreline velocity patterns on Wykeham Glacier are coincident with a trough in the basal topography, which reaches a maximum of >200 m below sea level (Figure 2-6c, Appendix A). Ice motion is slower (<1 m d^{-1}) where the glacier is pinned at the margins of this trough on subglacial features located at 0 km and 6 km from the terminus (Figure 2-3c). The remainder of Wykeham Glacier is grounded mainly below sea level for a distance of ~30 km up-glacier from the terminus.

Annual average velocities for Wykeham Glacier follow the same overall acceleration pattern, increasing from ~1 m d^{-1} in 2009 to ~2 m d^{-1} in 2018 (Figure 2-6b). The highest velocities were located in the lowermost ~10 km of the glacier trunk, and since 2014 there has been a clear propagation of elevated ice motion between 10 and 20 km up-glacier from the terminus. There was also a shift in variability between annual and winter velocities around the year 2014, as prior to this annual velocities were generally higher than winter velocities, whereas since winter 2015 there has been a clear increase in winter velocities which match or exceed those observed during the rest of the year. This is especially evident ~5 km from the terminus and in the regions 10-20 km up-glacier from it.

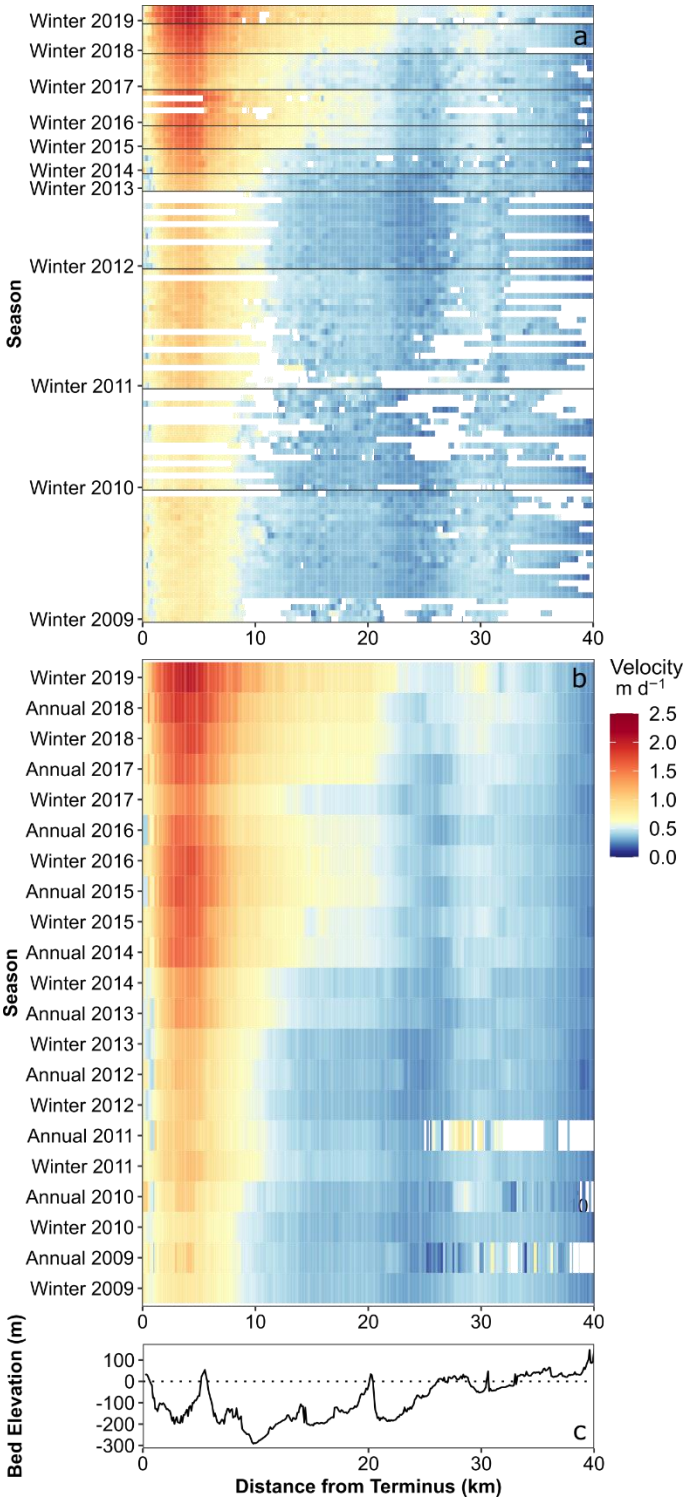

Figure 2-6: For the centreline of Wykeham Glacier: a) Radarsat-2 speckle-tracking derived winter velocities, 2009-2019, b) Comparison between average Radarsat-2 derived winter velocities and ITS_LIVE feature-tracking derived annual velocity composites, 2009-2019, c) NASA 3D tomography derived bed elevations along the glacier centreline shown in Figure 1.

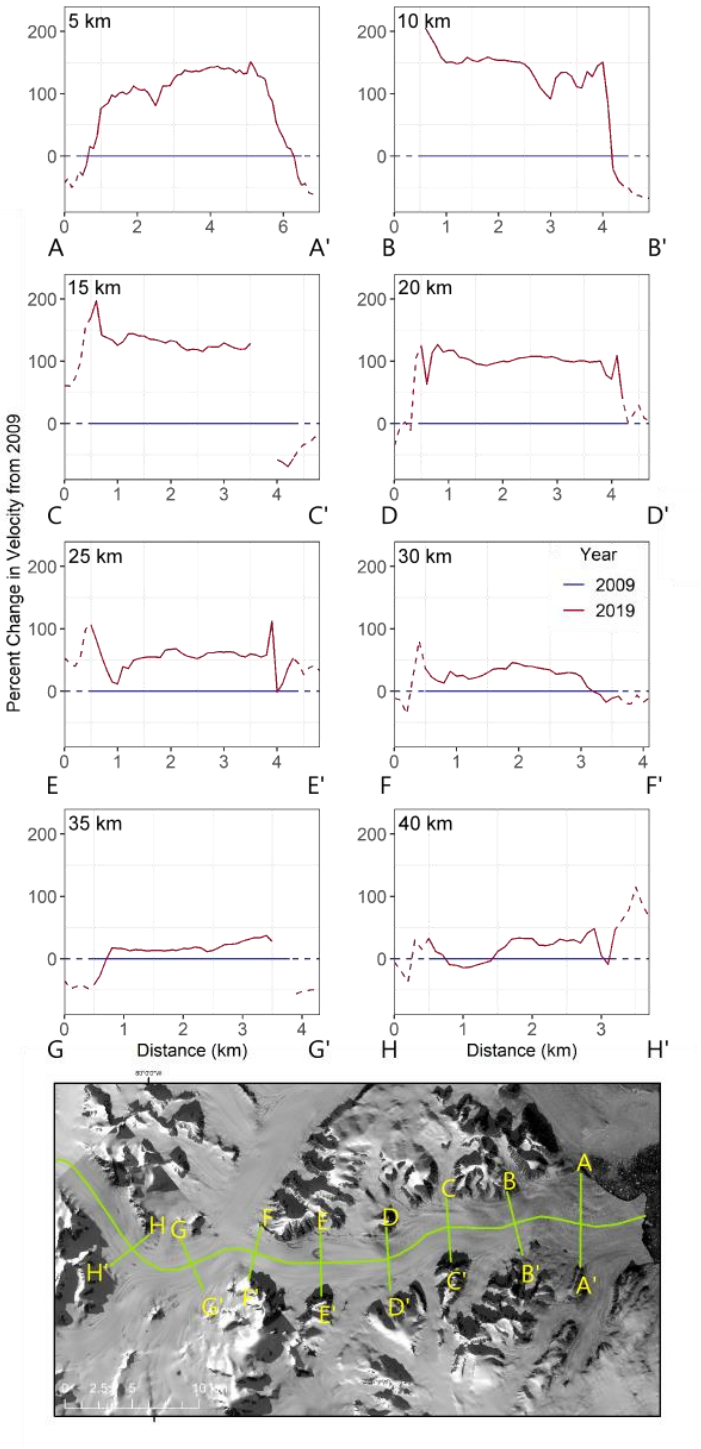

Figure 2-7: Percent change in velocity for Wykeham Glacier between 2009 and 2019 along 5 km cross sections up-glacier from the terminus (see base map at bottom for locations). Dashed lines represent an area of greater uncertainty in the velocity data resulting from a combination of bedrock and moving glacier in the matching window of the cross-correlation algorithm. Base image: Landsat-8, August 9, 2019, USGS/NASA Landsat.

Trinity Glacier shows similar velocity patterns to Wykeham Glacier during winter, with an acceleration between 2009 and 2019, from a peak of ~2 m d^{-1} in the earlier years to ~3 m d^{-1} in more recent years (Figure 2-8a). These results are consistent with those of previous studies from this region (Millan et al. 2017; Sánchez-Gámez and Navarro 2017; Harcourt et al., 2020; Van Wychen et al. 2014, 2016; 2021). Between 2009 and 2016, the highest velocities were concentrated in the lowermost ~18 km of the glacier. This region of elevated flow corresponds with a subglacial trough (previously identified in Harcourt et al. (2020)), which extends ~16 km up-glacier from the terminus at a depth of ~100-200 m below sea level (Figure 2-3c, Appendix A). The remainder of Trinity Glacier is grounded below sea level for ~40 km up-glacier from the terminus (Figure 2-8c). Since 2016, higher velocities of >1 m d^{-1} have begun propagating up-glacier into the region that lies between 18 and 30 km from the terminus, where velocities previously did not exceed ~ 0.5-0.8 m d^{-1} (Figure 2-8a). On Trinity, velocity increases of ~50% between 2009 and 2019 were observed near the terminus, but the greatest percent change was observed in the 20-30 km area where an approximate doubling of velocity occurred (Figure 2-9).

Within individual years, Trinity Glacier has also undergone seasonal variations in velocity (Figure 2-8a). For example, during winter 2012 there was a clear increase in velocity from ~2.3 m d^{-1} to ~3 m d^{-1} between January and March. Throughout the velocity dataset, we see evidence of apparent oscillations of speed-up occurring in multi-year repeating periods. For example, from 2013 to 2016, velocities consistently increased from ~2.1 m d^{-1} to ~2.8 m d^{-1} over the lower 18 km of the Trinity Glacier trunk. In 2017, velocities decreased from 2016 values, but within the same region between 2017 and 2019 ice motion once again consistently increased from ~2.4 m d^{-1} to ~3.2 m d^{-1}, suggesting the start of a second distinct period of speed-up.

When comparing average winter velocities with average annual velocities for Trinity, there are two distinct periods of ice motion in the lower ~18 km of the glacier (Figure 2-8b). From 2009 to 2013, winter velocities were consistently lower than the annual average. However, from 2014 to 2019, the discrepancy between ‘winter’ and ‘annual’ flow speeds became negligible, with Trinity flowing at approximately the same speed during winter as during the remainder of the year. By winter 2019, Trinity was flowing at about the same rate (3.2 m d^{-1}) as the annual average in 2009. Since ~2017, higher velocities are occurring year-round in the region 18-25 km up-glacier from the terminus, and are no longer limited to just the lowermost glacier trunk (Figure 2-8b).

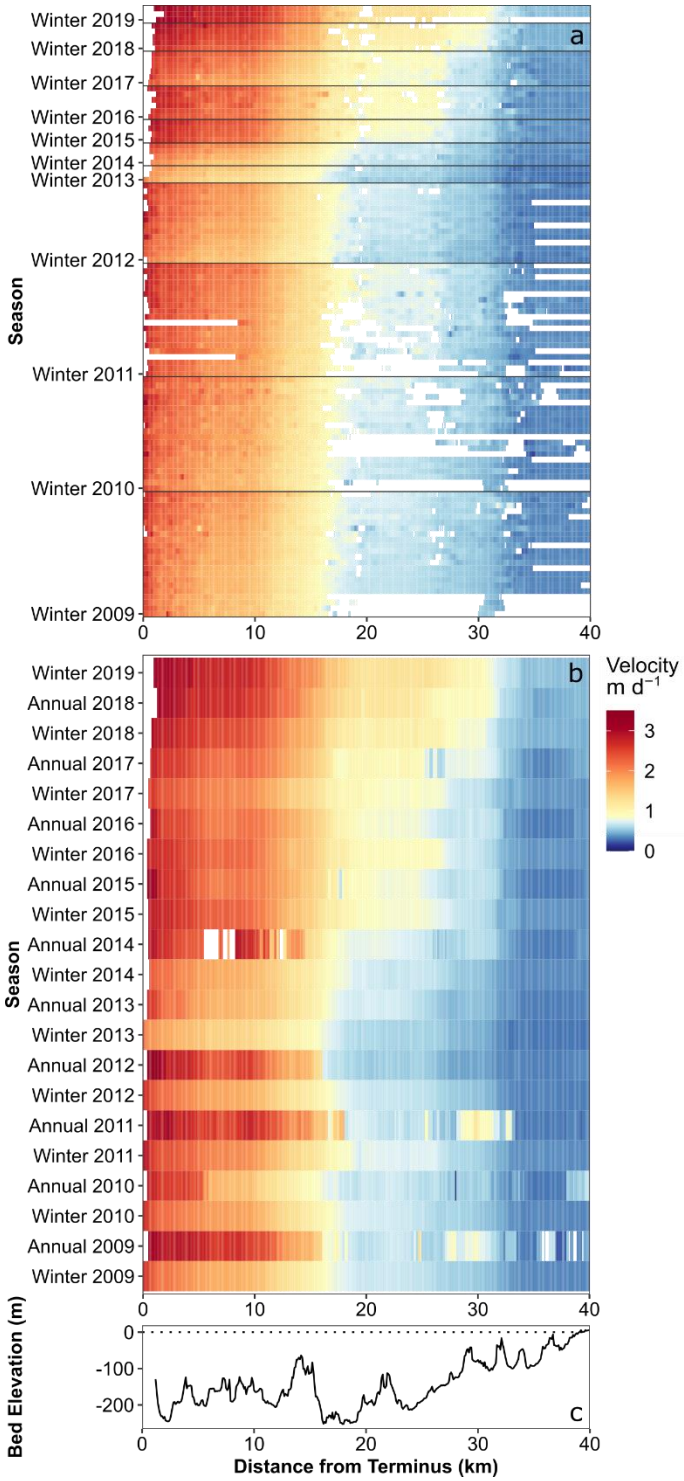

Figure 2-8: For the centreline of Trinity Glacier: a) Radarsat-2 speckle-tracking derived winter velocities, 2009-2019, b) Comparison between average Radarsat-2 derived winter velocities and ITS_LIVE feature-tracking derived annual velocity composites, 2009-2019, c) NASA 3D tomography derived bed elevations along the glacier centreline shown in Figure 1.

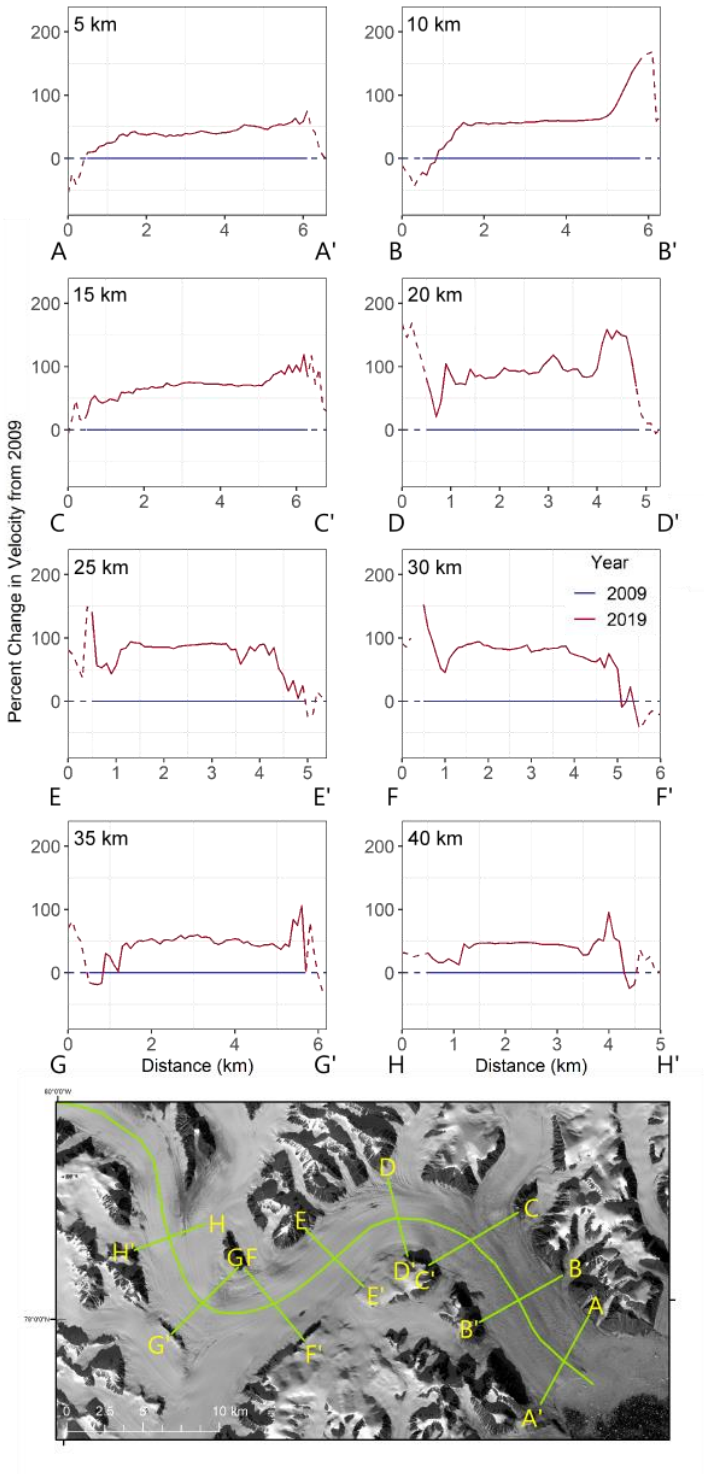

Figure 2-9: Percent change in velocity for Trinity Glacier between 2009 and 2019 along 5 km cross sections up-glacier from the terminus (see base map at bottom for locations). Dashed lines represent an area of greater uncertainty in the velocity data resulting from a combination of bedrock and moving glacier in the matching window of the cross-correlation algorithm. Base image: Landsat-8, August 9, 2019, USGS/NASA Landsat.

To determine whether there were connections between changes in velocity and surface elevation, we used our CryoSat-2 data (Figure 2-10) and ASTER DEM results from Hugonnet et al. (2021) (Figure 2-4) to identify surface elevation change for Trinity and Wykeham glaciers since 2010. On both glaciers, the greatest changes in surface height were observed in the near-terminus area, coincident with observations of elevated velocities. On average between 2010 and 2014, Wykeham thinned at a rate of 3-4 m a^{-1} in the lowermost ~8 km of the glacier trunk (Figure 2-4a). For the period 2015-2019 average thinning rates near the terminus of Wykeham decreased slightly to ~3 m a^{-1} (Figure 2-4b), while elevated thinning rates continued to extend 10-20 km up-glacier from the terminus (Hugonnet et al., 2021). Rate of elevation decrease in the area 0-300 m a.s.l. slows starting in 2016 (Figure 2-10b). Overall, between 2010 and 2020, there was ~23 m loss in surface height on Wykeham Glacier near the terminus (0-300 m a.s.l.) (Figure 2-10b).

For Trinity, the majority of the lowermost 10 km of the glacier thinned at a rate of 3-5.5 m a^{-1} between 2010 and 2014 (Figure 2-4a). During this time period, thinning rates exceeding 1 m a^{-1} were observed over a distance of nearly 40 km up-glacier from the terminus. Between 2015 and 2019, thinning rates decreased over the lower 10 km of the glacier, averaging ~3 m a^{-1}, with the exception of the glacier front which continued to thin at a rate of 4-6 m a^{-1} (Figure 2-4b). In the region 15-25 km up-glacier from the terminus of Trinity Glacier, thinning rates decreased overall. There was a total of ~25 m loss in surface height for Trinity Glacier near the terminus (0-300 m a.s.l.) between 2010 and 2020 , with a clear decrease in rate of height change beginning in 2016 (Figure 2-10a).

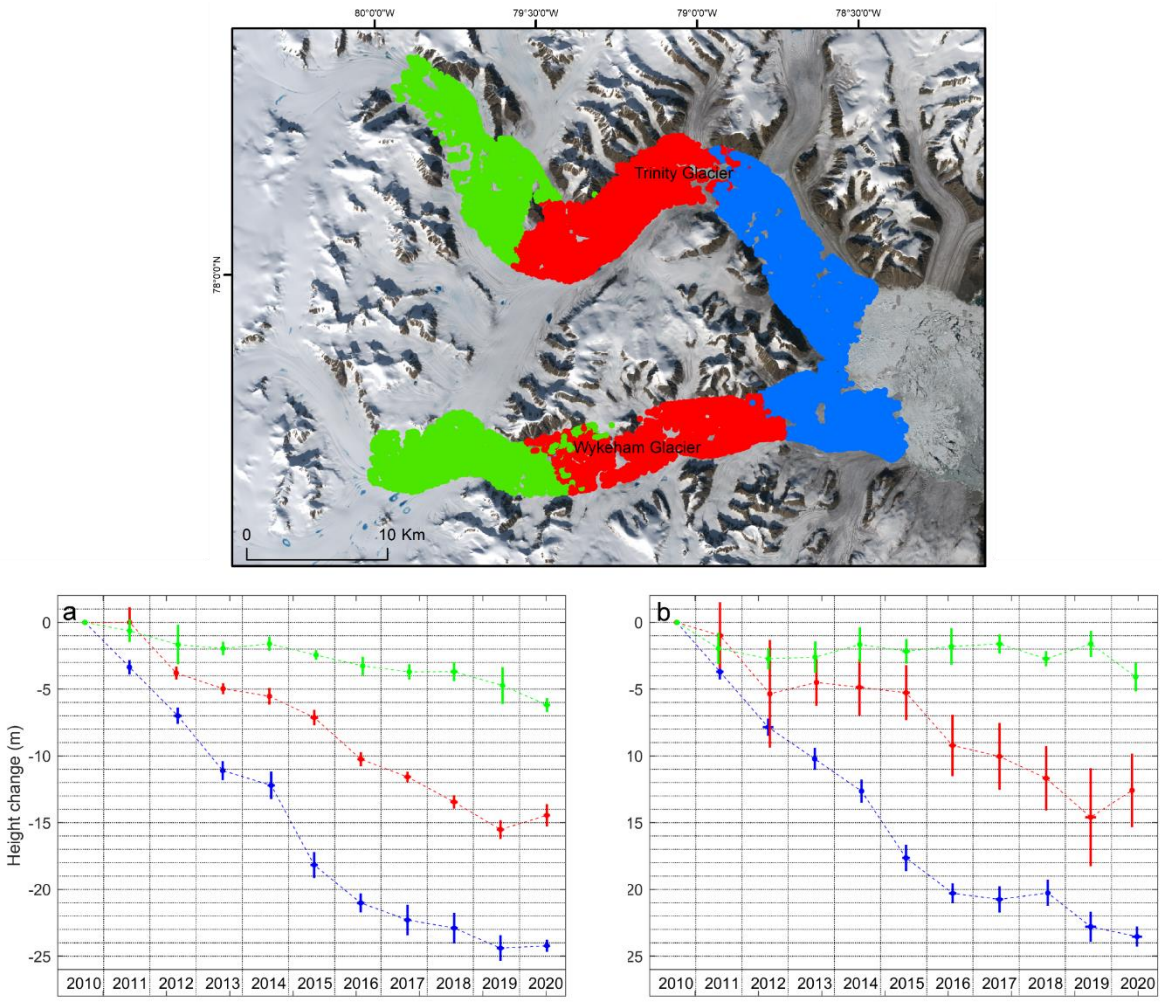

Figure 2-10: Cryosat-2 derived surface elevation changes between 2010 and 2020 for: a) Trinity Glacier, and b) Wykeham Glacier. The elevation bands are 0-300 m (blue points), 300-550 m red points), and 550-800 m (green points) above the WGS84 Ellipsoid. The vertical lines at each point represents plus and minus two times the standard error of the mean. Base image: Landsat-8, August 9, 2019, USGS/NASA Landsat.

To investigate whether the termini of Trinity and Wykeham glaciers have reached flotation, and the potential impact of this on retreat, acceleration, and thinning, we use ArcticDEM surface elevations and NASA 3D tomography bed elevation data to calculate how near to flotation the terminus of each glacier is, and how this has changed through time (Figure 2-11). In 2012, the lowermost ~2 km of Trinity Glacier was within 10 m of flotation which propagated to ~3 km up-glacier by 2017, with the exception of a pinning point located in the centre of the terminus. Trinity Glacier thinned by 20-25 m on this pinning point (Figure 2-3c) between 2012 and 2017, the area of which decreased by about half during this period. The ice underlain by an additional area of elevated basal topography located directly behind the current pinning point has also decreased in area but, as of 2017, had not yet reached flotation. A similar pattern is visible on Wykeham Glacier, where in 2012, the lowermost 2 km of the trunk was within 10 m of flotation, with the exception of a pinning point at the terminus. This pinning point decreased in area by approximately half and the ice above it thinned by ~25-30 m between 2012 and 2017. By 2017, the area of Wykeham Glacier within 10 m of flotation had propagated to ~3 km up-glacier from the terminus. Given the continuation of thinning in low elevation areas for Trinity and Wykeham beyond 2017 (Figure 2-10), it is likely that portions of each termini have since reached flotation.

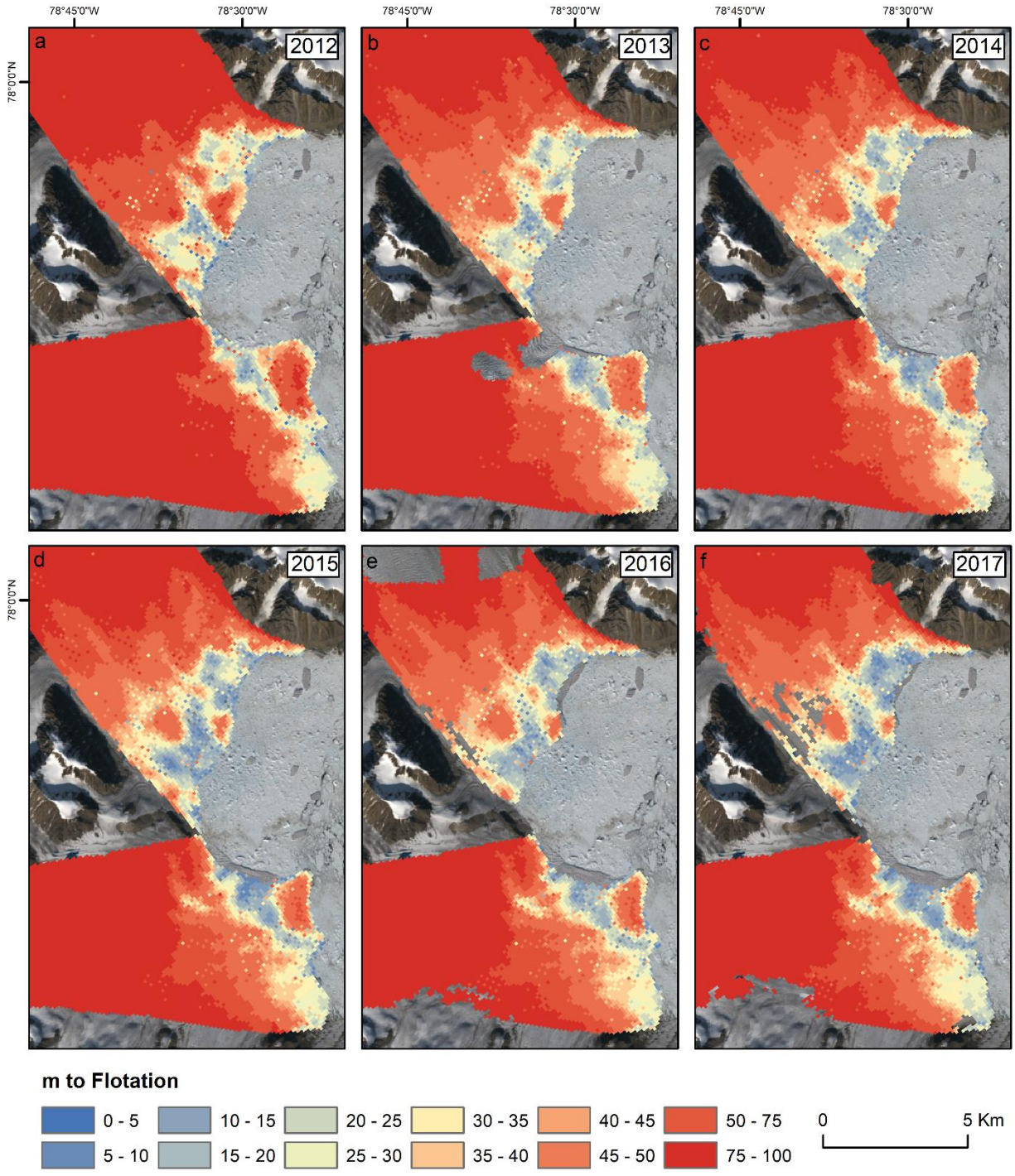

Figure 2-11: Thickness of ice in excess of flotation for the terminus regions of Trinity and Wykeham glaciers, 2012-2017. Derived using measured ice thickness and density of water and ice (see Equation 1). Base image: Landsat-8, August 9, 2019, USGS/NASA Landsat.

2.5 Discussion

Glaciers of the QEI have been previously classified by flow type (Copland et al., 2003; Burgess et al., 2005; Medrzycka et al., 2019; Van Wychen et al. 2016, 2017; 2021) into four main categories:

(a) 'Normal' tidewater glaciers in the QEI are generally slow flowing (30-90 m a^{-1}) in their main trunk near the equilibrium line, before increasing to ~300 m a^{-1} near the terminus (Van Wychen et al. 2014; 2020). For 'normal' land-terminating glaciers in the QEI, main trunk velocities range between 20-50 m a^{-1} and do not generally exceed 75 m a^{-1} at the terminus (Van Wychen et al,, 2020). While these glaciers can undergo seasonal velocity variability, there are not typically large velocity variations over longer time periods (Van Wychen et al., 2014).

(b) Surge-type glaciers are characterized by periods of irregular flow which cycle between a long quiescent phase of decreased velocities (which can last for decades or longer), and a surge phase involving a rapid increase in velocity over most of the glacier length (which can last for up to a decade or longer) (Raymond et al., 1987). In the QEI, at least 51 surge-type glaciers were identified by Copland et al. (2003) and Van Wychen et al. (2014) through changes including heavy crevassing, rapid increases in velocity, looped medial moraines, and rapid terminus advance.

(c) Pulse-type glaciers were first identified in the QEI by Van Wychen et al. (2016) and are characterized by periods of multi-year velocity variability on tidewater glaciers, where the highest velocities occur near the terminus and are restricted to regions of the glacier that are grounded well below sea level.

(d) Consistent acceleration refers to glaciers which have undergone a long-term increase in velocity which appears to be unrelated to surging or pulsing and is thought to be driven by external climatic factors (Van Wychen et al., 2016; 2021). Only two glaciers in the QEI, Trinity and Wykeham have been observed to consistently accelerate while also retreating over the last two decades, although there is an indication that Belcher and Sydkap glaciers have undergone speed-ups in the last decade that could be attributed to consistent acceleration (Van Wychen et al., 2016, 2020; Millan et al., 2017; Harcourt et al., 2020).

Based on these definitions, the four glaciers in this study share behaviour with two previously-identified flow types: pulse-type and consistent acceleration. These are discussed further below.

2.5.1 Cadogan & Ekblaw Glaciers

Between 2009 and 2019, we observed flow patterns on both Cadogan and Ekblaw which were consistent with the characteristics of 'pulse-type' glaciers (Van Wychen et al., 2016). Their flow consisted of a deceleration from about 2013 to 2016, followed by an acceleration from 2017-2019.

On Ekblaw Glacier, the highest velocities were concentrated at the glacier front and propagated up-glacier (Figure 2-2a). Ekblaw velocities were higher overall compared to Cadogan and were concentrated in the lowermost ~1-2 km of the glacier, which coincides with the location of a deep trough that reaches up to ~350 m below sea level for the lowermost ~6 km of the glacier, and then gradually slopes upwards towards sea level over the next ~35 km (Figures 2-2c, 2-3a). Consistent with Van Wychen et al (2016), velocity variability on Ekblaw coincides with the portion grounded below sea level, initiating in the terminus region and propagating up-glacier during periods of faster flow (e.g. 2017-2019), and remains largely confined to the terminus during periods of slower flow (e.g. 2014-2017).

Seasonally, Ekblaw Glacier appears to flow slower in the winter compared to the rest of the year in the area 2-40 km up-glacier from the terminus, suggesting that seasonal changes in basal hydrology connected to the input of surface meltwater to the bed are likely important controls on dynamics in this system (Burgess et al., 2005; Cuffey & Paterson, 2010). However, the lack of accurate ITS_LIVE data in the near-terminus area for Ekblaw Glacier makes it difficult to consistently identify this pattern (Figure 2-2b). The near terminus area of Ekblaw where the highest velocities were observed is also where the greatest surface thinning occurred between 2010 and 2019 (Figure 2-4; Hugonnet et al., 2021). Near ~40 km up-glacier, changes in flow speed on Ekblaw are negligible, but as the ice flows down a gradual bed slope towards the terminus, velocities increase (Appendix A). This is likely the result of a transition from ice frozen at the bed to warmer basal conditions where the presence of subglacial water can contribute to basal sliding and lead to extensional flow and thinning of the ice near the terminus (Burgess et al., 2005; Cuffey & Paterson, 2010). The lack of sills and underlying bedrock pinning points beneath the glacier trunk (Figure 2-3a) results in the highest velocities at the terminus of Ekblaw.

Cadogan Glacier was not previously classified as 'pulse-type' by Van Wychen et al. (2016), but the behaviour observed in this study is consistent with pulse-type glaciers. For Cadogan, there is more variability in basal topography than at Ekblaw, including a subglacial ridge located ~9 km up-glacier from the terminus which reaches ~100 m.a.s.l. (Figure 2-3b, 2-5c), although it does not appear as a nunatak visible on the surface. Ice at this location appears heavily crevassed in Landsat-8 imagery (from August 9, 2019) as the glacier flows over the ridge and into a trough which extends to ~150 m below sea level. The fastest velocities observed between 2009 and 2019 were located down-glacier of this ridge in a subglacial trough in the lowermost 9 km of the trunk, which suggests that basal topography is an important control on glacier dynamics in this region (Figure 2-3b, 2-5c). Cadogan Glacier showed relatively stable velocities throughout the winter, which were consistently lower than average annual velocities, again suggesting that seasonal changes in glacier hydrology are important in the dynamics of this glacier (Figure 2-5b).

Temporally, Cadogan and Ekblaw glaciers exhibit similar flow patterns of multiyear variability. Spatially, Cadogan Glacier flows similarly to Dobbin and Parrish glaciers located on Agassiz Ice Cap to the north, and previously identified as 'pulse-type' (Van Wychen et al., 2016); present at all three glaciers are subglacial sills located in the lower part of the trunk which inhibit flow up-glacier of their location. As ice flows over the sill, high basal pressures would be created as ice thickens locally up-glacier. This likely leads to enhanced basal meltwater production, which can flow over the ridge and induce faster flow on the down-glacier side of the sill and therefore extensional flow and surface thinning as the glacier accelerates (Cuffey & Patterson, 2010; Van Wychen et al., 2016; Harcourt et al., 2020).

2.5.2 Trinity & Wykeham Glaciers

Over the period 2009-2019 we observed a near constant acceleration of both Trinity and Wykeham glaciers, consistent with the findings of previous studies (Millan et al., 2017; Harcourt et al., 2020; Van Wychen et al., 2016, 2021). Our study builds upon this existing work by providing an in-depth analysis of seasonal and inter-annual velocity changes for Trinity and Wykeham Glaciers over the last decade.

On Wykeham Glacier, there was an overall doubling in winter velocities from ~1 m d^{-1} to ~2 m d^{-1} in the lowermost 5 km of the glacier between 2009 and 2019 (Figure 2-6a, 2-7) with the greatest velocity changes occurring down-glacier of a subglacial ridge located ~8 km from the terminus

(Figure 2-3c, 2-6c). Velocities on Wykeham were consistently lower than Trinity throughout the study period, likely as a result of a series of subglacial ridges which are oriented perpendicular to flow and hinder ice motion near the terminus (Figure 2-3c; Harcourt et al., 2020). Seasonally, there was a shift in flow type in 2014 for Wykeham Glacier. Our results, and those of Van Wychen et al. (2021), show that after 2014, higher velocities on Wykeham began to propagate ~25 km up-glacier from the terminus, with little difference between winter and annual flow rates. Prior to 2014, Wykeham consistently flowed slower during winter than during the remainder of the year (including summer).

For Trinity Glacier, the highest velocities were observed over the lowermost ~10 km of the terminus (Figure 2-8a), where ice in the lower trunk accelerates as it is channelled into two deep subglacial troughs near the terminus (Harcourt et al., 2020; Figure 2-3c). Trinity Glacier also underwent a shift in flow type after 2014 to a period when winter flow rates were nearly identical to those observed throughout the rest of the year. This shift also coincides with the propagation of higher velocities to a distance of 15-30 km up-glacier from the terminus on Trinity (Figure 2-8a), and an approximate doubling in speed in a region where elevated flow rates were not previously observed. This indicates that seasonality of flow has become less apparent in recent years and Trinity and Wykeham glaciers may now experience basal sliding throughout the year, with larger portions of the trunk engaged in increased motion. Further research that links climatic changes to rates of basal sliding should be investigated in future studies.

Between 2010 and 2020, Trinity Glacier thinned at an average rate of ~2.2 m a^{-1} over the elevation range 0-300 m a.s.l. (Figure 2-10a), while Wykeham Glacier thinned by ~2.1 m a^{-1} (Figure 2-10b), although local rates were much higher than this, particularly near the terminus (Figure 2-4). There is also a clear decrease in thinning rate for both glaciers after 2014 (Figure 4b; Figure 10a, b). To quantify the relative importance of surface melt in accounting for these changes, we computed ASTER DEM derived elevation changes from Hugonnet et al. (2021) for four glaciers located on the northern coast of Talbot Inlet (Figure 2-4a) which have not exhibited significant velocity variability since 2009 (Van Wychen et al., 2016; Van Wychen et al., 2021). We calculated average thinning rates for areas ≤ 300 m a.s.l. on these four glaciers of 0.91 m a^{-1} for 2010-2014 and 0.66 m a^{-1} for 2015-2019 to use as a proxy for surface melt. This is consistent with the findings of Noël (2017), who used 1 km downscaled regional climate model RACMO2.3 data to determine that on

average, surface mass balance (SMB) accounted for ~1 m a^{-1} of elevation loss between 1996 and 2015 for the areas of Trinity and Wykeham ≤ 300 m a.s.l.

When the surface mass balance losses computed from the Hugonnet et al. (2021) data are subtracted from the total thinning rates on Trinity and Wykeham glaciers over the same elevation range, we assume that the remaining elevation changes are primarily driven by changes in ice motion (i.e., dynamic thinning; Figure 2-12). Between 2010 and 2014, the lowermost 10 km of both glaciers underwent dynamic thinning between 1.5-4 m a^{-1}, before decreasing over 2015-2019 to 0-2 m a^{-1}. For both glaciers, the greatest rates of dynamic thinning were observed near the terminus. On Trinity Glacier, portions of the terminus underwent dynamic thinning at a rate of ~7 m a^{-1} for 2010-2014 and ~5.5 m a^{-1} for 2015-2019 (Figure 2-12). A similar trend was observed for Wykeham Glacier, with maximum thinning rates of ~10.5 m a^{-1} in the earlier time period and ~6 m a^{-1} in the later time period. Observed rates of thinning are therefore far beyond those which can be attributed to surface mass balance.

Given this combination of terminus acceleration, retreat (Van Wychen et al., 2016; Dalton et al., 2019), and rapid thinning, we suggest that Trinity and Wykeham glaciers have transitioned from a seasonal flow type to one dominated by dynamic thinning. These observations are similar to those on Columbia Glacier between the 1970s and 1990, when there was a dramatic collapse of the glacier front (Van der Veen, 1996; 2002). Columbia Glacier accelerated at the terminus, thinned, and retreated from its terminal moraine, which increased terminus buoyancy and reduced effective pressure at the bed, allowing the glacier to flow faster and for increased velocities to propagate up-glacier (Van der Veen, 1996; Benn et al., 2007; Cuffey & Paterson, 2010). At Columbia Glacier, ice front thickness is closely linked with calving and ice flow, with calving rates increasing when the terminus front thins to within ~50 m of flotation (Meier & Post, 1987; Van der Veen, 1996; 2002, Cuffey & Paterson, 2010).

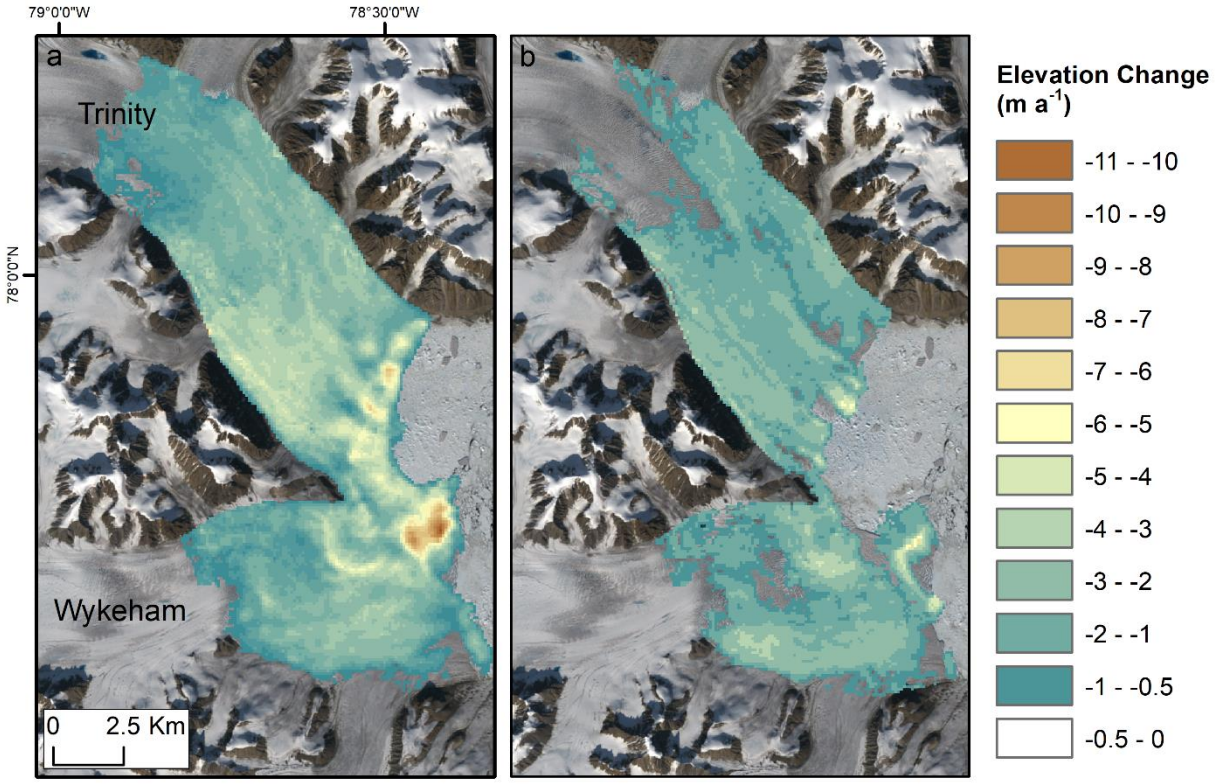

Figure 2-12: Surface elevation changes as a result of dynamic thinning (i.e., after mean regional surface mass balance has been subtracted) on Trinity and Wykeham glaciers for: a) 2010-2014, and b) 2015-2019. Base image: Landsat-8, August 9, 2019

It therefore seems likely that high rates of thinning, trunk geometry, and associated increases in buoyancy at the terminus have allowed Trinity and Wykeham glaciers to accelerate in recent years. Trinity and Wykeham both underwent significant thinning between 2010 and 2015 (Figure 2-4a, 2-10), coincident with apparent instability of terminus position and velocity, and a transition between seasonal and dynamic flow. Helheim Glacier on SE Greenland has also undergone periods of stable and unstable flow related to climatic changes and basal topography, most recently in 2003-2005, which coincided with significant acceleration, retreat, and dynamic thinning in the near-terminus region (Howat et al., 2005, 2008; Stearns & Hamilton, 2007; Joughin et al., 2008; Bevan et al., 2012). Similar to our findings for Trinity and Wykeham glaciers, Williams et al. (2021) identified a shift in dynamics (i.e. terminus velocity and retreat) on Helheim between 2014 and 2019, again coinciding with acceleration and retreat in the near terminus area, a region which is currently near (within 50 m) flotation. It is expected that continued mass loss, thinning, and retreat down the retrograde slope located in the lowermost 5 km of the terminus of Helheim will result in dramatic retreat.

Consistent with the findings of Harcourt et al. (2020) and Van Wychen et al. (2016; 2021) and similar to observations at Helheim Glacier (Williams et al., 2021), we suggest that beginning in 2014, Trinity and Wykeham glaciers have transitioned to a flow type of dynamic thinning which is strongly influenced by subglacial topography. In contrast to previous studies from this region (Millan et al., 2017, Harcourt et al., 2020; Van Wychen et al., 2016; 2021), we find that Trinity and Wykeham, while having undergone an overall increase in velocity since 2009, have not accelerated consistently as previously suggested, and are likely strongly influenced by subglacial topography which result in multi-year repeating periods of acceleration.

While Trinity and Wykeham glaciers are both currently grounded on basal pinning points, if thinning continues at the current rate, it is likely that a destabilization of their termini will occur, resulting in further acceleration in velocity and retreat in terminus position similar to that expected and previously observed at Helheim Glacier. Glaciers with deep basal topography and/or with wide trunks are likely closer to flotation near the terminus, and therefore require less thinning to initiate retreat and acceleration following a perturbation (Enderlin et al., 2013; Catania et al., 2018). The terminus at Wykeham glacier is currently ~9 km wide and narrows up-glacier. Destabilisation from the current pinning point at the terminus will likely result in retreat and acceleration in the

lowermost 5 km of the trunk which is underlain by a steep retrograde slope (Appendix A). However, while Wykeham is grounded below sea level behind the current pinning point, its narrowing trunk and a ridge oriented perpendicular to ice flow approximately 5 km up-glacier and extends above sea level may act to stabilize the terminus in the event of a rapid retreat.

Trinity Glacier is ~6 km wide at the terminus and trunk width remains relatively uniform for ~40 km up-glacier. Basal topography deepens behind the current pinning point at the terminus of Trinity and remains grounded approximately 150 m below sea level for up to 15 km up-glacier, increasing the potential for instability resulting from rapid retreat and acceleration (Appendix A). Glacier geometry and basal topography of Trinity and Wykeham glaciers are relevant as they point to the importance of the reorganization of basal and lateral pinning-points as the glacier thins, which act as critical controls on the future evolution of the flow. As such, these features may provide periodic buffers to the rapid acceleration and retreat of these glaciers in the future.

2.6 Conclusion

In this study, a dense temporal record of winter surface motion combined with annual velocity composites, ice thickness, and bed elevation data, offers insight into the process controlling glacier flow and ice discharge from the POW Icefield. Based on our observations, we identify Ekblaw Glacier as consistent with a "pulse-type" flow regime, first identified by Van Wychen et al. (2016). Glaciers of this type are characterized by variable velocity confined to the portion of the glacier grounded below sea level. Based on these criteria, our study expands the identification of pulse-type glaciers to include Cadogan Glacier. Both Cadogan and Ekblaw glaciers were observed to have slower velocities during winter, suggesting that seasonal changes in basal hydrology resulting from surface mass balance are the primary control on dynamics in these systems. This classification allows us to further understand the dynamics of Canadian Arctic glaciers and how their flow types and discharge may evolve in a warming climate.

Consistent with the results of previous studies (Millan et al., 2017, Harcourt et al., 2020; Van Wychen et al., 2016; 2021), we find that Trinity and Wykeham glaciers have undergone an overall increase in velocity since 2009. However, the acceleration of both glaciers was temporally variable, characterized by multi-year repeating periods of acceleration which are likely controlled

by subglacial topography (e.g., pinning points) and changes in surface meltwater input to the bed. Evidence of sustained thinning and near-flotation of the termini of both glaciers, in combination with this velocity increase, leads us to believe that Trinity and Wykeham glaciers are responding to external forcing by switching between seasonal flow and flow dominated by dynamic thinning. Both glaciers are grounded below sea level for a distance of 30-40 km up-glacier from their termini, and patterns of thinning, increased buoyancy, and acceleration are similar to those observed during the collapse of Columbia Glacier, Alaska (Van der Veen 1996; 2002; Cuffey & Paterson, 2010) and more recently at Helheim Glacier, Greenland (Williams et al., 2021). Based on our observations, we expect thinning, retreat, and acceleration of Trinity and Wykeham to continue in multi-year repeating periods, controlled by subglacial topography.

More investigation is needed to improve our understanding of the role that bed topography plays in controlling ice motion in this region. These results will be useful for continuing in-depth studies on the processes controlling Arctic glacier dynamics and the links between glacier motion and basal hydrology. Our dense record of winter velocities for the POW Icefield will be useful for modelling hydrology and dynamics to better understand the processes controlling ice flow. Future work should also focus on the impact of external forcing (e.g. ocean temperature and fiord geometry) on these glacier flow types, and identify the impact of increased glacier motion and ice discharge on Baffin Bay. As such, continued monitoring of these glaciers will be essential for developing an in-depth dataset to further investigate the dynamic processes of Canadian Arctic glaciers.

Data Availability

Radarsat-2 SAR imagery for speckle-tracking was acquired through partnerships with Natural Resources Canada (NRCan) and Environment, and Climate Change Canada (ECCC). Radarsat-2 imagery was processed using a MATLAB algorithm developed for speckle-tracking (Short & Gray, 2005; Van Wychen et al., 2012). Landsat-8 and Sentinel-2B satellite imagery was accessed through the Earth Explorer Data portal (https://earthexplorer.usgs.gov/). We downloaded annual CryoSat-2 baseline-D intermediate level 1b (L1b) SARIn altimetry data from the ESA ftp site (ftp://science-pds.cryosat.esa.int/). Cryosat-2 data was processed using MATLAB (Gray et al., 2015; 2021). Annual ITS_LIVE velocity composites were downloaded from the NASA ITS_LIVE portal (https://its-live.jpl.nasa.gov/). ArcticDEM MOSAIC and Strip Map products were accessed through the Polar Geospatial Center (https://www.pgc.umn.edu/data/arcticdem/). Bed topography data were created using airborne radar measurements from the Centre for Remote Sensing of Ice Sheet (CReSIS) Multichannel Coherent Data Depth Sounder (MCoRDS) which was downloaded from the University of Kansas (https://data.cresis.ku.edu/). Surface elevation change data produced by Hugonnet et al. (2021) is accessible at the Theia web portal (http://maps.theia-land.fr; https://doi.org/10.6096/13).

References

Benn, D. I., Warren, C. R., & Mottram, R. H. (2007). Calving processes and the dynamics of calving glaciers. *Earth-Science Reviews*, *82*(3–4), 143–179. https://doi.org/10.1016/j.earscirev.2007.02.002

Bevan, S. L., Luckman, A. J., & Murray, T. (2012). Glacier dynamics over the last quarter of a century at Helheim, Kangerdlugssuaq and 14 other major Greenland outlet glaciers. *The Cryosphere*, *6*(5), 923–937. https://doi.org/10.5194/tc-6-923-2012

Burgess, D. O., Sharp, M. J., Mair, D. W. F., Dowdeswell, J. A., & Benham, T. J. (2005). Flow dynamics and iceberg calving rates of Devon Ice Cap, Nunavut, Canada. *Journal of Glaciology*, *51*(173), 219–230. https://doi.org/10.3189/172756505781829430

Burgess, E. W., Larsen, C. F., & Forster, R. R. (2013). Summer melt regulates winter glacier flow speeds throughout Alaska. *Geophysical Research Letters*, *40*(23), 6160–6164. https://doi.org/10.1002/2013GL058228

Carr, J. R., Stokes, C. R., & Vieli, A. (2013). Recent progress in understanding marine-terminating Arctic outlet glacier response to climatic and oceanic forcing: Twenty years of rapid change. *Progress in Physical Geography: Earth and Environment*, *37*(4), 436–467. https://doi.org/10.1177/0309133313483163

Catania, G. A., Stearns, L. A., Sutherland, D. A., Fried, M. J., Bartholomaus, T. C., Morlighem, M., Shroyer, E., & Nash, J. (2018). Geometric Controls on Tidewater Glacier Retreat in Central Western Greenland. *Journal of Geophysical Research: Earth Surface*, *123*(8), 2024–2038. https://doi.org/10.1029/2017JF004499

Cogley, J. G., Hock, R., Rasmussen, L. A., Arendt, A. A., Bauder, A., Braithwaite, R. J., Jansson, P., Kaser, G., Möller, M., Nicholson, L., & Zemp, M. (2011). Glossary of glacier mass balance and related terms. https://doi.org/10.5167/UZH-53475

Consortium, R. G. I. (2017). Randolph Glacier Inventory 6.0 [Data set]. NSIDC. https://doi.org/10.7265/N5-RGI-60

Cook, A. J., Copland, L., Noël, B. P. Y., Stokes, C. R., Bentley, M. J., Sharp, M. J., Bingham, R. G., & van den Broeke, M. R. (2019). Atmospheric forcing of rapid marine-terminating glacier retreat in the Canadian Arctic Archipelago. *Science Advances*, *5*(3), eaau8507. https://doi.org/10.1126/sciadv.aau8507

Copland, L., Sharp, M. J., & Dowdeswell, J. A. (2003). The distribution and flow characteristics of surge-type glaciers in the Canadian High Arctic. *Annals of Glaciology*, *36*, 73–81. https://doi.org/10.3189/172756403781816301

CReSIS (2016) Multichannel Coherent Depth Sounder (MCoRDS) L3 Gridded Data. Digital Media http://data.cresis.ku.edu/

Cuffey, K., & Paterson, W. S. B. (2010). The Physics of Glaciers (4th ed). Butterworth-Heinemann/Elsevier.

Dalton, A., Copland, L., Tivy, A., Van Wychen, W., & Cook, A. (2019). Iceberg production and characteristics around the Prince of Wales Icefield, Ellesmere Island, 1997-2015. *Arctic, Antarctic, and Alpine Research, 51*(1), 412–427. https://doi.org/10.1080/15230430.2019.1634442

Danielson, B., & Sharp, M. (2013). Development and application of a time-lapse photograph analysis method to investigate the link between tidewater glacier flow variations and supraglacial lake drainage events. *Journal of Glaciology, 59*(214), 287–302. https://doi.org/10.3189/2013JoG12J108

Dee, D. and National Center for Atmospheric Research Staff (Eds). Last modified 09 Oct 2021. "The Climate Data Guide: ERA5 atmospheric reanalysis." Retrieved from https://climatedataguide.ucar.edu/climate-data/era5-atmospheric-reanalysis.

Enderlin, E. M., Howat, I. M., & Vieli, A. (2013). High sensitivity of tidewater outlet glacier dynamics to shape. The Cryosphere, 7(3), 1007–1015. https://doi.org/10.5194/tc-7-1007-2013

Gardner, A. S., Moholdt, G., Scambos, T., Fahnstock, M., Ligtenberg, S., van den Broeke, M., & Nilsson, J. (2018). Increased West Antarctic and unchanged East Antarctic ice discharge over the last 7 years. *The Cryosphere*, *12*(2), 521–547. https://doi.org/10.5194/tc-12-521-2018

Gardner, A., Fahnestock, M., & Scambos, T. (2019). MEASURES ITS_LIVE Regional Glacier and Ice Sheet Surface Velocities [Data set]. NASA National Snow and Ice Data Center DAAC. https://doi.org/10.5067/6II6VW8LLWJ7

Gourmelen, N., Escorihuela, M. J., Shepherd, A., Foresta, L., Muir, A., Garcia-Mondéjar, A., Roca, M., Baker, S. G., & Drinkwater, M. R. (2018). CryoSat-2 swath interferometric altimetry for mapping ice elevation and elevation change. *Advances in Space Research, 62*(6), 1226–1242. https://doi.org/10.1016/j.asr.2017.11.014

Gray, L., Burgess, D., Copland, L., Cullen, R., Galin, N., Hawley, R., & Helm, V. (2013). Interferometric swath processing of Cryosat data for glacial ice topography. *The Cryosphere, 7*(6), 1857–1867. https://doi.org/10.5194/tc-7-1857-2013

Gray, L., Burgess, D., Copland, L., Demuth, M. N., Dunse, T., Langley, K., & Schuler, T. V. (2015). CryoSat-2 delivers monthly and inter-annual surface elevation change for Arctic ice caps. The Cryosphere, 9(5), 1895–1913. https://doi.org/10.5194/tc-9-1895-2015

Gray, L. (2021). Brief communication: Glacier run-off estimation using altimetry-derived basin volume change: case study at Humboldt Glacier, northwest Greenland. *The Cryosphere, 1*5(2), 1005–1014. https://doi.org/10.5194/tc-15-1005-2021

Harcourt, W. D., Palmer, S. J., Mansell, D. T., Le Brocq, A., Bartlett, O., Gourmelen, N., Tepes, P., Dowdeswell, J. A., Blankenship, D. D., & Young, D. A. (2020). Subglacial controls on dynamic

thinning at Trinity-Wykeham Glacier, Prince of Wales Ice Field, Canadian Arctic. International *Journal of Remote Sensing, 41*(3), 1191–1213. https://doi.org/10.1080/01431161.2019.1658238

Hugonnet, R., McNabb, R., Berthier, E., Menounos, B., Nuth, C., Girod, L., Farinotti, D., Huss, M., Dussaillant, I., Brun, F., & Kääb, A. (2021). Accelerated global glacier mass loss in the early twenty-first century. *Nature, 592*(7856), 726–731. https://doi.org/10.1038/s41586-021-03436-z

Jezek, K., Wu, X., Paden, J., & Leuschen, C. (2013). Radar mapping of Isunnguata Sermia, Greenland. *Journal of Glaciology, 59*(218), 1135–1146. https://doi.org/10.3189/2013JoG12J248

Joughin, I., Howat, I., Alley, R. B., Ekstrom, G., Fahnestock, M., Moon, T., Nettles, M., Truffer, M., & Tsai, V. C. (2008). Ice-front variation and tidewater behavior on Helheim and Kangerdlugssuaq Glaciers, Greenland. *Journal of Geophysical Research*, *113*(F1), F01004. https://doi.org/10.1029/2007JF000837

Joughin, I., Howat, I. M., Fahnestock, M., Smith, B., Krabill, W., Alley, R. B., Stern, H., & Truffer, M. (2008). Continued evolution of Jakobshavn Isbrae following its rapid speedup. *Journal of Geophysical Research, 113*(F4), F04006. https://doi.org/10.1029/2008JF001023

Koerner, R. M. (1979). Accumulation, Ablation, and Oxygen Isotope Variations on the Queen Elizabeth Islands Ice Caps, Canada. *Journal of Glaciology, 22*(86), 25–41. https://doi.org/10.3189/S0022143000014039

Koerner, R. (2005). Mass balance of glaciers in the Queen Elizabeth Islands, Nunavut, Canada. *Annals of Glaciology, 42,* 417-423. doi:10.3189/172756405781813122

Mair, D., Burgess, D., Sharp, M., Dowdeswell, J. A., Benham, T., Marshall, S., & Cawkwell, F. (2009). Mass balance of the Prince of Wales Icefield, Ellesmere Island, Nunavut, Canada. *Journal of Geophysical Research, 114*(F2), F02011. https://doi.org/10.1029/2008JF001082

Medrzycka, D., Copland, L., Van Wychen, W., & Burgess, D. (2019). Seven decades of uninterrupted advance of Good Friday Glacier, Axel Heiberg Island, Arctic Canada. *Journal of Glaciology, 65*(251), 440–452. https://doi.org/10.1017/jog.2019.21

Meier, M. F., & Post, A. (1987). Fast tidewater glaciers. *Journal of Geophysical Research, 92*(B9), 9051. https://doi.org/10.1029/JB092iB09p09051

Millan, R., Mouginot, J., & Rignot, E. (2017). Mass budget of the glaciers and ice caps of the Queen Elizabeth Islands, Canada, from 1991 to 2015. *Environmental Research Letters*, *12*(2), 024016. https://doi.org/10.1088/1748-9326/aa5b04

Moon, T., Joughin, I., & Smith, B. (2015). Seasonal to multiyear variability of glacier surface velocity, terminus position, and sea ice/ice mélange in northwest Greenland. *Journal of Geophysical Research: Earth Surface, 120*(5), 818–833. https://doi.org/10.1002/2015JF003494

Mortimer, C. A., Sharp, M., & Wouters, B. (2016). Glacier surface temperatures in the Canadian High Arctic, 2000–15. *Journal of Glaciology, 62*(235), 963–975. https://doi.org/10.1017/jog.2016.80

Nick, F. M., Vieli, A., Howat, I. M., & Joughin, I. (2009). Large-scale changes in Greenland outlet glacier dynamics triggered at the terminus. *Nature Geoscience, 2*(2), 110–114. https://doi.org/10.1038/ngeo394

Noël, B. (2017): Average surface mass balance (SMB) components at 1 km for the Canadian Arctic Archipelago (1958-1995 and 1996-2015), links to RACMO2.3 model results in NetCDF format. PANGAEA, https://doi.org/10.1594/PANGAEA.881315

Supplement to: Noël, B., van de Berg, W.J., Lhermitte, S., Wouters, B., Schaffer, N., van den Broeke, M.R. (2018). Six decades of glacial mass loss in the Canadian Arctic Archipelago. *Journal of Geophysical Research-Earth Surface, 123*(6), 1430-1449, https://doi.org/10.1029/2017JF004304

Paden, J., Akins, T., Dunson, D., Allen, C., & Gogineni, P. (2010). Ice-sheet bed 3-D tomography. *Journal of Glaciology, 56*(195), 3–11. https://doi.org/10.3189/002214310791190811

Rasmussen, L. A., Conway, H., Krimmel, R. M., & Hock, R. (2011). Surface mass balance, thinning and iceberg production, Columbia Glacier, Alaska, 1948–2007. *Journal of Glaciology, 57*(203), 431–440. https://doi.org/10.3189/002214311796905532

Raup, B., Racoviteanu, A., Khalsa, S. J. S., Helm, C., Armstrong, R., & Arnaud, Y. (2007). The GLIMS geospatial glacier database: A new tool for studying glacier change. Global and Planetary Change, 56(1–2), 101–110. https://doi.org/10.1016/j.gloplacha.2006.07.018

Raymond, C. F. (1987). How do glaciers surge? A review. *Journal of Geophysical Research, 92*(B9), 9121. https://doi.org/10.1029/JB092iB09p09121

Sánchez-Gámez, P., & Navarro, F. (2017). Glacier Surface Velocity Retrieval Using D-InSAR and Offset Tracking Techniques Applied to Ascending and Descending Passes of Sentinel-1 Data for Southern Ellesmere Ice Caps, Canadian Arctic. *Remote Sensing, 9*(5), 442. https://doi.org/10.3390/rs9050442

Schoof, C. (2010). Ice-sheet acceleration driven by melt supply variability. *Nature, 468*(7325), 803–806. https://doi.org/10.1038/nature09618

Sharp, M., Burgess, D. O., Cawkwell, F., Copland, L., Davis, J. A., Dowdeswell, E. K., Dowdeswell, J. A., Gardner, A. S., Mair, D., Wang, L., Williamson, S. N., Wolken, G. J., & Wyatt, F. (2014). Remote sensing of recent glacier changes in the Canadian Arctic. In J. S. Kargel, G. J. Leonard, M. P. Bishop, A. Kääb, & B. H. Raup (Eds.), Global Land Ice Measurements from Space (pp. 205–228). Springer Berlin Heidelberg. https://doi.org/10.1007/978-3-540-79818-7_9

Short, N. H., & Gray, A. L. (2004). Potential for RADARSAT-2 interferometry: Glacier monitoring using speckle tracking. *Canadian Journal of Remote Sensing, 30*(3), 504–509. https://doi.org/10.5589/m03-071

Short, N. H., & Gray, A. L. (2005). Glacier dynamics in the Canadian High Arctic from RADARSAT-1 speckle tracking. *Canadian Journal of Remote Sensing, 31*(3), 225–239. https://doi.org/10.5589/m05-010

Stearns, L. A., & Hamilton, G. S. (2007). Rapid volume loss from two East Greenland outlet glaciers quantified using repeat stereo satellite imagery. *Geophysical Research Letters*, *34*(5). https://doi.org/10.1029/2006GL028982

Thomas, R. H., Abdalati, W., Frederick, E., Krabill, W. B., Manizade, S., & Steffen, K. (2003). Investigation of surface melting and dynamic thinning on Jakobshavn Isbræ, Greenland. *Journal of Glaciology, 49*(165), 231–239. https://doi.org/10.3189/172756503781830764

van der Veen, C. J. (2002). Calving glaciers. *Progress in Physical Geography: Earth and Environment, 26*(1), 96–122. https://doi.org/10.1191/0309133302pp327ra

van der Veen, C. J. (1996). Tidewater calving. *Journal of Glaciology, 42*(141), 375–385. https://doi.org/10.1017/S0022143000004226

Van Wychen, W., Copland, L., Gray, L., Burgess, D., Danielson, B., & Sharp, M. (2012). Spatial and temporal variation of ice motion and ice flux from Devon Ice Cap, Nunavut, Canada. *Journal of Glaciology, 58*(210), 657–664. https://doi.org/10.3189/2012JoG11J164

Van Wychen, W., Burgess, D. O., Gray, L., Copland, L., Sharp, M., Dowdeswell, J. A., & Benham, T. J. (2014). Glacier velocities and dynamic ice discharge from the Queen Elizabeth Islands, Nunavut, Canada. *Geophysical Research Letters, 41*(2), 484–490. https://doi.org/10.1002/2013GL058558

Van Wychen, W., Copland, L., Jiskoot, H., Gray, L., Sharp, M., & Burgess, D. (2018). Surface Velocities of Glaciers in Western Canada from Speckle-Tracking of ALOS PALSAR and RADARSAT-2 data. *Canadian Journal of Remote Sensing, 44*(1), 57–66. https://doi.org/10.1080/07038992.2018.1433529

Van Wychen, W., Burgess, D., Kochtitzky, W., Nikolic, N., Copland, L., & Gray, L. (2021). RADARSAT-2 Derived Glacier Velocities and Dynamic Discharge Estimates for the Canadian High Arctic: 2015–2020. *Canadian Journal of Remote Sensing, 46*(6), 695–714. https://doi.org/10.1080/07038992.2020.1859359

Vijay, S., & Braun, M. (2017). Seasonal and Interannual Variability of Columbia Glacier, Alaska (2011–2016): Ice Velocity, Mass Flux, Surface Elevation and Front Position. *Remote Sensing, 9*(6), 635. https://doi.org/10.3390/rs9060635

Williams, J. J., Gourmelen, N., & Nienow, P. (2020). Dynamic response of the Greenland ice sheet to recent cooling. *Scientific Reports, 10*(1), 1647. https://doi.org/10.1038/s41598-020-58355-2

Williams, J. J., Gourmelen, N., Nienow, P., Bunce, C., & Slater, D. (2021). Helheim Glacier Poised for Dramatic Retreat. *Geophysical Research Letters, 48*(23). https://doi.org/10.1029/2021GL094546

Wu, X., Jezek, K. C., Rodriguez, E., Gogineni, S., Rodriguez-Morales, F., & Freeman, A. (2011). Ice Sheet Bed Mapping With Airborne SAR Tomography. IEEE Transactions on Geoscience and *Remote Sensing, 49(*10), 3791–3802. https://doi.org/10.1109/TGRS.2011.2132802

Chapter 3: Long-term field tracking of icebergs in the eastern Canadian Arctic

3.1 Introduction

Icebergs primarily calved from tidewater glaciers in the Queen Elizabeth Islands (QEI) and western Greenland usually drift into Baffin Bay, where they typically transit in a counter-clockwise direction before drifting southwards along the east coast of Canada (Valeur et al., 1996). Icebergs have both an above-water (sail) and below-water (keel) portion and are subject to a number of influences including wind and ocean currents, bathymetry, and sea ice conditions (Bigg et al., 1996). They can also pose a potential risk to marine traffic and offshore activities in northern and eastern Canada. This is of particular concern given the recent increase in ship traffic throughout this region as a result of increased sea ice navigability, at least partly driven by climate change (Pizzolato et al., 2016; Dawson et al., 2018). However, little is currently known about the drift patterns of icebergs in the Canadian Arctic, and the potential future risks they may pose as vessel traffic increases.

Iceberg production occurs from the calving of marine-terminating glaciers. From 2010-2020, 4.28 ± 1.18 Gt a^{-1} of ice was discharged into Baffin Bay and adjacent waters from the Queen Elizabeth Islands (QEI; Kochtitzky et al., 2022). Between 2010 and 2018, the Greenland Ice Sheet lost 126 ± 9 Gt a^{-1} to ice discharge, of which ~76 Gt a^{-1} drained into Nares Strait and into fiords that empty into Baffin Bay from northern and western regions of the ice sheet (Mouginot et al., 2019). Mass loss from the Greenland Ice Sheet through glacier dynamics (i.e., ice motion) increased between 1972 and 2018, with a particular acceleration since the start of the 21st century, with dynamics controlling 66 ± 8% of mass loss over this period, compared to 34 ± 8% from surface mass balance (Mouginot et al., 2019). This highlights the important role that glacier ice discharge plays in the total mass budget and overall contribution of icebergs in Baffin Bay.

Automated iceberg detection in satellite imagery is challenging, which hinders the ability of agencies such as the Canadian Ice Service (CIS) and International Ice Patrol (IIP) to map their locations and provide near real-time information for Arctic shipping (Scheick et al., 2019). There is also a great deal of variability between years in the number of icebergs that reach the Grand Banks in offshore Newfoundland (Bigg et al., 2018). Previous studies have successfully used satellite-tracking beacons to monitor iceberg and ice island movement within Baffin Bay (Robe et al., 1980; Marko et al., 1982; Larsen et al., 2015). However, there is limited data in Canadian

coastal waters, and many drift tracks do not extend beyond a year and have not monitored icebergs through their entire life cycle from their source to sink. As a result, there remains uncertainty concerning the origins of icebergs in Canadian waters, whether patterns exist in their drift, and their locations of deterioration.

The CIS currently uses the North American Ice (NAIS) iceberg drift model to provide information on the distribution of icebergs in Canadian Waters. The model is widely used in Eastern Canada but there has been little testing of its efficacy into Baffin Bay and the eastern Canadian Arctic due in part to the lack of in-situ iceberg drift observations (Garbo, 2022). There is also a general assumption that icebergs drift at ~2% of the wind speed (Garrett, 1985; Smith and Donaldson, 1987; Smith, 1993; Bigg et al., 1997), although this rule-of-thumb has mainly been evaluated using iceberg drift models for Newfoundland/Labrador (Smith and Donaldson, 1987; Smith, 1993) and Antarctica (Wagner et al., 2017), rather than the Canadian Arctic.

Using a multi-year dataset of iceberg drift locations collected through the deployment of global navigation satellite system (GNSS) equipped tracking beacons, the purpose of this study is to:

(i) characterize spatial and seasonal patterns in regional iceberg drift throughout the eastern Canadian Arctic;
(ii) evaluate the applicability of the 2% rule for icebergs drifting in the eastern Canadian Arctic, and;
(iii) using reanalysis data, describe local environmental variables (e.g. wind, ocean, and tidal currents) on select iceberg tracks as potential drivers of drift.

3.2 Study Area

3.2.1 Baffin Bay

Baffin Bay is an oceanic basin located in the Arctic, connecting the Arctic Ocean to Davis Strait and the Labrador Sea (Figure 3-1). Meteorological conditions in Baffin Bay are strongly controlled by the surrounding Greenland and North American landmasses. Winter winds generally blow from the northwest, while during summer strong winds typically blow from the south-southeast and are most persistent off the coast of Greenland. These wind conditions influence surface ocean currents

and therefore other factors such as temperature, sea ice variability, fog, and precipitation in Baffin Bay (Valeur et al., 1996; Tang et al., 2004). Mean air temperatures in the region are generally below 5°C year-round, with mean winter temperatures of -20°C and summer temperatures remaining around 4°C (Valeur et al., 1996). Sea ice and icebergs in Baffin Bay are influenced by two main ocean currents: the relatively warm West Greenland Current (WGC) and the colder Baffin Island Current (BIC) (Figure 3-1). The WGC flows northward along the west coast of Greenland until Smith Sound where it flows westward, and then begins moving southward along the eastern coast of Baffin Island (Melling et al., 2001; Tang et al., 2004). Icebergs and sea ice can be carried by this current around Baffin Bay and may eventually drift south into Davis Strait and the Labrador Sea (Valeur et al., 1996; Tang et al., 2004; Münchow et al., 2015).

Minimum sea ice cover occurs in September when remaining sea ice is only present near the coast of Baffin Island due to the relatively warm northward flowing WGC in the east (Tang et al., 2004). Sea ice begins to form in mid-October and is typically present in Baffin Bay throughout the year, reaching a maximum cover in March when it extends into Davis Strait (Valeur et al., 1996). Along the eastern Canadian Arctic coast, icebergs can often become frozen in sea ice as they follow the BIC close to the shores of Baffin Island (Marko et al., 1982; Tang et al., 2004) and will remain static until the sea ice is free to move again. Previous studies which used satellite tracking beacons to monitor iceberg drift in Baffin Bay found icebergs averaged drift speeds of ~10 km d^{-1}, with periods of rapid drift between 10 and 30 km d^{-1} during the summer and fall (Robe et al., 1980; Marko et al., 1982; Valeur et al., 1996).

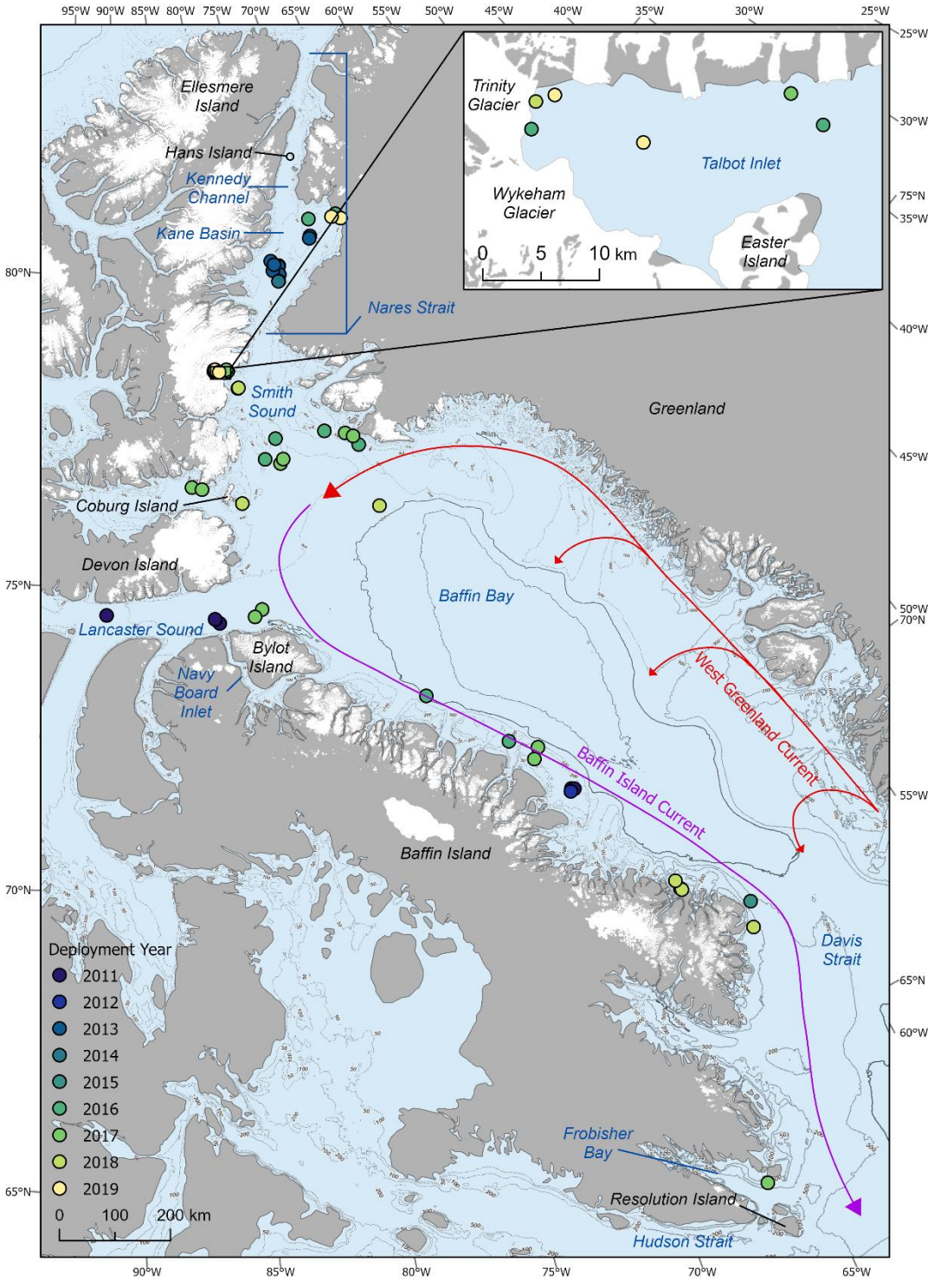

Figure 3-1: Location of beacon deployments on icebergs and ice islands in the eastern Canadian Arctic between 2011 and 2019. Inset map shows locations of beacon deployment in Talbot Inlet, Ellesmere Island. Bathymetry: General Bathymetric Chart of the Oceans (GEBCO), NOAA National Centers for Environmental Information (NCEI), Glacier outlines: Randolph Glacier Inventory (RGI) version 6.0 (RGI Consortium, 2017).

3.2.2 Nares Strait/Smith Sound

Nares Strait is a 500-km long channel approximately 40 km wide located between Ellesmere Island and NW Greenland, which connects the Arctic Ocean to northern Baffin Bay (Figure 3-1). Nares Strait is one of the windiest locations in the Arctic (Gutjahr & Heinemann, 2018; Kohnemann & Heinemann, 2021), caused in part by steep surrounding topography which channels northerly low-level winds through its narrowest areas (e.g., Smith Sound) (Samelson & Barbour, 2008; Kohnemann & Heinemann, 2021). Mean wind speeds of 6-8 m s^{-1} occur in Nares Strait, although observations of wind speeds exceeding 20 m s^{-1} have been recorded as early as the 1860s (Ito, 1982; Ingram et al., 2002) and >40 m s^{-1} in Smith Sound in winter 1979 (Steffen, 1985). Between 2017 and 2019, an average sea ice area of ~86,000 km^2 was transported annually through Nares Strait from the Arctic Ocean (Moore et al., 2021). Most commonly, this takes place after July due to the formation of ice arches at the northern and southern ends of the strait in mid- to late-winter which block sea ice drift (Kwok, 2005), although these arches have been less common recently (Moore et al., 2021). Between September and November, mean sea ice drift speed through Nares Strait can vary between 20-40 km d^{-1} (0.23-0.46 m s^{-1}; Kwok, 2005), but limited research has been conducted on the drift characteristics of icebergs through this region (Nutt, 1966; Crawford et al., 2018; Crawford and Mueller, 2023).

The ice arch and wind through Nares Strait also play an important role in the formation of the Pikialasorsuaq (also known as the North Water Polynya) in Smith Sound (Ito, 1982; Steffen, 1985; Melling et al., 2001). The Pikialasorsuaq and Kane Basin region of Nares Strait are the location of some of the strongest tidal currents in the Canadian Arctic, with M_2 major axis amplitudes exceeding 20 cm s^{-1} (Dunphy et al., 2005; Davis et al., 2018; Baumann et al., 2020). The Pikialasorsuaq covers an area of ~80,000 km^2 and is typically covered by close pack sea ice (7-8/10 concentration) that contains several leads and polynyas throughout the winter, including in Lancaster and Smith Sounds (Steffen, 1986), allowing for movement of sea ice and icebergs throughout the year. Sea ice in Lancaster Sound generally begins forming in October, reaching a maximum in March. By June, polynyas within the Pikialasorsuaq in Lancaster and Smith sounds begin to merge, with less than half the area covered with sea ice by July (Valeur et al., 1996; Tang et al., 2004).

3.2.3 Talbot Inlet

Trinity and Wykeham glaciers are located at the head of Talbot Inlet on SE Ellesmere Island (Figure 3-1). Both are large tidewater outlet glaciers that drain the SE Prince of Wales (POW) Icefield into Smith Sound, and then northern Baffin Bay. As of 2020, Trinity and Wykeham glaciers were responsible for ~50% of total solid ice discharge from tidewater glaciers in the QEI (1.60 Gt a^{-1}), compared to ~22% (0.55 Gt a^{-1}) in 2000 (Van Wychen et al., 2021). Both glaciers have undergone a significant increase in velocity and discharge over the last 10-15 years (Van Wychen et al., 2021; Dalton et al., 2022) that has coincided with a terminus retreat of ~3-4 km for Trinity Glacier and ~1 km for Wykeham Glacier (Cook et al., 2019). Given the significant recent increases in calving from these glaciers, Talbot Inlet was selected as an area of focus for deploying iceberg tracking beacons between 2016 and 2019 near to their calving source.

3.3 Methods & Data

3.3.1 Iceberg tracking beacon deployment

Between 2016 and 2019, we deployed 50 satellite tracking beacons by helicopter from the CCGS Amundsen icebreaker onto icebergs and ice islands in Nares Strait, Baffin Bay, Talbot Inlet and surrounding areas (Figure 3-1). Of the 50 beacons deployed during this time, 11 were MetOcean iSVP and CALIB Iridium beacons deployed on behalf of Environment and Climate Change Canada, 23 used RockSTAR GNSS trackers (https://www.groundcontrol.com/us/product/rockstar-global-satellite-messaging-tracking), six were Solara Iridium beacons, and 10 used the 'Cryologger' ice tracking beacon (ITB) (https://cryologger.org) built specifically for this project (Figure 3-2). The RockSTAR units were connected to an 18Ah rechargeable sealed lead acid battery and a solar panel housed within a waterproof Nanuk case. The Cryologger system is comprised of a custom-built system of an Arduino platform, GNSS receiver, Iridium telemeter, temperature and pressure sensors, and lithium batteries housed inside a Nanuk case.

The Cryologger ITB is a low-cost, modular, and user-friendly data logger and telemeter based on the open-source Arduino electronics platform. Constructed using off-the-shelf components, it does not require specialized tools or expertise to build and can be easily modified to meet individual

application requirements. Intended for deployments of 3 years or more, the Cryologger provides long-term measurements of multiple variables, including GNSS position, temperature, pressure, pitch, roll, tilt-compensated heading, and battery voltage. Data are recorded hourly and transmitted over the Iridium satellite network at specified intervals, which can be remotely configured by the end user. A more detailed description of the design and a complete bill of materials are made freely available on GitHub (https://github.com/cryologger/ice-tracking-beacon).

The iSVP, Solara, RockSTAR, and Cryologger systems were designed with the ability to maintain two-way communication, so that their transmission frequency could be changed remotely based on their activity and battery level. For example, in the summer months when there is little sea ice and icebergs are more likely to drift, the beacons were set at a high transmission frequency (typically once per hour). In the winter when many of the icebergs are frozen in sea ice and drifting little, the transmission frequency was reduced (e.g., once per day) to reduce battery consumption. Despite this, the battery levels of some beacons still became too low to transmit due to extreme cold winter temperatures, while Solara beacons often experienced transmission malfunction. Between approximately October and July, RockSTAR units stopped transmitting likely due to heavy snow cover.

When selecting icebergs suitable for beacon deployment, characteristics such as size, shape, and location were taken into account. Due to the nature of helicopter deployment, icebergs were required to be large enough and primarily tabular in shape so that they were stable for landing and unlikely to calve, roll, or break apart in the short term. As a result, beacons were generally deployed onto icebergs that were >100 m in length, tabular, and located far enough away from a coast so as to not become immediately grounded in shallow waters. Locations of beacon deployments were also constrained spatially and temporally by the timing and location of CCGS *Amundsen*-based fieldwork. Field beacon deployment occurred from 2016 to 2019 between July and September near the coasts of Baffin and Ellesmere Islands, NW Greenland, and in Nares Strait (60°N - 82°N).

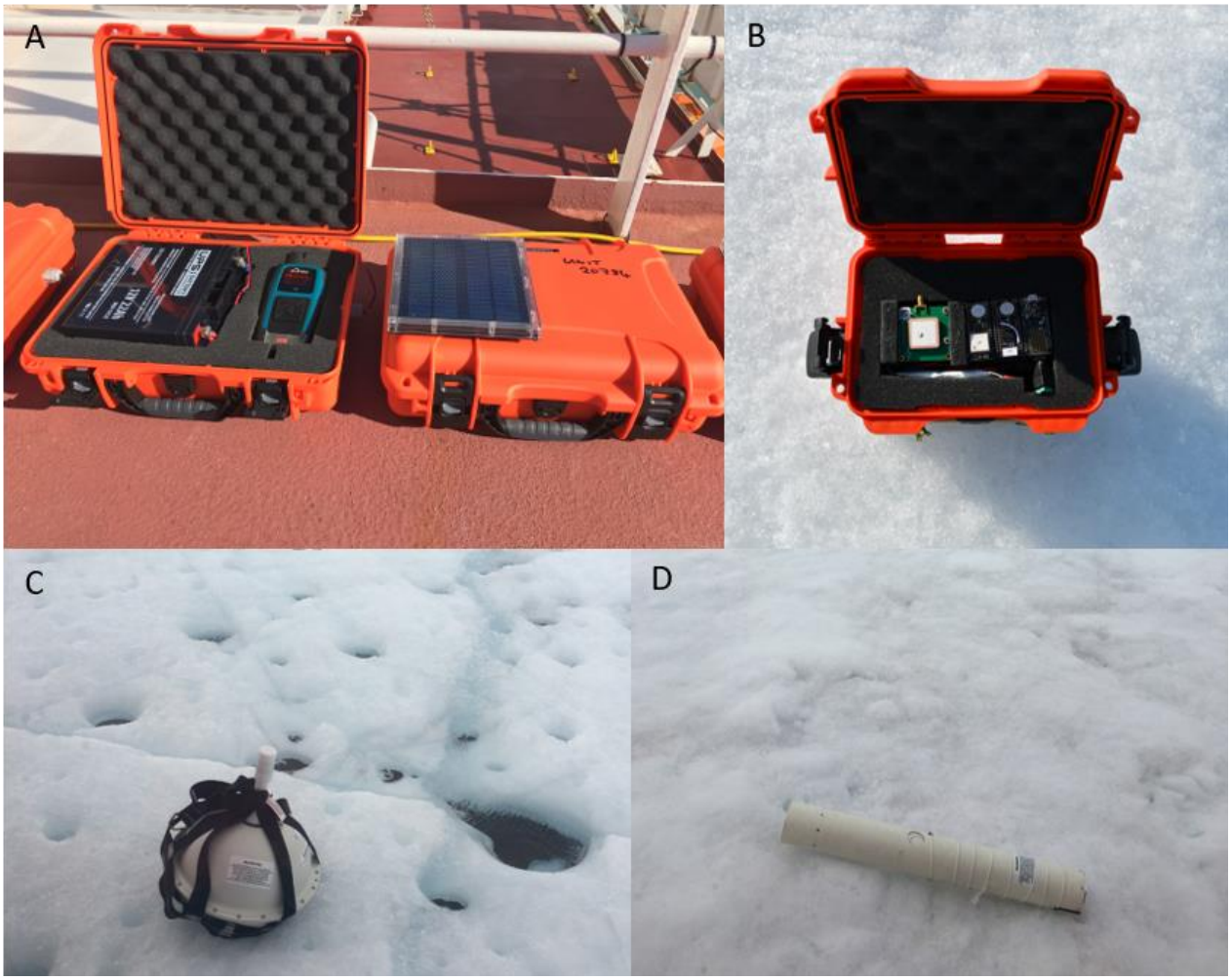

Figure 3-2: Examples of iceberg tracking beacons deployed for this study: (a) RockStar; (b) Cryologger; (c) MetOcean iSVP; (d) MetOcean CALIB.

3.3.2 Canadian Ice Service Database: 1997-2022

Iceberg drift track data from our deployments were included in a database compiled by Carleton University and the CIS, which includes iceberg tracking beacon data from 1997 to 2022. Iceberg drift tracks from the CIS database were selected for use in our study based on the following criteria:

i) Observations were located between 50°N & 80.5°N and 85°W & 50°W
ii) Start of iceberg track was north of 60°N
iii) Observation transmission interval did not exceed six hours
iv) Drift track duration was ≥ 10 days
v) Transmissions occurred between 2011 and 2019

Drift tracks were limited to a geographical area that extends approximately from Kennedy Channel to the Labrador Sea. Beacons that were deployed north of 60°N and drifted south of this boundary were also included. Beacons which transmitted data for fewer than 10 days, or which had a transmission interval exceeding six hours, were excluded due to their limited coverage. While five iceberg tracking beacons that were deployed in 2018 and 2019 continued transmitting data until 2020-2021 (Figures 3-4 to 3-7), due to availability of environmental variable data we focus our analysis on the time period 2011-2019.

For deployments within Talbot Inlet (between 77.5°N & 78°N and 76°W & 78.5°W; Figure 3-1), observations were only included for icebergs once they drifted outside the above bounds of the inlet. Due to lack of reliable environmental data within Talbot Inlet and the likely influence of fiord geometry on iceberg drift patterns (Carlson et al., 2017; Sulak et al., 2017), we have omitted the inlet tracks for the purposes of this study.

For some beacon types, observations were recorded hourly while new positional data was only transmitted every three hours. For these cases, the data were filtered to only include positional transmissions (i.e., every three hours). Observations from ARGOS-based beacon types were excluded from the database due to poor location accuracy. Based on these criteria, a subset of 54 beacons from the CIS database (36 from our deployments from the CCGS *Amundsen*, 18 from other deployments) were used in this study (Table 3-1).

As this subset contained seven different beacon types with variable transmission intervals, speed and distance plots were manually analysed to check for inconsistences and potential errors in

observations. In cases where iceberg drift speeds were unrealistically high (>8 m s^{-1}), or there were unexplained long distances between subsequent transmissions, observations were removed from the dataset. To determine the minimum velocity that could be detected by the GNSS receivers, apparent motion was calculated for a Cryologger beacon initially deployed on an ice island fragment near Qikiqtarjuaq, Nunavut. Satellite imagery showed the beacon to be grounded on shore and immobile between 2019 and 2022. The GNSS data during this period indicated mean velocities of 0.001 ± 0.04 m s^{-1}, so speeds < 0.01 m s^{-1} were excluded from the entire dataset.

3.3.3 Environmental Variables

The influence of environmental variables on iceberg drift was quantified using input data from ERA5 wind reanalysis, GLORYS12 ocean reanalysis (subsequently referred to as GLORYS), and the CIS MANICE (Manual of Standard Procedures for Observing and Reporting Ice Conditions) datasets for 2011-2019. To determine the potential influence of wind, ocean, and sea ice variables on iceberg drift tracks, the nearest (spatially and temporally) point of environmental data to each corresponding iceberg drift observation point were selected. As a result, the extracted environmental data could have occurred before or after the iceberg location transmission, but never >3 hours for ERA5 wind reanalysis data or >12 hours for GLORYS ocean reanalysis data from the transmission time.

3.3.3.1 ERA5 wind reanalysis data

The influence of wind speed and direction on iceberg drift patterns was assessed using ERA5 climate reanalysis data. The ERA5 dataset provides hourly estimates of a large number of atmospheric, land and oceanic climate variables using a latitude-longitude grid with 1/4°-1/2° horizontal resolution. The u and v-components (m s^{-1}) of the 10 m height wind data were used to calculate wind speed and heading for the study area between 2011 and 2019. This dataset was accessed from the "Hourly data on single levels from 1979 to present" dataset through the Copernicus Climate Data Store (https://www.ecmwf.int/en/forecasts/datasets/reanalysis-datasets/era5).

Table 3-1: Summary drift track start and end date, duration, maximum speed, and total distance for the 54 beacons used in this study.

Beacon ID	Start Latitude (°N)	Start Longitude (°W)	Start Date	End Date	Distance (km)	Duration (days)	Maximum Speed (m s^{-1})
300034013463170[1*]	74.264	87.943	30/08/2011	23/10/2012	152.8	54	0.65
300234010031950[2*]	73.923	81.274	30/07/2011	08/09/2011	901.8	39	0.83
300234010035940_PII-B[2*]	69.649	65.928	06/11/2011	21/10/2014	1888.8	1080	0.76
300234010955690[2*]	73.999	81.511	30/07/2011	08/09/2011	823.0	39	0.74
300234010958690_PII-B[2*]	69.625	65.803	23/10/2011	26/09/2012	736.4	338	0.81
300234010959690[2*]	74.004	81.511	30/07/2011	12/09/2011	812.5	43	0.71
9999999999999993[*]	69.607	66.003	02/08/2012	19/08/2013	19.2	381	0.30
300034013460170[1*]	79.575	67.783	30/08/2013	06/10/2014	12.6	402	0.12
300034013461170[1*]	79.304	71.198	25/08/2013	26/07/2014	1420.4	335	1.05
300034013464160[1*]	79.295	71.240	25/08/2013	11/07/2014	687.3	320	1.02
300034013468160[1]	79.546	67.909	05/09/2013	25/08/2014	30.8	353	0.16
300234011240410[4]	79.170	71.397	25/08/2013	21/04/2014	4069.6	238	1.30
300234011241410[4]	79.292	71.445	25/08/2013	19/05/2014	5279.5	266	1.12
300234011242410[4]	79.258	71.817	25/08/2013	27/10/2014	2372.5	427	2.31
300234011938510[4]	79.341	71.555	26/08/2013	30/11/2014	675.5	461	0.89
300234060544160[2*]	79.073	71.623	05/08/2014	29/08/2015	196.1	388	0.34
300234061763040[2*]	79.070	71.657	06/08/2014	03/07/2015	422.9	331	0.57
300234060104820[4*]	67.390	63.312	20/10/2015	05/12/2017	596.4	777	0.31
300234060435010[4*]	66.671	60.890	22/10/2015	07/08/2016	2987.3	290	1.30
300234061762030[4*]	67.390	63.312	20/10/2015	07/12/2016	84.1	413	0.20
300234060172440[5]	76.564	71.869	08/08/2016	11/11/2016	382.1	95	0.59
300234060172670[5]	70.763	67.857	05/09/2016	18/10/2016	102.2	43	0.29
300234061761040[5]	76.668	75.284	17/08/2016	19/10/2016	1174.1	62	1.38
300234061763030[6*]	71.938	71.063	05/08/2016	23/08/2016	219.5	18	0.32
300234061768060[6*]	79.836	67.357	20/08/2016	10/08/2017	3914.4	354	1.36
300234063513450[6*]	79.743	64.962	19/08/2016	23/12/2017	747.4	490	0.76
300234063515450[6*]	76.387	76.331	12/08/2016	28/01/2018	1812.6	533	0.87
300234064808170[5]	77.950	78.524	11/08/2016	09/10/2016	116.3	59	0.12
300234064808210[5]	77.905	77.481	11/08/2016	09/11/2016	326.1	90	0.45
300434063218800[5]	76.175	69.939	08/08/2016	22/09/2016	229.5	45	0.51
300234010025000[5]	76.426	70.542	27/07/2017	14/08/2017	150.4	17	0.55
300234060169280[5]	77.934	77.571	04/08/2017	12/10/2017	759.2	68	1.07
300234060177480[5]	74.021	78.657	02/08/2017	30/08/2017	715.4	27	1.08
300234060270020[5]	73.925	79.157	02/08/2017	21/08/2017	467.6	18	0.70
300234060272000[5]	76.231	75.549	25/07/2017	21/09/2017	288.2	57	0.64
300234060563100[5]	76.339	70.100	02/08/2017	09/09/2017	99.4	37	0.63
300234060692710[5]	76.177	81.629	04/08/2017	10/09/2017	728.4	36	1.21

300234062324750[2]	70.492	66.642	30/08/2017	21/09/2017	298.9	22	0.48
300234062325760[2]	70.333	67.027	30/08/2017	15/09/2017	177.7	15	0.60
300234062327750[2]	76.121	80.975	19/10/2017	24/02/2018	1779.6	128	0.95
300234062328750[2]	76.316	75.145	25/07/2017	06/12/2017	2018.9	134	1.24
300234063516450[6]	62.338	65.053	26/07/2017	22/10/2017	38.3	88	0.97
300234060367670[5]	75.157	70.184	29/08/2018	12/11/2018	1226.0	74	0.65
300234062807520[5+]	77.598	77.043	28/08/2018	02/10/2018	295.9	34	0.39
300434063411050[7]	77.970	78.488	30/08/2018	08/04/2020	321.0	587	0.49
300434063415110[7]	75.771	78.516	28/08/2018	03/07/2019	3980.4	308	1.70
300434063415160[7]	67.358	63.271	02/09/2018	28/03/2021	564.7	938	1.10
300434063416060[7]	67.539	63.364	03/09/2018	22/09/2019	98.3	384	0.54
300434063418130[7]	66.219	61.486	03/09/2018	12/11/2019	1429.3	434	1.12
300434063419120[7+]	77.607	76.974	28/08/2018	10/04/2020	1252.4	590	0.88
300234060206850[5]	79.646	64.694	31/07/2019	02/10/2019	57.8	62	0.09
300434063392070[7]	79.725	65.390	01/08/2019	27/09/2019	9.0	57	0.07
3004340633941107	77.972	78.414	06/08/2019	10/04/2020	104.1	248	0.30
300434063495310[7]	77.923	78.136	06/08/2019	30/10/2019	177.6	84	0.38

Beacon type: [1]Oceanetics, [2]MetOcean iSVP, [3]Navidatum, [4]Canatec, [5]RockSTAR, [6]CALIB IRIDIUM, [7]Cryologger; Iceberg source: *Ice island fragment, [+]Petermann Glacier

3.3.3.2 GLORYS12 ocean reanalysis data

GLORYS provides 3D daily mean values for ocean temperature, salinity, currents, and other oceanographic variables. It is based on the NEMO ocean current model platform and driven by ECMWF ERA-Interim and ERA5 climate reanalysis data. GLORYS data is available for 50 depth layers between 0 and 5500 m and uses a regular latitude-longitude grid with a horizontal resolution of 1/12° and vertical resolution of 1 m up to 100 m depth in the upper 22 layers. In this study we use surface (0.494 m) ocean depth data to account for the variation in iceberg thickness and keel depth for the 54 icebergs analysed. We calculated ocean current speed (m s^{-1}) and direction (heading) using u and v-components provided with the data, accessed using the MOTU Client Command Line Interface (CLI) through the Copernicus Marine Environment Monitoring Service website (CMEMS; https://marine.copernicus.eu/).

3.3.3.3 CIS ice chart archive

Weekly regional digital ice charts were used to determine the presence and type of sea ice in Baffin Bay during the drift paths of the icebergs in this study. The classification of sea ice is based on the CIS MANICE classification system. The MANICE provides definitions and procedures for observing, recording, and reporting ice conditions (sea, lake, and river ice, and ice of land origin). The "Egg Code" is used for ice charts and contains data on the stage of development (age), form (flow size), and concentration of sea ice. For example, land-fast sea ice is identified as Form of Ice Code 8 and a triangle symbol denotes the presence of icebergs (CIS, 2005). Regional ice charts are most useful for larger areas such as Baffin Bay where less detail is needed. The online archive of historical weekly ice charts for the eastern Arctic was downloaded from the CIS website (https://iceweb1.cis.ec.gc.ca/Archive/page1.xhtml?lang=en).

3.4 Results & Discussion

For the 54 icebergs analyzed for this study, the seasonal distribution of speed observations used for analysis for the eastern Canadian Arctic are shown in Figure 3-3. Drift tracks are first plotted by season to characterize their spatial and temporal patterns on a regional basis throughout the study area (Figures 3-4 to 3-7). We provide an analysis of the 2% rule for all icebergs in the study,

followed by a review of the main mechanisms controlling iceberg drift, using examples from specific locations.

3.4.1 Seasonal iceberg drift patterns

3.4.1.1 Summer

Of the 54 total beacons deployed, 48 beacons transmitted data during the summer months (June, July, August) between 2011 and 2019. The majority of these observations are concentrated in the area north of 70°N, between Kane Basin and the entrance of Lancaster Sound, with only a few tracks located south of 65°N (Figure 3-4a, b). The highest median drift speeds of ~0.73 m s^{-1} were observed around 55°N off the coast of Labrador (Figure 3-4c). Higher drift speeds of between 0.4 and 0.6 m s^{-1} were observed around 73°N, near the entrance of Lancaster Sound, and 63°N near the entrance of Hudson Strait and Frobisher Bay on southern Baffin Island. However, most summer median speeds did not exceed ~0.4 m s^{-1}. Greater variability in speed was observed near the entrance of Lancaster Sound and in Davis Strait (Figure 3-4f).

Drift direction was highly variable during the summer months, especially within Kane Basin and Smith Sound (Figure 3-4d). Icebergs located closest to the coast of Devon Island were observed to drift southwest from Smith Sound into Lancaster Sound. Icebergs located farther from the coast drifted generally southeast from Smith Sound along the east coast of Baffin Island. As icebergs move south of 65°N, their drift direction becomes more variable near the entrance of Hudson Strait and along the mid-coast of Labrador.

Areas of highest mean residence time, defined as the mean time an iceberg is located in a given 50 x 50 km cell, are coincident with regions of lower drift speeds, and are more prevalent in Kane Basin, near Coburg Island, and along the coast of Baffin Island around 67°N (Figure 3-4e). Mean residence times increase further south along the east coast of Baffin Island, reaching a maximum of 183 days near 67°N. In Smith Sound and northern Baffin Bay, mean residence times were not observed to exceed 25 days during the summer months.

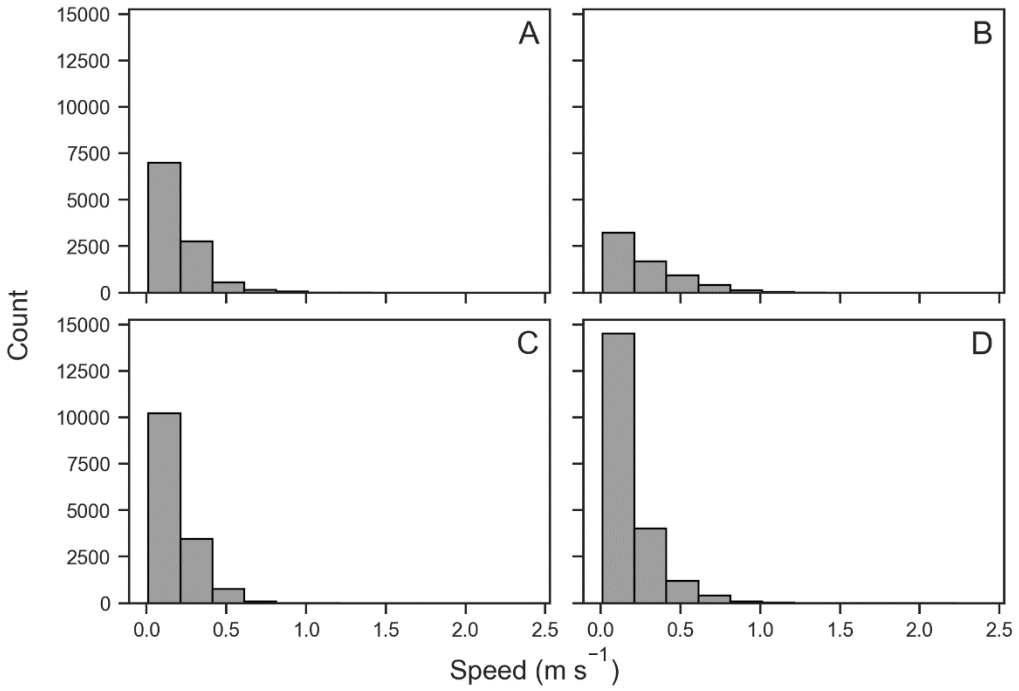

Figure 3-3: Histogram of number of seasonal iceberg drift speed observations used in this study for the eastern Canadian Arctic during: a) winter; b) spring; c) summer; and d) fall.

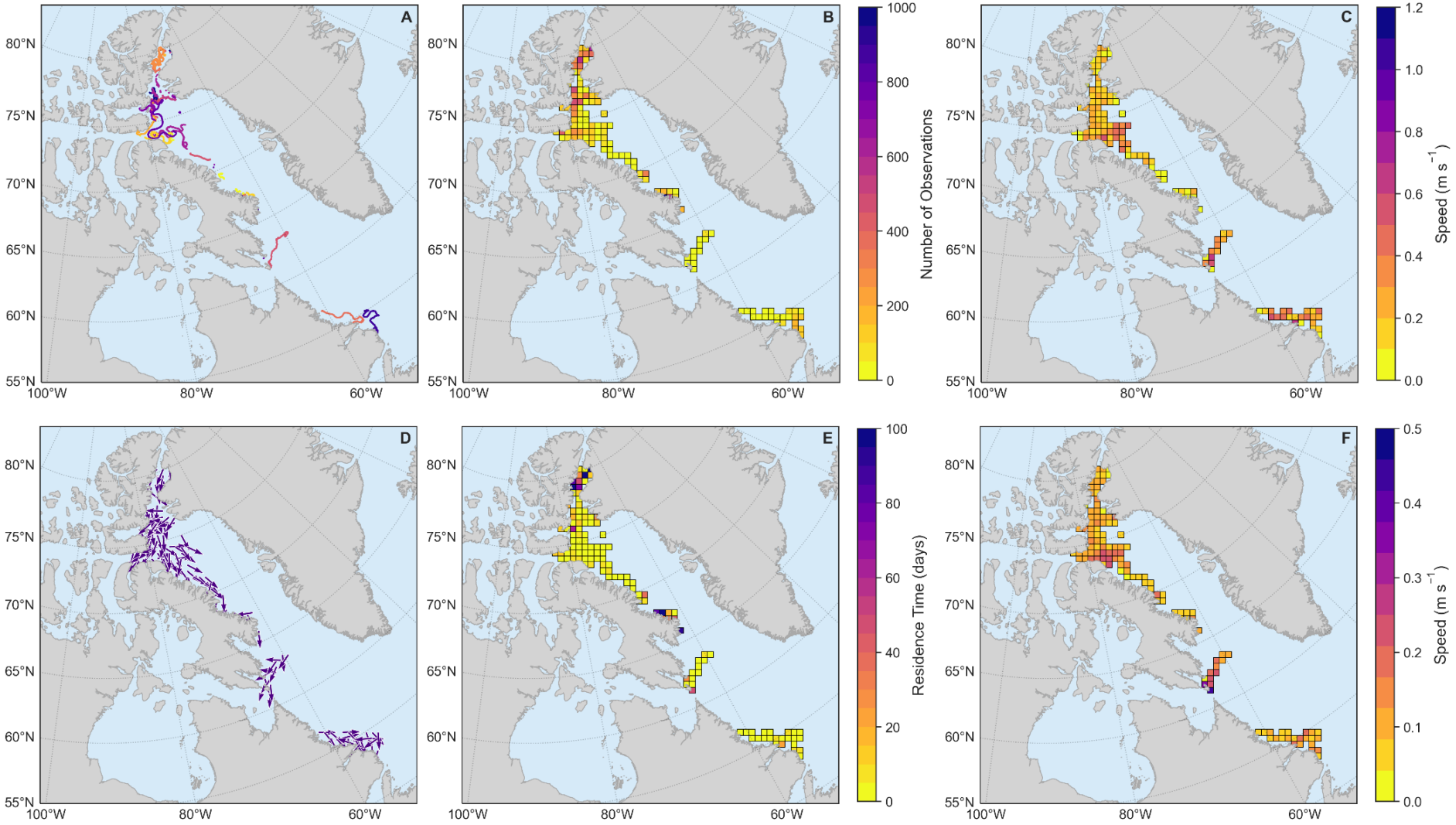

Figure 3-4: a) Drift tracks (one colour per iceberg); b) number of observations; c) median drift speed; d) mean drift direction, e) mean residence time and f) standard deviation of drift speed during the summer (June, July, August) for 48 icebergs tracked between 2011 and 2020, calculated for 50 x 50 km grid cells.

3.4.1.2 Fall

Observations were recorded for 49 icebergs during the fall months (September, October, November) between 2011 and 2019, concentrated between 60°N and 80°N (Figure 3-5a, b). Highest median speeds occurred near the entrance of Lancaster Sound and along the mid-coast of Baffin Island and reached a maximum of ~0.79 m s^{-1} (Figure 3-5c). Fall is the only season in this study when iceberg drift was observed in northeastern Baffin Bay, where median speeds ranged between 0.2 and 0.3 m s^{-1}. Variation in speed was greatest off the coast of SE Ellesmere Island and within Lancaster Sound (Figure 3-5f).

Drift direction was generally uniform, with icebergs moving south and southeast throughout the entire study area. Near the coast of Devon Island, icebergs tended to drift into the entrance of Lancaster Sound (Figure 3-5d). Similar to the summer months, icebergs located farther from the coast of Devon Island drifted southeast towards the coast of Baffin Island. Mean residence time was low (<50 days) for nearly the entire study area, except for the southeast coast of Baffin Island where the highest mean residence time of 464 days was observed (Figure 3-5e).

3.4.1.3 Winter

A total of 21 beacons transmitted data during the winter (December, January, February) between 2011 and 2019, from Kane Basin to the Labrador coast (80°N-56°N; Figure 3-6a, b). Higher drift speeds were observed in areas located >50 km from the coast, with the highest speeds of 1.0 to 1.2 m s^{-1} in Nares Strait, Smith Sound, and off the northeastern coast of Labrador (Figure 3-6c). This was also the location of the greatest variation in drift speed (Figure 3-6f). Along the east coast of Baffin Island, speeds were lower in the areas closest to the coast and higher farther away from the coast.

Mean drift direction was spatially consistent during the winter months as icebergs flow generally south/southeast along the coast of Ellesmere, Devon, and Baffin Islands (Figure 3-6d). Residence times generally did not 25 exceed days, with the exception of Kane Basin, Coburg Island, and the southeast coast of Baffin Island, which ranged from a minimum of 42 to a maximum of 89 days, the latter being consistent with other seasons (Figure 3-6e).

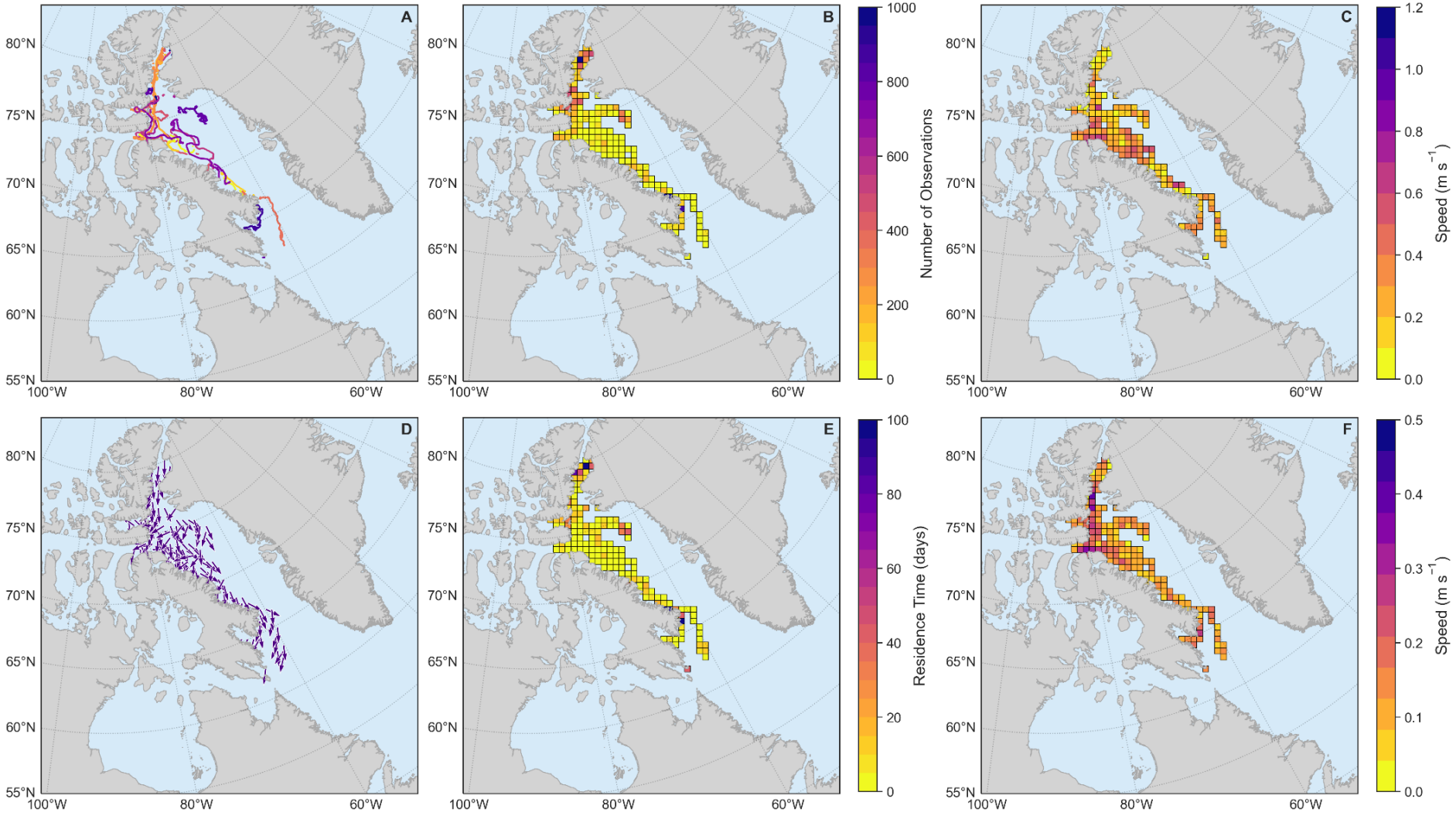

Figure 3-5: a) Drift tracks (one colour per iceberg); b) number of observations; c) median drift speed; d) mean drift direction, e) mean residence time and f) standard deviation of drift speed during the fall (September, October, November) for 49 icebergs tracked between 2011 and 2020, calculated for 50 x 50 km grid cells.

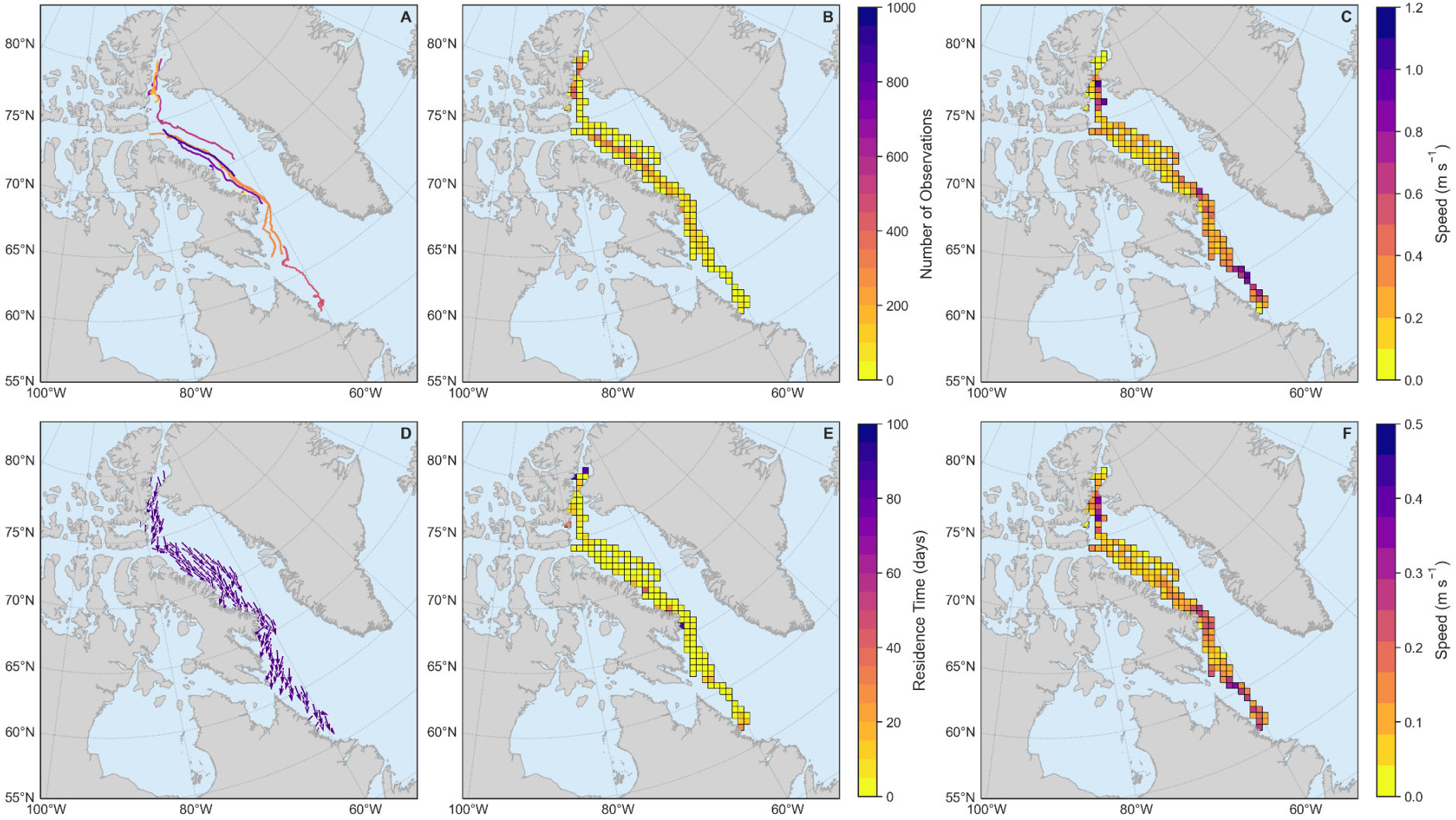

Figure 3-6: a) Drift tracks (one colour per iceberg); b) number of observations; c) median drift speed; d) mean drift direction, e) mean residence time and f) standard deviation of drift speed during the winter (December, January, February) for 21 icebergs tracked between 2011 and 2021, calculated for 50 x 50 km grid cells.

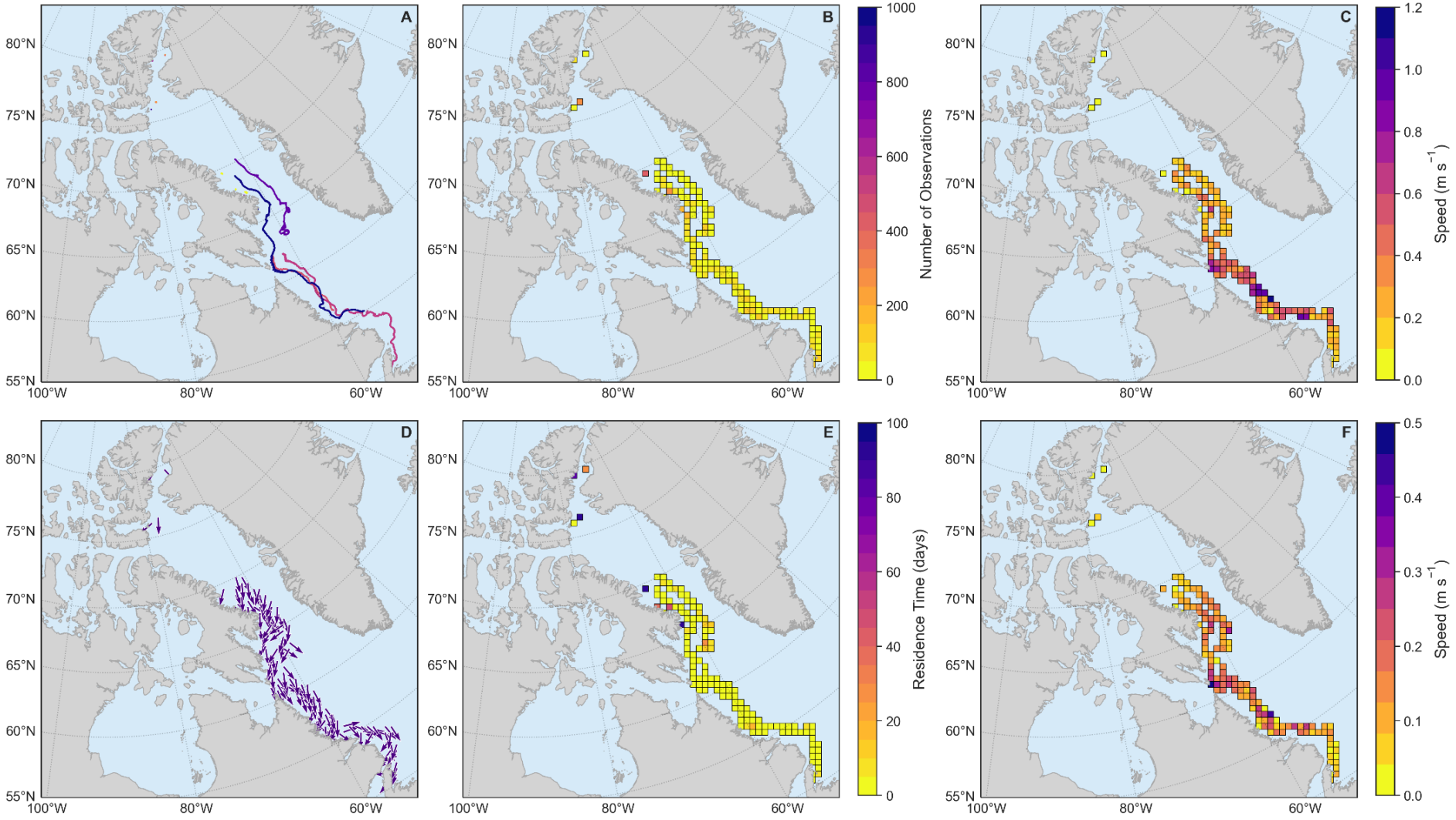

Figure 3-7: a) Drift tracks (one colour per iceberg); b) number of observations; c) median drift speed; d) mean drift direction, e) mean residence time and f) standard deviation of drift speed during the spring (March, April, May) for 14 icebergs tracked between 2012 and 2021, calculated for 50 x 50 km grid cells.

3.4.1.4 Spring

During the spring (March, April, May), a total of 14 beacons transmitted data between 2012 and 2019. Observations are mainly concentrated in the area south of 70°N, with some transmissions in Kane Basin and Smith Sound (Figure 3-7a, b). Speeds were highest along the coast of Labrador, with median drift speeds reaching 1.2 m s^{-1} around 57°N (Figure 3-7c), coincident with the area of greatest variability (Figure 3-7f). Drift speeds are also observed to be higher (~0.8 m s^{-1}) at the entrance of Hudson Strait. Median iceberg drift speeds decreased as icebergs drifted south towards Newfoundland.

Similar to the remainder of the year, mean iceberg drift direction was south/southeast along the coast of Baffin Island and Labrador (Figure 3-7d). As icebergs drifted south, the drift direction became more variable, especially as median speeds increased. The majority of mean iceberg residence times generally did not exceed 50 days, with the exception of icebergs located in Kane Basin and Smith Sound, which reached as high as 91 days on the southeast coast of Baffin Island (Figure 3-7e).

3.4.2 Evaluation of the 2% rule for iceberg drift speed

To determine whether the operational rule-of-thumb that icebergs drift at 2% of the wind speed can be applied to icebergs tracked in this study, we calculated the ratio (V_i/V_a) of iceberg speed (V_i) to ERA5 wind speed (V_a; Ettle, 1974) (Figure 3-8). The ratio was calculated for ERA5 wind speeds >1 m s^{-1} based on the assumption that icebergs can continue drifting under the influence of additional forces (e.g. ocean currents) when the potential influence of wind speeds is minimal. The speed ratio consistently exceeded 0.02 (2%) at all wind speeds, with a median speed ratio for all icebergs of 3.04%. The majority, 66.3%, of icebergs drifted at speeds => 2% of the wind speed, while the speed ratio was <=2% for the remaining 33.7%. For wind speeds below 5 m s^{-1}, the speed ratios were generally higher, and in some cases reached over 100%. In contrast, for wind speeds above 15 m s^{-1} the speed ratio was lower and generally did not exceed 20%, indicating that multiple factors are likely to influence iceberg drift at any given time.

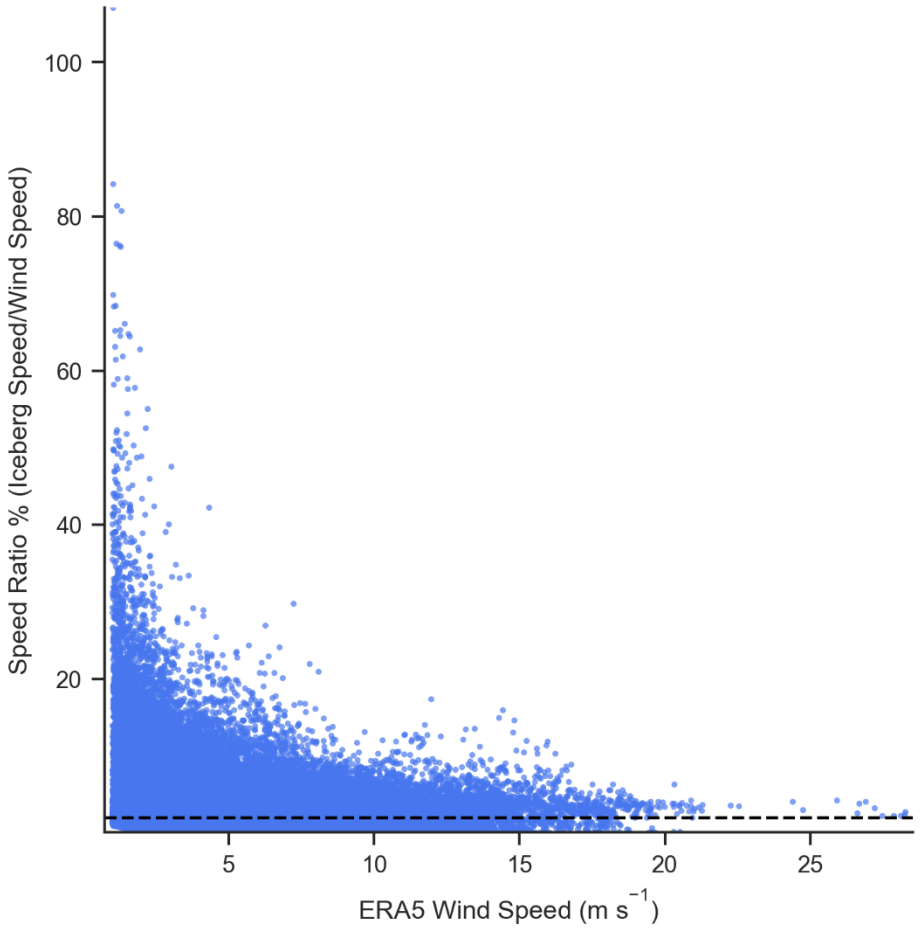

Figure 3-8: Ratio between iceberg drift speed and ERA5 wind speed for all icebergs in the study. The dashed black line represents a speed ratio of 2%.

We used polynomial regression to determine whether a statistical relationship exists between ERA5 wind speed and speed ratio. Results show a low, but significant correlation ($p < .0001$), for both a linear relationship ($R^2 = 0.07$) and 2nd and 3rd degree polynomials ($R^2 = 0.10$ and 0.12, respectively). This analysis indicates that while variability exists, it is likely that iceberg drift is more wind driven when wind speeds are higher, but drift is driven by a combination of factors such as ocean and tidal currents when wind speeds are lower. We investigate these factors further below.

3.4.3 Drift characteristics

Given the large spatial and temporal scope of our regional iceberg drift dataset, which extends >4000 km from north to south over a period of up to 10 years in all seasons, it is difficult to make broad statements concerning the controls on iceberg motion. However, when looking at our complete dataset and auxiliary environmental data in detail there are three iceberg drift characteristics that stand out:

i) High drift speeds and acceleration of icebergs between Kane Basin and Smith Sound;
ii) High surface currents and intrusion of icebergs into the entrance of Lancaster Sound and meandering east of Bylot Island, and;
iii) Tidal influence and looping of icebergs at the southern entrance to Baffin Bay in western Davis Strait.

The following discussion focuses on the iceberg drift patterns in these locations, using a subset of nine particularly long duration drift tracks. We first provide a detailed description of iceberg speed for each subset. We then investigate the potential relationships between iceberg drift and environmental variables including wind, ocean currents, tides, and sea ice using ERA5 and GLORYS reanalysis data, WebTide Tidal Prediction models, and CIS digital ice charts.

3.4.3.1 High drift speeds

Beacon *300234011242410* was deployed August 25, 2013 onto a tabular iceberg in Kane Basin (79.258°N, 71.817°W), with a surface extent of ~600 m x 300 m and a freeboard of ~20 m (Figure 3-9a). The iceberg had a mean speed of 0.17 m s^{-1} within Kane Basin for over a year, drifting between approximately 79-80°N in a looping pattern. The section of Nares Strait between Kane Basin and Smith Sound is characterized by strong tidal currents which can lead to bidirectional

movement (northward and southward) of sea ice, depending on tidal direction (Vincent & Marsden, 2008). The highest speed observed in our entire dataset occurred from October 1-4, 2014, when the iceberg accelerated south, reaching a drift speed of 2.31 m s^{-1} (Figure 3-10). Drift speeds decreased to <1.5 m s^{-1} south of approximately 76°N as the iceberg drifted along the coasts of Coburg and Devon islands and into the entrance of Lancaster Sound, before contact was lost on October 27, 2014. Beacon *300234061768060* was deployed on 17 August 2016 onto a tabular iceberg in Kane Basin (79.836°N, 67.357°W; Figure 3-9b), ~300 m x 185 m in size. Four months after deployment, the iceberg began drifting south through Nares Strait and into Smith Sound where, similar to *300234011242410*, it began to accelerate, reaching a maximum drift speed of 1.36 m s^{-1} on 19 December 2016 before decelerating south of approximately 75°N (Figure 3-10).

Limited observations exist of iceberg drift through Nares Strait, although the WH-5 ice island fragment, initially part of the Ward Hunt Ice Shelf, was tracked from Kennedy Channel to Smith Sound using radio tracking beacons and oil drums in August 1963 (Nutt, 1966). Through this portion of Nares Strait, WH-5 drifted south under the influence of northerly winds, reaching maximum reported drift speeds of ~0.19 m s^{-1} and occasionally moving northward or becoming immobile. Consistent with our observations of beacon *300234011242410*, WH-5 fragments appeared to disintegrate shortly after reaching the relatively warmer open waters of Smith Sound and northern Baffin Bay (Nutt, 1966). Increased mobility is also likely influenced by bathymetry, which deepens abruptly from <200 m in Kane Basin to >500 m in northern Smith Sound (Davis et al., 2018; Jakobsson et al., 2020; Figure 3-10).

To investigate factors controlling the observed drift speed for iceberg *300234011242410* during the high velocity period in October 2014 we explored relationships with GLORYS ocean currents, sea ice drift, and ERA5 wind speed. Within Nares Strait, the median difference between iceberg speed and surface ocean current speed was 0.08 m s^{-1}. CIS historical ice charts show that a dense sea ice pack (9/10 concentration) was present in Nares Strait between September 29, 2014, and October 6, 2014, which opened to bergy water (1/10 concentration) in Smith Sound.

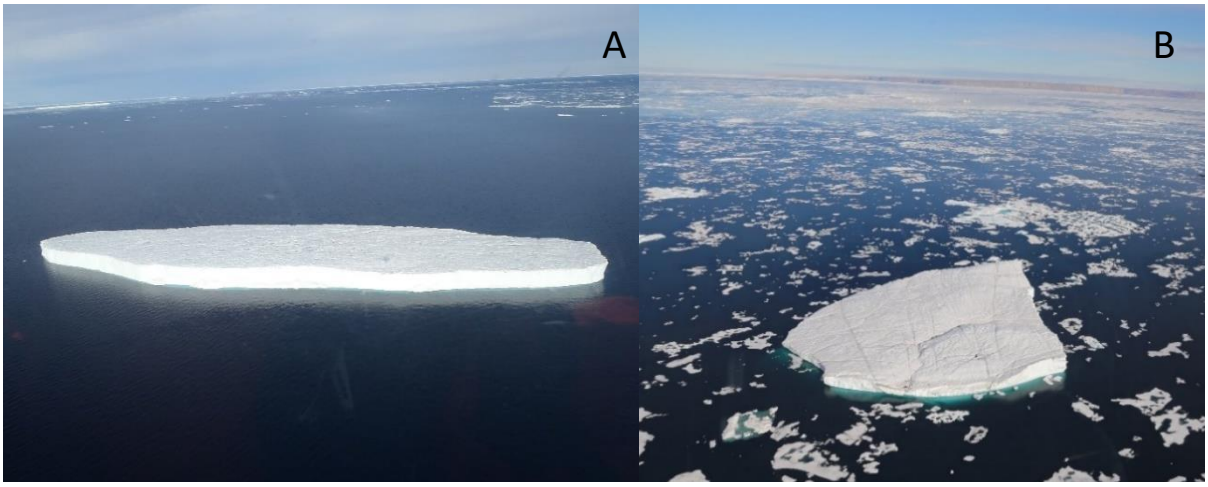

Figure 3-9: a) Iceberg *300234011242410* on August 25, 2013 at 79.258°N, 71.817°W (approx. 300 m x 600 m) and b) Iceberg *300234061768060* on August 17, 2016 at 79.836°N, 67.357° (approx. 185 m x 300 m).

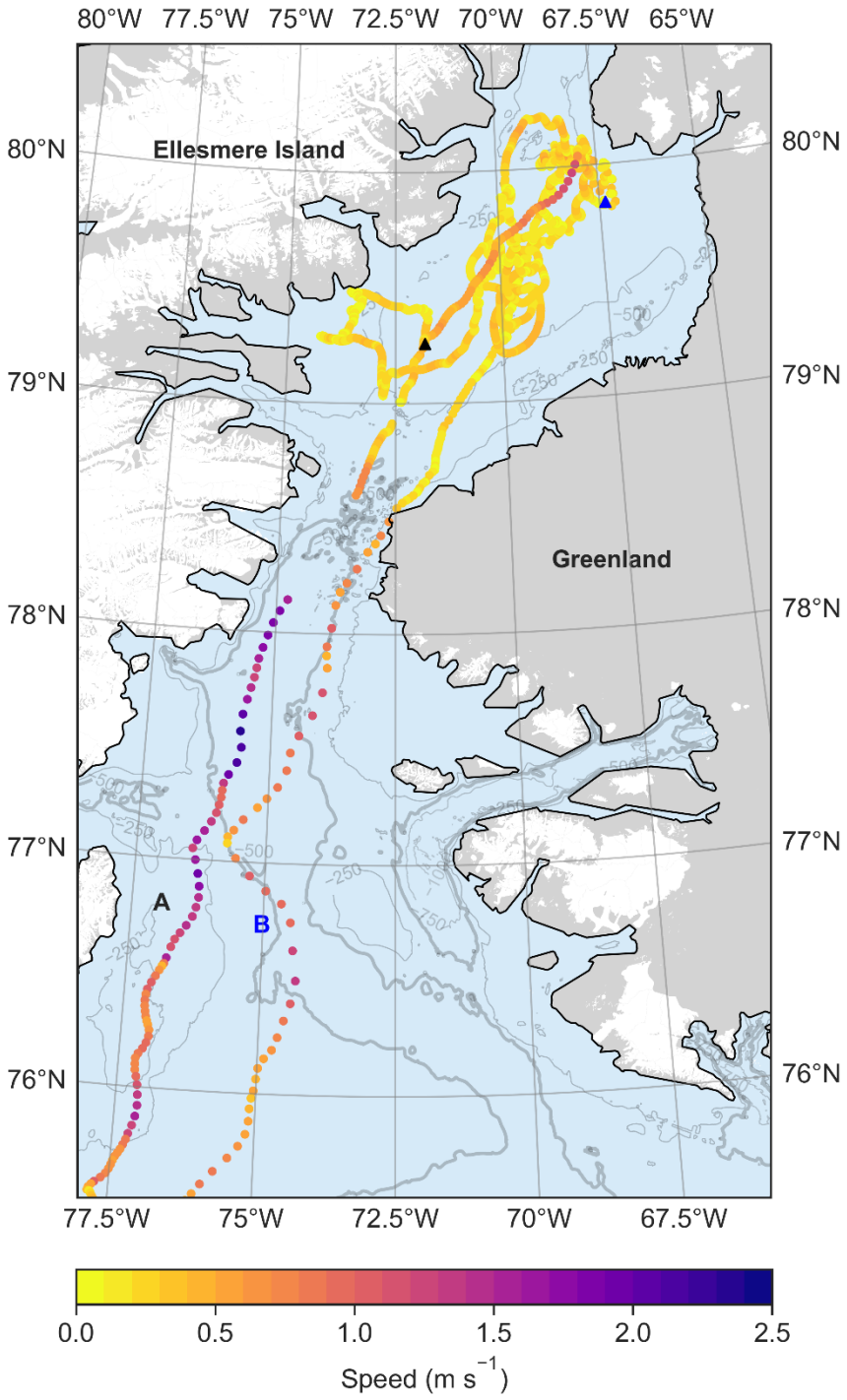

Figure 3-10: Drift speed (m s^{-1}) through Nares Strait of iceberg *300234011242410* (track A, deployment location at black triangle) and iceberg *300234061768060* (track B, deployment location at blue triangle). Glacier outlines: RGI 6.0 (RGI Consortium, 2017) and Mouginot & Rignot (Greenland; 2019). Bathymetry: International Bathymetric Chart of the Arctic Ocean (GEBCO), Jakobsson et al. (2020)

In Figure 3-11 we present analysis of hourly wind and ocean speed data compared to iceberg speed for the period 25 September to 10 October 2014. Both ERA5 and automatic weather station (AWS) data from Hans Island (80.828°N, 66.459°W; Figure 3-1) show that the period of maximum iceberg drift between 1-4 October 2014, and the build up to it, corresponded with a similar increase and then decrease in wind speeds (Figure 3-11). This station, located in the northern part of Nares Strait, has public data available from 2014 to 2020 (https://dataservices.sams.ac.uk/aws/; Wilkinson et al., 2009). Iceberg speed is more highly correlated with ERA5 wind speeds (R^2 = 0.66; $p < .00001$), although we also found iceberg speed to be moderately correlated with GLORYS ocean surface current speeds ($R^2 = 0.48$) over the same time period. This suggests that there is likely a combination of factors influencing iceberg drift during high speed events, including both wind and ocean currents.

According to GEBCO, this region also has relatively shallower bathymetry (200-250 m depths) compared to Smith Sound (>500 m depth). Once icebergs drift south from Nares Strait speeds tend to increase (>1 m s^{-1}) into Smith Sound and the Pikialasorsuaq, as the sea ice concentration decreases. Comparison with GLORYS ocean surface currents extracted along the same tracks from December 14-20 2014 showed a higher, but still moderate, correlation with iceberg drift speeds (R^2=0.38, $p <0.0001$).

Given the presence of low-level atmospheric jets in Nares Strait during winter (Samelson & Barbour, 2008; Kohnemann & Heinemann, 2021), it is likely that southerly iceberg drift at high speeds in this region is influenced by local wind events in combination with increased ocean surface current speed. These results suggest that high wind events and increased ocean surface currents through Nares Strait may play a significant role in influencing short-term iceberg drift, even in the presence of a close sea ice pack in Kane Basin. It is therefore likely that for the duration of these drift tracks, a combination of factors including sea ice cover and ocean and wind conditions are the controlling factors on iceberg speed and direction.

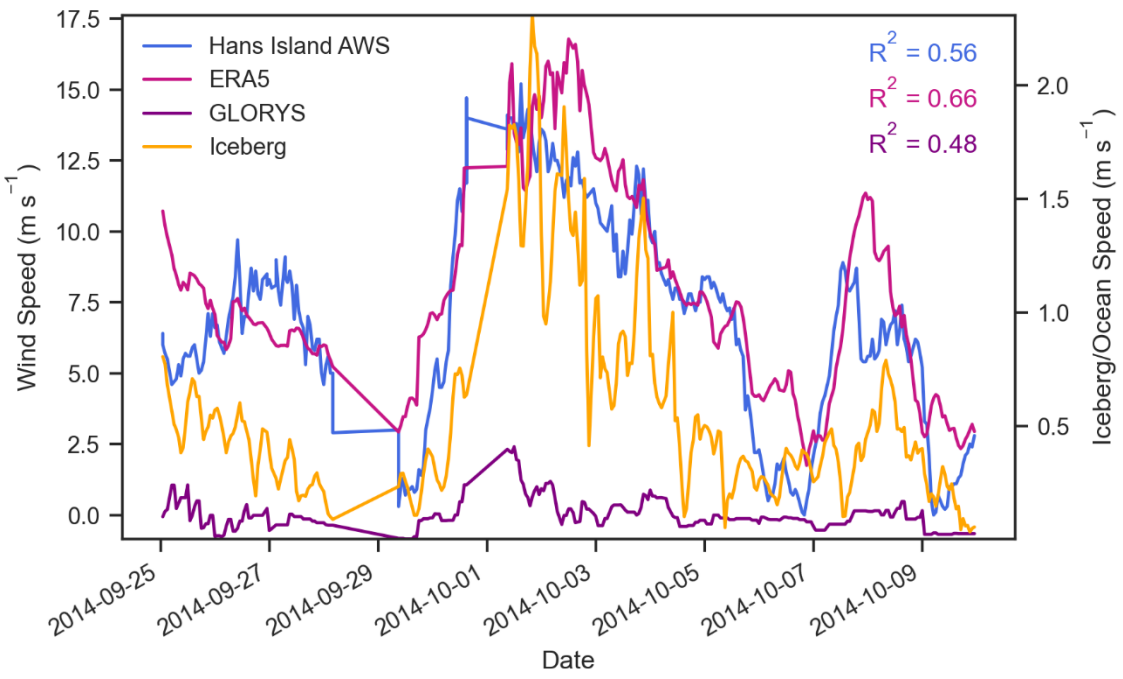

Figure 3-11: Time series of iceberg drift speed, Hans Island AWS observed mean wind speed, GLORYS ocean surface current speed, and ERA5 wind speed for iceberg *300234011242410*.

3.4.3.2 Surface ocean currents

The locations of four tabular icebergs from this study that drifted south through Baffin Bay before drifting west and intruding into Lancaster Sound, following the BIC (Fissel et al., 1982), are shown in Figure 3-12. Beacon *300234063515450* was deployed August 12, 2016 (Figure 3-12a), beacon *300234060692710* was deployed July 30, 2017 (Figure 3-12b), beacon *300234062328750* was deployed July 25, 2017 (Figure 3-12c), and beacon *300234062327750* was deployed July 30, 2017 (Figure 3-12d).

Icebergs *300234063515450* and *300234062327750* both closely followed the eastern coast of Devon Island while drifting south, before drifting west along the northern edge of Lancaster Sound. Iceberg *300234062328750* drifted farther from the coast of Devon Island before entering the northern side of Lancaster Sound. These three icebergs then drifted along the northern side of Lancaster Sound, generally following the BIC along the 500 m isobath (Fissel et al., 1982; Melling et al., 2001; Crawford & Mueller, 2023). Between approximately 80° and 82.5°W, the icebergs began drifting southward to cross Lancaster Sound before moving east along the northern coast of Bylot Island and exiting Lancaster Sound. One iceberg, *300234060692710*, did not follow this trajectory and instead drifted south across the entrance to Lancaster Sound, before drifting west through the centre of the sound, and then accelerating southwards into Navy Board Inlet where it became grounded on the shore of Bylot Island. We received confirmation of the likely deterioration of iceberg *300234060692710* when the tracking beacon was located on a beach in Navy Board Inlet by a community member from Pond Inlet, Nunavut in March 2020 (T. Allooloo & C. Innuarak, personal communication, March 9, 2020).

The BIC reaches speeds of 1 m s^{-1} around the southeastern coast of Devon Island and maintains surface flow speeds of 0.75 m s^{-1} at its centre 20-25 km offshore during its intrusion into Lancaster Sound (Fissel et al., 1982). Currents at all depths in Lancaster Sound tend to be stronger in the summer and fall than in the winter and spring (Tang et al., 2004). The influence of this pattern is provided by the acceleration of icebergs *300234063515450* and *300234062327750* as they drifted south past Devon Island and westward into Lancaster Sound. East of Bylot Island, where the BIC detaches from the coast and begins to move southward along Baffin Island, meanders, eddies, and northerly counter-flows are common which we observed for the drift paths of icebergs *300234063515450, 300234062327750, and 300234062328750* (Figure 3-13a). For all four

icebergs, the median difference between iceberg speed and surface ocean current speed was 0.11 m s^{-1}. Each of these four icebergs drifted into Lancaster Sound between August and October when CIS ice charts for August-October 2016 and 2017 show that the region was largely clear of sea ice (concentration <5/10, bergy water) until late October, when concentrations reached 9+/10.

To investigate the potential influence of tides on iceberg drift in this region, we used data from the WebTide Tidal Prediction Model Application to predict historical tidal current speed in Lancaster Sound (74°N, 80°W). For August-October in 2016 and 2017, when these four icebergs drifted into Lancaster Sound, maximum daily tidal currents reached 0.11 m s^{-1} in both years. There are no consistent semi-diurnal drift patterns that match tidal periodicity for the icebergs in this region.

Previous studies state that while iceberg drift into Lancaster Sound is a common trajectory, icebergs in this region do not exceed drift speeds of ~0.3 m s^{-1} (Robe et al., 1980; Marko et al., 1982; Tang et al., 2004). However, our study indicates that icebergs drifting near the entrance of Lancaster Sound can move much more quickly, consistently exceeding 0.3 m s^{-1} and reaching maximum speeds of ~1.2 m s^{-1} (Figure 3-13a). Analysis of GLORYS ocean surface vectors extracted nearest to the time of observation show an acceleration of ocean currents around the SE coast of Devon Island to ~0.5 m s^{-1}, generally following the 500 m isobaths (Figure 3-13b). Ocean surface current velocity decreases through the middle of Lancaster Sound before reaching its peak of ~1.2 m s^{-1} along the north coast of Bylot Island. Velocities once again decrease and current direction becomes more variable east of Bylot Island in the region where the BIC and WGC converge.

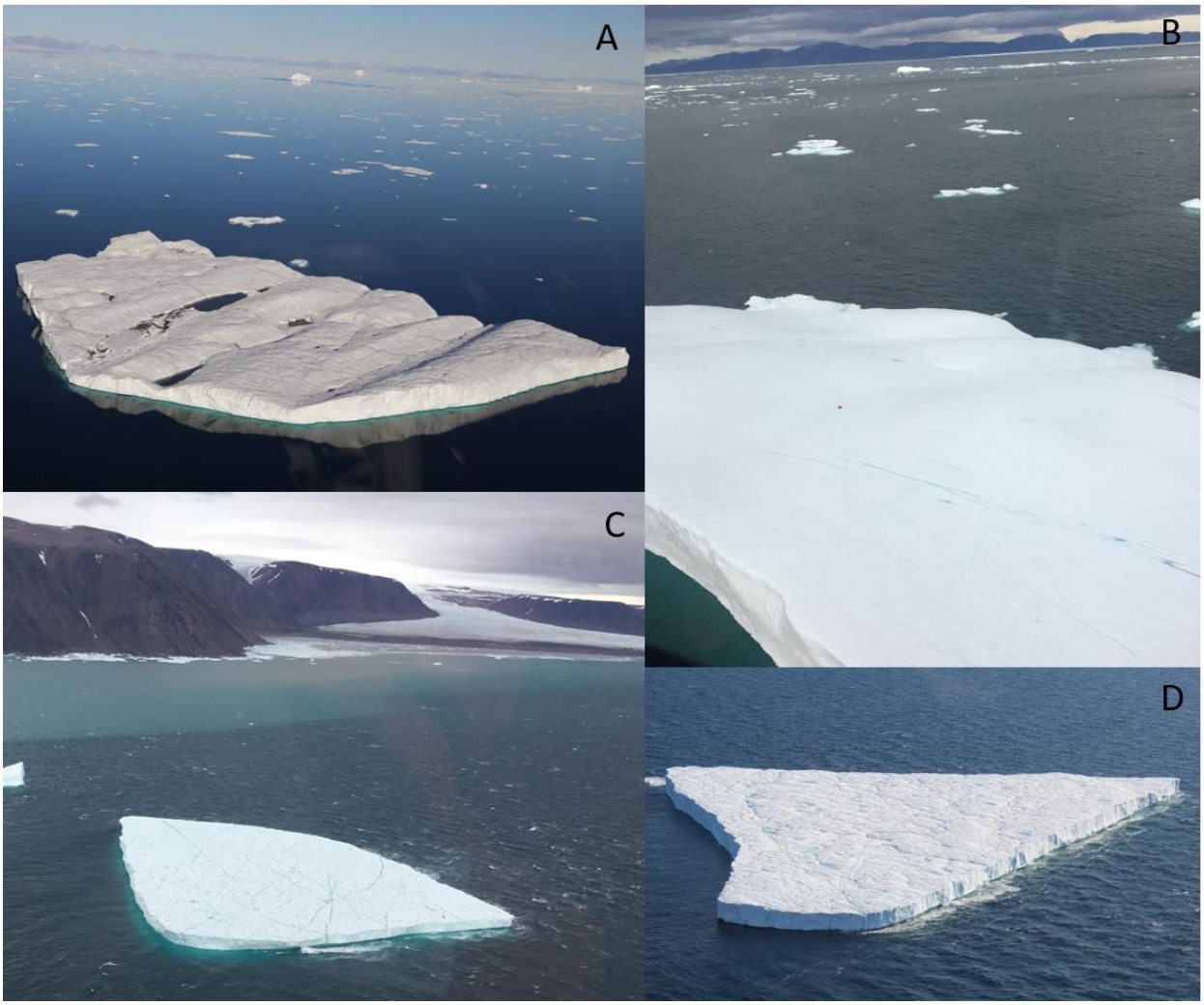

Figure 3-12: Iceberg a) *300234063515450* at 76.387°N, 76.331°W on August 12, 2016 (420 m x 320 m), b) *300234060692710* at 76.177°N, 81.629°W on July 30, 2017 (150 m x 75 m), c) *300234062327750* at 76.121°N, 80.975°W on July, 30 2017 (315 m x 215 m), and d) *300234062328750* at 76.316°N, 75.145°W on July, 25 2017 (600 m x 425 m).

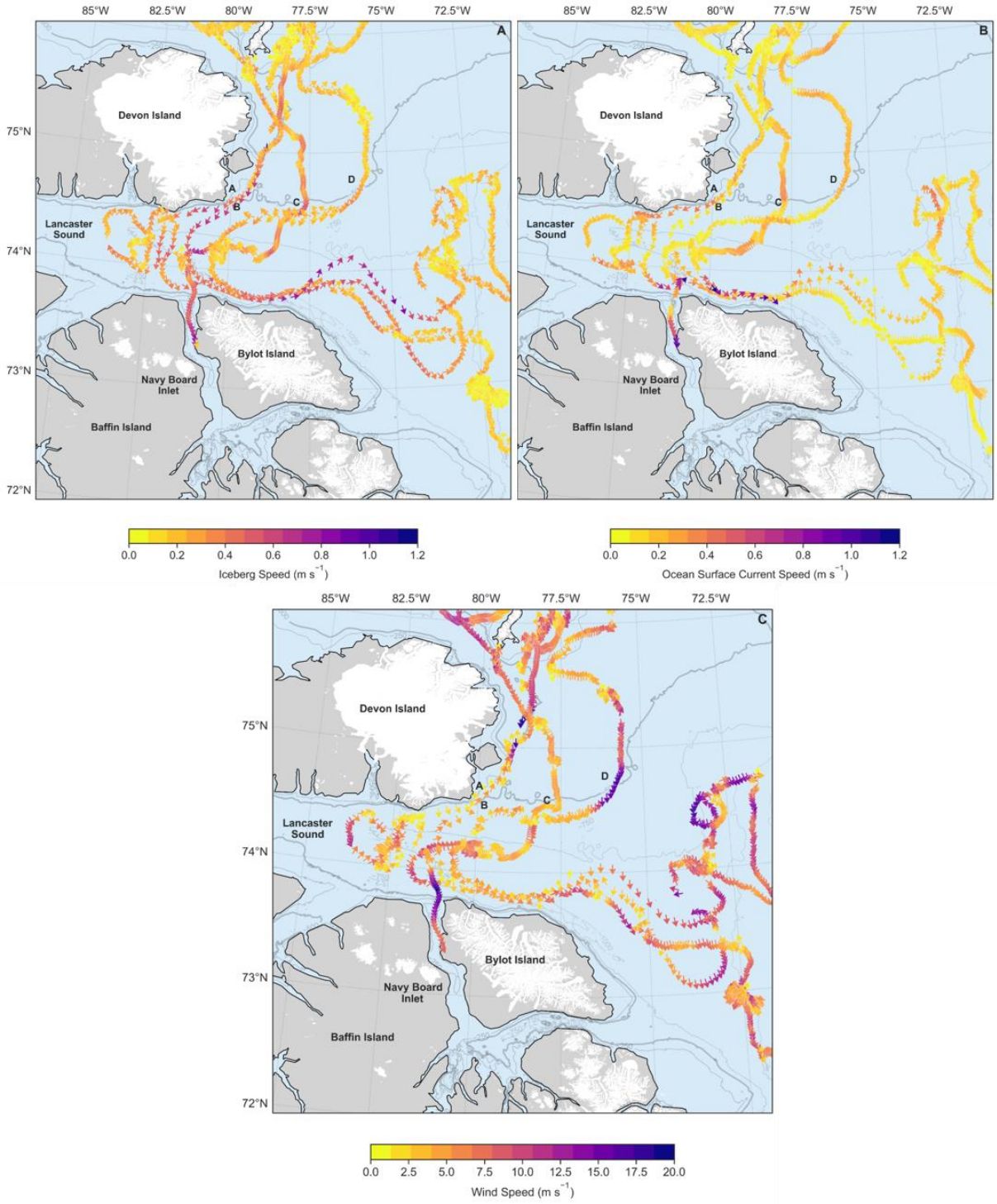

Figure 3-13: a) Iceberg drift speed (m s^{-1}); b) GLORYS ocean surface current velocity (m s^{-1}); and, c) ERA5 wind velocity (m s^{-1}) in Lancaster Sound of icebergs A: *300234063515450* (August 12-October 10, 2016), B: *300234062327750* (October 19-December 13, 2017), C: *300234060692710* (August 4-September 10, 2017), and D: *300234062328750* (July 25-October 9, 2017). Glacier outlines: RGI 6.0 (RGI Consortium, 2017). Bathymetry: International Bathymetric Chart of the Arctic Ocean (GEBCO), Jakobsson et al., (2020).

ERA5 wind speed and direction vary throughout Lancaster Sound, including the presence of localized high wind events. For example, iceberg *300234060692710* followed the pattern of intrusion into Lancaster Sound south of Devon Island before drifting towards Bylot Island. At the entrance of Navy Board Inlet, GLORYS ocean surface currents were observed to be moving approximately eastward at speeds of <0.2 m s^{-1}. Simultaneously, ERA5 reanalysis data showed a localized southerly wind event exceeding 19 m s^{-1} which likely influenced the southern drift of iceberg *300234060692710* into Navy Board Inlet (Figure 3-13c). These iceberg drift patterns observed in Lancaster Sound are consistent with those observed in previous studies (Riggs et al., 1980; Fissel et al., 1982; Marko et al., 1982) and can likely be attributed to surface ocean currents and eddies. Icebergs that drifted south close to the SE coast of Devon Island within the BIC were observed to drift faster (>1 m s^{-1}) than those which drifted south offshore (<1 m s^{-1}) before intruding into Lancaster Sound.

3.4.3.3 Tidal influence

Davis Strait is a 350 km wide strait that connects Baffin Bay to the Labrador Sea with a sill depth of ~650 m (Tang et al., 2004; Wu et al., 2013). It marks one of the areas in Baffin Bay where the WGC diverts flows from northward to westward, connecting with the southward flowing BIC and eventually connecting with the Labrador Current (LC; Figure 3-1). Davis Strait is characterized by strong tidal and non-tidal currents, which can reach speeds of up to 2 m s^{-1} near the entrance of Hudson Strait (Wu et al., 2013).

Three icebergs from this study that drifted through Davis Strait and past the entrance of Hudson Strait are shown in Figure 3-14. Beacon *300234011240410* was deployed on August 25, 2013 (79.169°N, 71.397°W) onto a tabular iceberg 500 m x 500 m in size (Figure 3-14a). Beacon *300234011241410* was also deployed on August 25, 2013 (79.292°N, 71.445°W) onto a tabular iceberg 1500 m x 300 m in size (Figure 3-14b). Beacon *300434063415110* was deployed on August 27, 2018 (75.771°N, 78.516°W) onto a tabular iceberg 270 m x 200 m in size (Figure 3-14c). Each iceberg drifted south through Baffin Bay and Davis Strait towards Resolution Island and the entrance of Hudson Strait. Icebergs *300234011240410* and *300234011241410* reached this area by February 2014 and iceberg *300434063415110* reached it by April 2019.

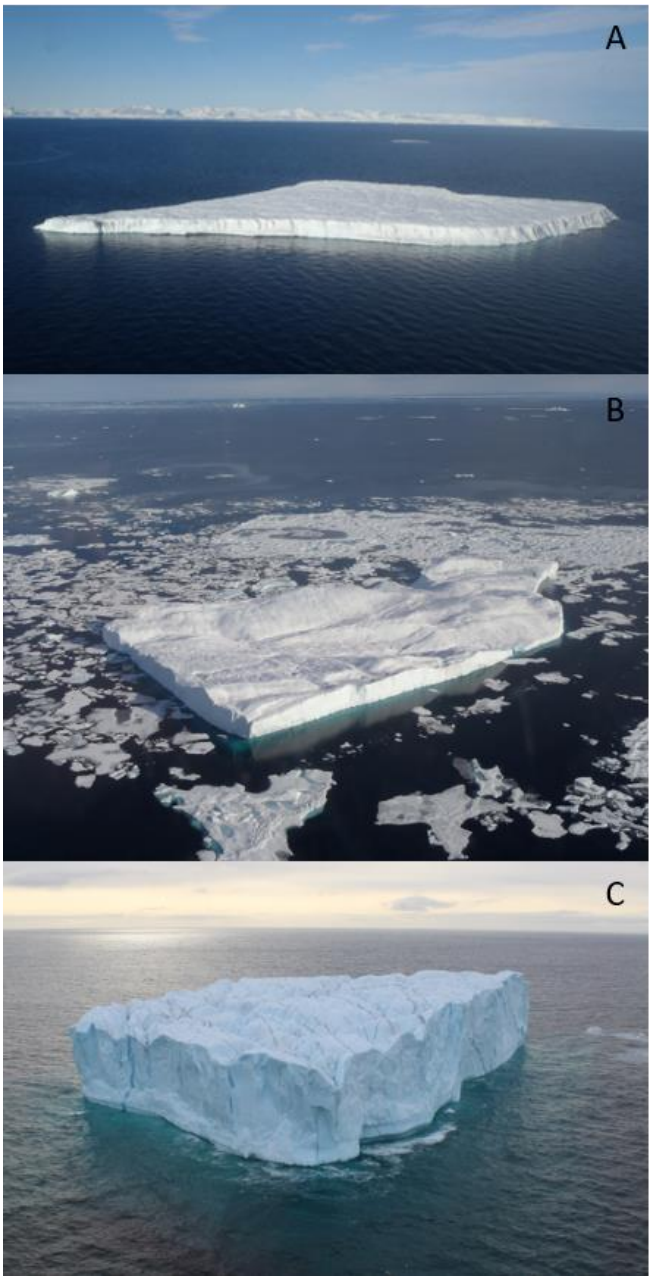

Figure 3-14: Icebergs a) *300234011240410* at 79.170°N, 71.397°W on August 25, 2013 (500 m x 500 m), b) *300234011241410* at 79.292°N, 71.445°W on August 25, 2013 (1500 m x 300 m), and c) *300434063415110* at 75.771°N, 78.516°W on August 27, 2018 (270 m x 200 m).

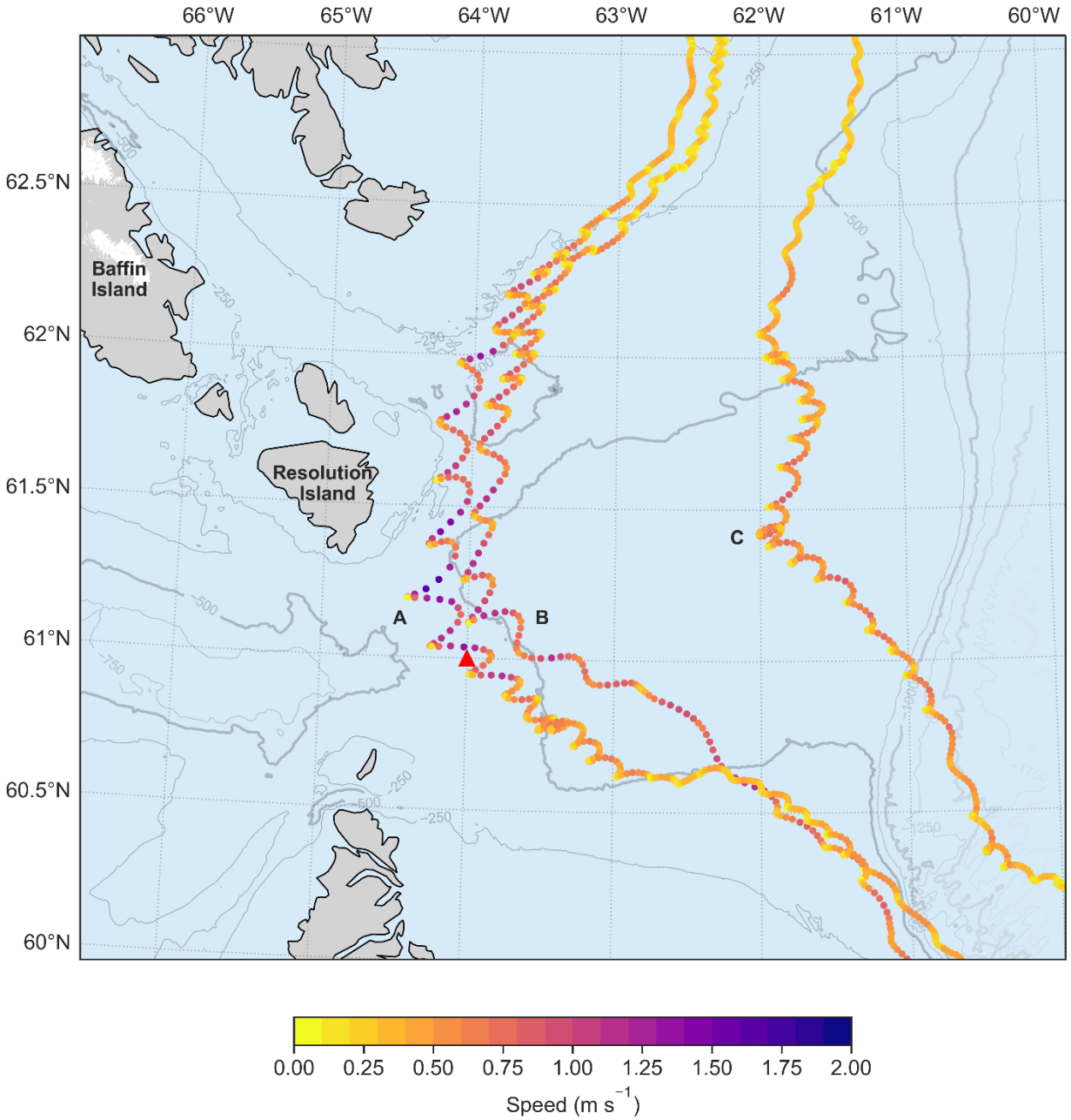

Figure 3-15: Iceberg drift speed (m s^{-1}) near the entrance of Hudson Strait of icebergs A: *300434063415110*, B: *300234011240410*, and C: *300234011241410*. Glacier Outlines: Randolph Glacier Inventory (RGI) Consortium (RGI Consortium, 2017). Red triangle denotes location of WebTide tidal current data. Bathymetry: General Bathymetric Chart of the Oceans (GEBCO), GEBCO Compilation Group (2022).

All three icebergs began to accelerate through Davis Strait upon approaching Resolution Island and the entrance to Hudson Strait, approximately following the Baffin Island shelf (~600 m; Figure 3-15). During this approach, each iceberg also exhibited clear semi-diurnal oscillations. Although currents in this region are dominated by both strong tidal and non-tidal currents (Wu et al., 2013), this relationship would likely not be detectable in the GLORYS model data as it does not consider tides. We found a median difference of 0.16 m s^{-1} between iceberg speed and surface ocean current speed for icebergs *300234011240410, 300234011241410,* and *300434063415110* as they drifted through Davis Strait (60-65°N).

To determine whether tidal currents influence iceberg drift in this region, we compared hourly iceberg drift speed with hourly tidal current speed using data from the WebTide Tidal Prediction Model Application (https://www.bio.gc.ca/science/research-recherche/ocean/webtide/index-en.php) for the location 61°N, 64°W for iceberg *300434063415110* (Figure 3-16). The iceberg drifted past the entrance of Hudson Strait (~60-63°N) between April 10 and May 2, 2019, and the subsequent increase in iceberg drift speed closely followed the gradual increase in tidal amplitude, albeit with an apparent lag for some periods. Preceding the tidal current maximum from April 10-15, the iceberg speed underwent approximately 24h oscillations. As the tidal current speed increased from April 15-21, iceberg speed oscillations increased to approximately every 6h, consistent with the modelled tidal current, and continued in coupled oscillations until tidal current speed decreased to ~0.5 m s^{-1} (Figure 3-16). Maximum tidal current speed of 1.17 m s^{-1} occurred on April 20 at 11:00:00, while the maximum iceberg speed of 1.69 m s^{-1} (Figures 3-15 and 3-16) occurred on April 22 at 12:00:00, which is in agreement with the results of Garbo (2022).

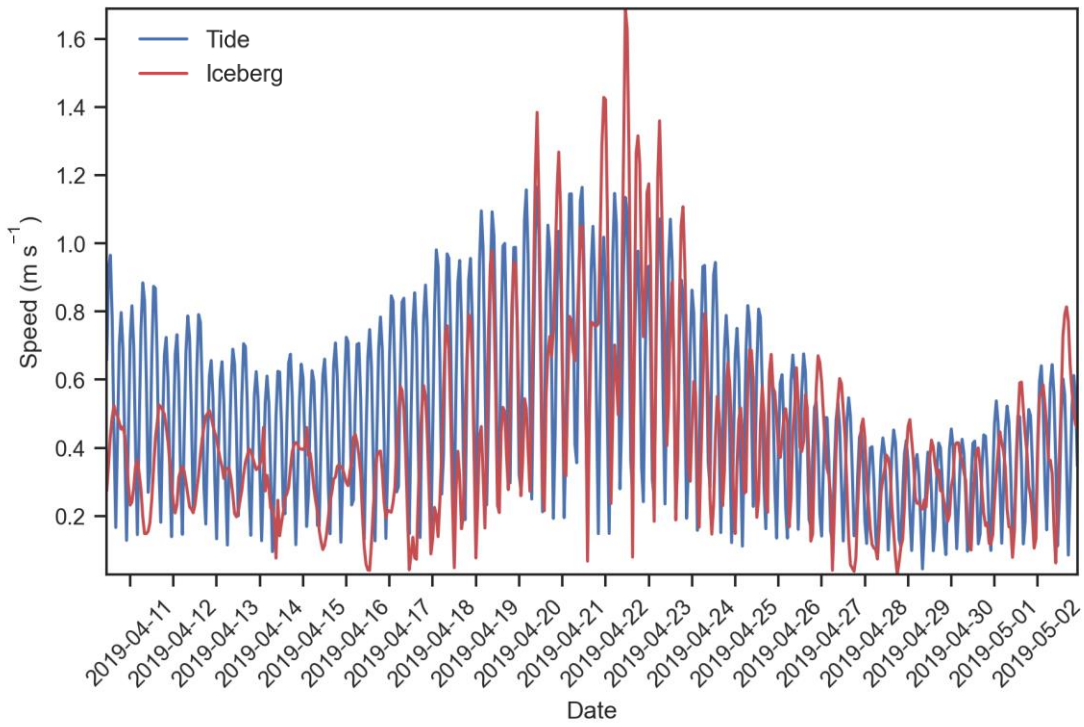

Figure 3-16: a) Hourly iceberg drift speed for iceberg *300434063415110* and hourly tidal current speed (at 61°N, 64°W), April 10-May 2, 2019.

Winds in Davis Strait are generally strongest during the winter (January-April), which contributes to the movement of sea ice from Baffin Bay to the Labrador Sea (Tang et al., 2004). Sea ice starts to form in western Davis Strait after September, along with the rest of Baffin Bay, while eastern Davis Strait will remain largely ice free throughout the winter season due to the relatively warmer WGC (Tang et al., 2004). In February 2014, when *300234011240410* and *300234011241410* were drifting through western Davis Strait, CIS historical ice charts show sea ice concentration of 9+/10 throughout the entire month. From April 1-15, 2019, when iceberg *300434063415110* was drifting through western Davis Strait, sea ice concentration ranged from 5 to 9+/10 concentration east of Resolution Island, before becoming 9+/10 concentration by May 6, 2019. Despite the presence of sea ice in both 2014 and 2019, icebergs *300234011240410*, *300234011241410*, and *300434063415110* continued drifting south past the entrance of Hudson Strait in a consistent oscillating pattern before returning to a relatively straight southeastward trajectory into the Labrador Sea.

3.5 Conclusion

In summary, our iceberg beacon database provides the most comprehensive record of long-term iceberg motion in the eastern Canadian Arctic to date, enabling a detailed description of the dominant iceberg drift patterns observed in Baffin Bay between 2011 and 2019. This fills a significant gap in our knowledge of the patterns of iceberg drift in Baffin Bay and provides important insights into the processes controlling their motion.

Icebergs in the eastern Canadian Arctic consistently drifted south/southeast along the east coast of Baffin Island and Labrador. The highest median speeds occurred during the winter and spring seasons, with areas of fastest flow through Nares Strait and through Davis Strait into the Labrador Sea. Consistent with the results of Crawford & Mueller (2023), which investigated common ice island fragment grounding locations in Baffin Bay, icebergs in this study commonly became grounded near eastern Coburg Island and along the SE coast of Baffin Island, where mean residence time exceeded 180 days in all seasons. Based on our observations of iceberg patterns through Baffin Bay between 2011 and 2019, it is apparent that the influence of environmental variables such as wind speed, surface ocean currents, and tidal currents varies with local

conditions. The relative importance of each environmental variable is often governed by local bathymetry and is likely further modulated by iceberg geometry.

For all icebergs in this study, drift speed often exceeded 2% of the wind speed, in particular when wind speeds were low, indicating that multiple factors are likely to influence iceberg drift at any given time. Results showed the median ratio for icebergs in this study was 3.04%. Based on this analysis, the rule-of-thumb used by operational forecasters to model iceberg drift in Canadian waters should be revisited for icebergs drifting in the eastern Canadian Arctic. The highest iceberg drift speed observed in this study of 2.31 m s^{-1} was likely influenced by a combination low-level atmospheric jets through Nares Strait (Samelson & Barbour, 2008; Kohnemann & Heinemann, 2021), resulting in strong winds in excess of 14 m s^{-1}, strong ocean currents, and bidirectional tidal currents (Melling et al., 2001; Vincent & Marsden, 2008). These variables, in combination with a deepening of bathymetry and the presence of the Pikialasorsuaq which results in lower sea ice concentrations, were likely the controlling factors in high drift rates for iceberg *300234011242410*. Consistent with the results of other studies (Fissel et al., 1982; Melling et al., 2001), strong surface currents of the BIC carry southward drifting icebergs from SE Devon Island into the entrance of Lancaster Sound, before returning them eastward of Bylot Island where they experience eddies, meandering, and northward flow. Oscillations in iceberg speed that were consistent with semi-diurnal tides lead us to believe that tidal currents were the primary factor controlling iceberg drift and contributing to high drift speeds in western Davis Strait.

Continued monitoring of iceberg drift through Canadian waters will be essential for further developing this dataset. Previous work suggests that the NAIS model is suitable for use north of 60°N (Garbo, 2022), but further validation is required to prove this, which relies on continued collection of in-situ iceberg observations like those monitored in this study. To reduce bias in the existing database, future iceberg tracking beacon deployment should occur during fall, winter, and spring seasons when possible, and capture non-tabular iceberg geometries. More investigation is needed to collect in-situ ocean and wind current data throughout Baffin Bay, which is currently scarce, to better quantify the influence of these factors on iceberg drift both in model and observational analysis. In this study, ERA5 and GLORYS models did not fully capture the influence of environmental variables on local iceberg drift patterns, likely due to their relatively low resolution. There is also a lack of direct bathymetric measurements in Canada (Chénier et al.,

2017), which would enhance our understanding of iceberg drift processes, particularly in inlets and fiords. Future work should focus on further refining estimates of the relative importance of winds, ocean currents, tides, and sea ice on iceberg drift. Given the recent increase in shipping traffic in the Canadian Arctic since the 1990s (Pizzolato et al., 2016; Dawson et al., 2022), results from this study can be used to identify the potential risks posed by icebergs along primary shipping routes and in offshore oil exploration areas along the east coast of Canada.

Data Availability

ERA5 wind reanalysis data are available through the Copernicus Climate Data Store (https://www.ecmwf.int/en/forecasts/datasets/reanalysis-datasets/era5). GLORYS12 ocean reanalysis data can be accessed through the Copernicus Marine Environment Monitoring Service website (CMEMS; https://marine.copernicus.eu/). Canadian Ice Service (CIS) weekly ice charts are available for download through the historical archive (https://iceweb1.cis.ec.gc.ca/Archive/page1.xhtml?lang=en).

References

Baumann, T. M., Polyakov, I. V., Padman, L., Danielson, S., Fer, I., Janout, M., Williams, W., & Pnyushkov, A. V. (2020). Arctic tidal current atlas. *Scientific Data*, 7(1), 275. https://doi.org/10.1038/s41597-020-00578-z

Bigg, G.R., Wadley, M., Stevens, D., and Johnson, A.J. (1996) Prediction of iceberg trajectories for the North Atlantic and Arctic Oceans. *Geophysical Research Letters*. 23. 10.1029/96GL03369.

Bigg, G. R., Wadley, M. R., Stevens, D. P., & Johnson, J. A. (1997). Modelling the dynamics and thermodynamics of icebergs. *Cold Regions Science and Technology*, 26(2), 113–135. https://doi.org/10.1016/S0165-232X(97)00012-8

Bigg, G. R., Cropper, T. E., O'Neill, C. K., Arnold, A. K., Fleming, A. H., Marsh, R., Ivchenko, V., Fournier, N., Osborne, M., & Stephens, R. (2018). A model for assessing iceberg hazard. *Natural Hazards*, 92(2), 1113–1136. https://doi.org/10.1007/s11069-018-3243-x

Canadian Ice Service (CIS). (2005) MANICE. Online. https://www.canada.ca/en/environment-climate-change/services/weather-manuals-documentation/manice-manual-of-ice.html.

Carlson, D. F., Boone, W., Meire, L., Abermann, J., & Rysgaard, S. (2017). Bergy Bit and Melt Water Trajectories in Godthåbsfjord (SW Greenland) Observed by the Expendable Ice Tracker. *Frontiers in Marine Science*, 4, 276. https://doi.org/10.3389/fmars.2017.00276

Chénier, R., Abado, L., Sabourin, O. and Tardif, L. (2017) Northern marine transportation corridors: Creation and analysis of northern marine traffic routes in Canadian waters. *Transactions in GIS*. 21. 10.1111/tgis.12295

Cook, A., Copland, L., Noël, B., Stokes, C., Bentley, M., Sharp, M., Bingham, R., Van den Broeke, M. 2019. Atmospheric forcing of rapid marine-terminating glacier retreat in the Canadian Arctic Archipelago. *Science Advances*¸ 5(3), 11pp, eaau8507. doi: 10.1126/sciadv.aau8507

Crawford, A. J., Mueller, D., Desjardins, L., & Myers, P. G. (2018). The Aftermath of Petermann Glacier Calving Events (2008–2012): Ice Island Size Distributions and Meltwater Dispersal. *Journal of Geophysical Research: Oceans*, 123(12), 8812–8827. https://doi.org/10.1029/2018JC014388

Crawford, A., & Mueller, D. (2023). Assessing Ice Island Drift Patterns, Ice Island Grounding Locations, and Gridded Bathymetry Products between Nares Strait and the North Atlantic. *Arctic*. https://doi.org/10.14430/arctic76227

Dalton, A., Van Wychen, W., Copland, L., Gray, L., & Burgess, D. (2022). Seasonal and Multiyear Flow Variability on the Prince of Wales Icefield, Ellesmere Island: 2009–2019. *Journal of Geophysical Research: Earth Surface*, 127(4). https://doi.org/10.1029/2021JF006501

Davis, P. E. D., Johnson, H. L., & Melling, H. (2019). Propagation and Vertical Structure of the Tidal Flow in Nares Strait. *Journal of Geophysical Research: Oceans*, 124(1), 281–301. https://doi.org/10.1029/2018JC014122

Dawson J., Pizzolato, L., Howell, S.E.L., Copland, L., and Johnston, M.E. (2018). Temporal and Spatial Patterns of Ship Traffic in the Canadian Arctic from 1990 to 2015. *Arctic*. 71(7), 15-26.

Dunphy, M., F. Dupont, C. G. Hannah, D. Greenberg. (2005). Validation of a Modelling System for Tides in the Canadian Arctic Archipelago. Canadian Technical Report of Hydrography and Ocean Sciences 243: vi + 70 pp.

Ettle, R. E. (1974). Statistical Analysis of Observed Iceberg Drift. *Arctic*, 27(2), 121–127. https://doi.org/10.14430/arctic2863

Fissel, D. B., Lemon, D. D., & Birch, J. R. (1982). Major Features of the Summer Near-Surface Circulation of Western Baffin Bay, 1978 and 1979. *Arctic*, 35(1), 180–200. https://doi.org/10.14430/arctic2318

Garbo, A. (2022) Validation of the North American Ice Service Iceberg Drift Model. *MSc thesis, University of Ottawa*. http://dx.doi.org/10.20381/ruor-27682.

Garrett, C. (1985). Statistical prediction of iceberg trajectories. *Cold Regions Science and Technology,* 11(3), 255-266.

GEBCO Compilation Group (2022) GEBCO_2022 Grid (doi:10.5285/e0f0bb80-ab44-2739-e053-6c86abc0289c)

Gutjahr, O., & Heinemann, G. (2018). A model-based comparison of extreme winds in the Arctic and around Greenland. *International Journal of Climatology*, 38(14), 5272–5292. https://doi.org/10.1002/joc.5729

Ingram, R. G., Bâcle, J., Barber, D. G., Gratton, Y., & Melling, H. (2002). An overview of physical processes in the North Water. Deep Sea Research Part II: *Topical Studies in Oceanography*, 49(22–23), 4893–4906. https://doi.org/10.1016/S0967-0645(02)00169-8

Ito, H. (1982). Wind Through a Channel—Surface Wind Measurements in Smith Sound and Jones Sound in Northern Baffin Bay. *Journal of Applied Meteorology*, 21(8), 1053–1062. https://doi.org/10.1175/1520-0450(1982)021<1053:WTACWM>2.0.CO;2

Jakobsson, M., Mayer, L. A., Bringensparr, C., Castro, C. F., Mohammad, R., Johnson, P., Ketter, T., Accettella, D., Amblas, D., An, L., Arndt, J. E., Canals, M., Casamor, J. L., Chauché, N., Coakley, B., Danielson, S., Demarte, M., Dickson, M.-L., Dorschel, B., … Zinglersen, K. B. (2020). The International Bathymetric Chart of the Arctic Ocean Version 4.0. *Scientific Data*, 7(1), 176. https://doi.org/10.1038/s41597-020-0520-9

Kochtitzky, W., Copland, L., Van Wychen, W., Hugonnet, R., Hock, R., Dowdeswell, J. A., Benham, T., Strozzi, T., Glazovsky, A., Lavrentiev, I., Rounce, D. R., Millan, R., Cook, A., Dalton, A., Jiskoot, H., Cooley, J., Jania, J., & Navarro, F. (2022). The unquantified mass loss of Northern Hemisphere marine-terminating glaciers from 2000–2020. *Nature Communications*, 13(1), 5835. https://doi.org/10.1038/s41467-022-33231-x

Kohnemann, S. H. E., & Heinemann, G. (2021). A climatology of wintertime low-level jets in Nares Strait. *Polar Research*, 40. https://doi.org/10.33265/polar.v40.3622

Lake, R. A., & Walker, E. R. (1976). A Canadian Arctic Fjord with Some Comparisons to Fjords of the Western Americas. *Journal of the Fisheries Research Board of Canada*, 33(10), 2272–2285. https://doi.org/10.1139/f76-274

Larsen, P.-H., Hansen, M. O., Buus-Hinkler, J., Krane, K. H., and Sønderskov, C. (2015). Field tracking (GPS) of ten icebergs in eastern Baffin Bay, offshore Upernavik, northwest Greenland. *J. Glaciol*. 61, 421–437. doi: 10.3189/2015JoG14J216

Marko, J., Birch, J., and Wilson, M. (1982). A Study of Long-Term Satellite-Tracked Iceberg Drifts in Baffin Bay and Davis Strait. *Arctic*, 35(1), 234-240. Retrieved from http://www.jstor.org/stable/40509318

Melling, H., Gratton, Y. and Ingram, G. (2001). Ocean circulation within the North Water polynya of Baffin Bay, *Atmosphere-Ocean*, 39:3, 301-325, DOI: 10.1080/07055900.2001.9649683

Moore, G. W. K. (2021). Impact of model resolution on the representation of the wind field along Nares Strait. *Scientific Reports*, 11(1), 13271. https://doi.org/10.1038/s41598-021-92813-9

Mouginot, J., & Rignot, E. (2019). Glacier catchments/basins for the Greenland Ice Sheet (Version 1, p. 4137543 bytes) [Data set]. Dryad. https://doi.org/10.7280/D1WT11

Mouginot, J., Rignot, E., Bjørk, A. A., Van Den Broeke, M., Millan, R., Morlighem, M., ... and Wood, M. (2019). Forty-six years of Greenland Ice Sheet mass balance from 1972 to 2018. *Proceedings of the National Academy of Sciences*, 116(19), 9239-9244.

Münchow, A., Falkner, K. K., & Melling, H. (2015). Baffin Island and West Greenland Current Systems in northern Baffin Bay. *Progress in Oceanography*, 132, 305–317. https://doi.org/10.1016/j.pocean.2014.04.001

Nutt, D. C. (1966). The Drift of Ice Island WH-5. *Arctic*, 19(3), 244–262. https://doi.org/10.14430/arctic3432

Pizzolato, L., Howell, S.E.L., Dawson, J., Laliberté, F., and Copland, L. (2016). The influence of declining sea ice on shipping activity in the Canadian Arctic, *Geophysical Research Letters*, 43, 12,146–12,154, doi:10.1002/2016GL071489.

RGI Consortium. (2017). Randolph Glacier Inventory – A Dataset of Global Glacier Outlines: Version 6.0: Technical Report, Global Land Ice Measurements from Space, Colorado, USA [Data set]. Digital Media. https://doi.org/10.7265/N5-RGI-60

Riggs, N. P., Thangam Babu, P. V., Sullivan, M. A., & Russell, W. E. (1980). Iceberg drift observations in Lancaster Sound. *Cold Regions Science and Technology*, 1(3–4), 283–291. https://doi.org/10.1016/0165-232X(80)90056-7

Robe, R. Q., Maier, D. C., & Russell, W. E. (1980). Long-term drift of icebergs in Baffin Bay and the Labrador Sea. *Cold Regions Science and Technology*, 1(3–4), 183–193. https://doi.org/10.1016/0165-232X(80)90047-6

Samelson, R. M., & Barbour, P. L. (2008). Low-Level Jets, Orographic Effects, and Extreme Events in Nares Strait: A Model-Based Mesoscale Climatology. *Monthly Weather Review*, 136(12), 4746–4759. https://doi.org/10.1175/2007MWR2326.1

Savage, S. B. (2001). Aspects of Iceberg Deterioration and Drift. In N. J. Balmforth & A. Provenzale (Eds.), Geomorphological Fluid Mechanics (Vol. 582, pp. 279–318). Springer Berlin Heidelberg. https://doi.org/10.1007/3-540-45670-8_12

Scheick, J., Enderlin, E. M., & Hamilton, G. (2019). Semi-automated open water iceberg detection from Landsat applied to Disko Bay, West Greenland. *Journal of Glaciology*, 65(251), 468–480. https://doi.org/10.1017/jog.2019.23

Smith, S. D. (1993). Hindcasting iceberg drift using current profiles and winds. *Cold Regions Science and Technology*, 22(1), 33–45. https://doi.org/10.1016/0165-232X(93)90044-9

Smith, S. D., & Donaldson, N. R. (1987). Dynamic modelling of iceberg drift using current profiles. Fisheries and Oceans Canada.

Steffen, K. (1985). Warm water cells in the North Water, Northern Baffin Bay during winter. *Journal of Geophysical Research*, 90(C5), 9129. https://doi.org/10.1029/JC090iC05p09129

Steffen, K. (1986). Ice Conditions of an Arctic Polynya: North Water in Winter. *Journal of Glaciology*, 32(112), 383–390. https://doi.org/10.3189/S0022143000012089

Squire, V. A. (2007). Of ocean waves and sea-ice revisited. *Cold Regions Science and Technology*, 49(2), 110–133. https://doi.org/10.1016/j.coldregions.2007.04.007

Sulak, D. J., Sutherland, D. A., Enderlin, E. M., Stearns, L. A., & Hamilton, G. S. (2017). Iceberg properties and distributions in three Greenlandic fjords using satellite imagery. *Annals of Glaciology*, 58(74), 92–106. https://doi.org/10.1017/aog.2017.5

Tang, C. C. L., Ross, C. K., Yao, T., Petrie, B., DeTracey, B. M., & Dunlap, E. (2004). The circulation, water masses and sea-ice of Baffin Bay. *Progress in Oceanography*, 63(4), 183–228. https://doi.org/10.1016/j.pocean.2004.09.005

Valeur, H. H., Hansen, C., Hansen, K. Q., Rasmussen, L., & Thingvad, N. (1996). Weather, sea and ice conditions in eastern Baffin Bay, offshore northwest Greenland: A review. Mineral Resources Administration for Greenland, 96–12 (December), 37 pp.

Van Wychen, W., Burgess, D., Kochtitzky, W., Nikolic, N., Copland, L. and Gray, L. (2021). RADARSAT-2 derived glacier velocities and dynamic discharge estimates for the Canadian High Arctic: 2015-2020. *Canadian Journal of Remote Sensing*, 46(6), 695-714. doi: 10.1080/07038992.2020.1859359.

Vincent, R. F., & Marsden, R. F. (2009). A Study of Tidal Influences in the North Water Polynya using Short Time Span Satellite Imagery. *Arctic*, 61(4), 373–380. https://doi.org/10.14430/arctic45

Wagner, T. J. W., Dell, R. W., & Eisenman, I. (2017). An Analytical Model of Iceberg Drift. *Journal of Physical Oceanography*, 47(7), 1605–1616. https://doi.org/10.1175/JPO-D-16-0262.1

Wilkinson, J. P., Gudmandsen, P., Hanson, S., Saldo, R., & Samelson, R. M. (2009). Hans Island: Meteorological Data From an International Borderline. Eos, Transactions American Geophysical Union, 90(22), 190. https://doi.org/10.1029/2009EO220002

Wu, Y., Hannah, C. G., Petrie, B., Pettipas, R., Peterson, I., Prinsenberg, S., Lee, C. M., & Moritz, R. (2013). Ocean current and sea ice statistics for Davis Strait (No. 284; Canadian Technical Report of Hydrography and Ocean Sciences, p. 55).

Chapter 4: Coexistence of icebergs and ships in the eastern Canadian Arctic: 2012-2019

4.1 Introduction

Ship traffic throughout the Canadian Arctic Archipelago (CAA) has more than tripled in recent decades, with the average number of voyages increasing from 104 yr^{-1} from 1990-1994 to 381 yr^{-1} from 2015-2019 (Dawson et al., 2022). The greatest increase has been observed in Hudson Strait, where many mines are located on adjacent lands, followed by the Beaufort Sea and Baffin Bay. Shipping has increased significantly while reductions in sea ice concentration have occurred in many parts of the CAA (Pizzolato et al., 2016). Many communities in the North are inaccessible by road and therefore heavily reliant on shipping, meaning that the primary purpose of much of the shipping is related to resource extraction and resupply (Stephenson et al., 2015; Dawson et al., 2018). Nevertheless, since 1990, the fastest growing shipping sector by kilometres travelled has been pleasure crafts, such as recreational sailboats and private yachts (Dawson et al., 2018). Spatially, this increase has particularly occurred through the Northwest Passage (NWP; Pizzolato et al., 2016; Dawson et al., 2018, 2022), which has seen an overall increase in traffic from all ship types due to increased accessibility of Arctic waters due to climate change (Haas & Howell, 2015; Copland et al., 2021; Mudryk et al., 2021).

Icebergs that calve from tidewater glaciers in the CAA and western Greenland frequently drift into Baffin Bay, where they typically transit in a counter-clockwise direction before drifting southwards along the east coast of Canada (Valeur et al., 1996). Icebergs have both an above-water (freeboard) and below-water (keel) portion and can range in size from smaller fragments called bergy bits (< 5 m length) and growlers (5 to <15 m length) to large tabular ice islands several km^2 in area (Bigg et al., 1996; CIS, 2005). Throughout the eastern Canadian Arctic (ECA), iceberg drift is largely controlled by a combination of local conditions including short-term wind events, ocean surface currents, and tidal oscillations (Garbo, 2022; Chapter 3). In the ECA, icebergs can often become frozen in sea ice in the winter as they follow the shore of eastern Baffin Island, posing a threat to ships as they are difficult to detect within the sea ice pack (Marko et al., 1982; AC, 2009).

There is a great deal of variability between years in the number of icebergs that reach ‘Iceberg Alley’, the area between Baffin Bay and the Grand Banks populated with offshore oil platforms, and large numbers of vessel movements (Sudom et al., 2014). Icebergs within Iceberg Alley have

been monitored since 1913, one year after the sinking of the RMS Titanic following an iceberg collision on April 14, 1912. The International Ice Patrol (IIP) works in conjunction with the Canadian Ice Service (CIS) to monitor iceberg presence in the North Atlantic Ocean and provide iceberg warnings and charts to those navigating off the coast of Newfoundland and Labrador. The IIP monitors this region from February to July each year, and the CIS from August to January. However, ice charts do not provide estimates of iceberg conditions north of 60°N in the ECA (Figure 4-1). Since the sinking of the Titanic, several collisions between ships and icebergs navigating the polar regions have been documented, including the sinking of the *Finnpolaris* cargo vessel in 1991 in Baffin Bay and the *M/V Explorer* passenger vessel in Antarctica in 2007 (Figure 4-1; Table 4-1).

The risk to vessels operating in the Arctic varies depending on factors such as their level of ice strengthening, and sea ice conditions and concentration (Dawson et al., 2022). The Arctic Ice Regime Shipping System (AIRSS) and Polar Operational Limitation Assessment Risk Indexing System (POLARIS) are used to manage operational limitations in Arctic Canada based on current sea ice conditions. Presently, the ice numeral used in POLARIS to asses risk only takes into account sea ice type and concentration and does not include icebergs. The lack of inclusion of icebergs in current navigational risk assessments in combination with the remoteness of the Canadian Arctic, limited search and rescue (SAR) capabilities (Ford & Clark, 2019), and lack of bathymetric data (Chénier et al., 2017), highlights the need for improved long-term monitoring of icebergs and improved assessment of their potential risk to navigation (AC, 2009; AMAP, 2009; Kujala et al., 2018; Dawson et al., 2022).

While previous research has focused on the relationships between sea ice and Arctic shipping (Pizzolato et al., 2014; 2016; Copland et al., 2021; Dawson et al., 2018; 2022), there has been little analysis completed on characterization of iceberg-ship coexistence. Earlier work has focused mainly on compilation of past collisions between ships and icebergs (Hill, 2010). This study therefore presents the first overview of spatial and temporal patterns in iceberg-ship coexistence throughout the ECA from 2012-2019. Using a comprehensive database of automatic identification system (AIS) ship locations and a multi-year dataset of known iceberg drift tracks, the purpose of this study is to:

i) identify spatial and temporal patterns in iceberg drift and ship traffic throughout the ECA during the shipping season (July-October);
ii) establish areas of coexistence between icebergs and ships; and
iii) quantify changes in iceberg-ship coexistence along ECA shipping routes.

4.2 Study Area

4.2.1 Baffin Bay

Baffin Bay is an oceanic basin located in the Arctic, connecting the Arctic Ocean to Davis Strait and the Labrador Sea (Figure 4-1). Sea ice and icebergs drifting in Baffin Bay are influenced by two main ocean currents: the West Greenland Current (WGC) and the colder Baffin Island Current (BIC). The WGC flows northward along the west coast of Greenland until Smith Sound where it bends westward, and then begins moving southward along the eastern coast of Baffin Island (Melling et al., 2001; Tang et al., 2004). Icebergs and sea ice can be carried by this current around Baffin Bay and may eventually drift south into Davis Strait and the Labrador Sea (Valeur et al., 1996; Tang et al., 2004; Münchow et al., 2015).

Minimum sea ice cover occurs in September when remaining sea ice is only present near the coast of Baffin Island due to the relatively warm northward flowing WGC in the east (Tang et al., 2004). Sea ice begins to form in mid-October and is typically present in Baffin Bay throughout the year, reaching a maximum cover in March when it extends into Davis Strait (Valeur et al., 1996). Along the ECA coast, icebergs can often become frozen in sea ice as they follow the Baffin Island Current close to the shores of Baffin Island (Marko et al., 1982; Tang et al., 2004) and will remain static until the sea ice is free to move again. Given the presence of sea ice throughout Baffin Bay from approximately November to June (Tang et al., 2004), we identify the shipping season as July to October (Stephenson et al., 2013; Eguíluz et al., 2016).

4.2.2 NORDREG zone

The NORDREG zone (Figure 4-1) is the region north of 60°N in the Canadian Arctic in which vessels above a certain size threshold are required to report their position and vessel characteristics (e.g. name, call sign) to the Canadian Coastguard. Other vessels (e.g. small pleasure crafts) may

voluntarily report their position. It has been stated that approximately 98% of all ships operating in the NORDREG zone notify the Canadian Coast Guard of their presence (Rompkey and Cochrane, 2008), even if not required to by law, in part due to the advantages accompanied with reporting such as enhanced search and rescue response (also see Johnston et al., 2017). Here, we use the NORDREG zone to define the eastern and southern extent of analysis for iceberg-ship coexistence.

4.3 Methods & Data

4.3.1 Ship collision with iceberg database

Hill (2010) compiled a database of over 200 years of historical iceberg and ship collisions throughout the northern hemisphere, which is available for download (https://newicedata.com/the-ship-iceberg-collision-database/). Collision details were compiled from a variety of sources, ranging from newspaper reports and shipping gazettes to official inquires. Based on this database, a total of 42 ship iceberg collisions occurred between 1800 and 2006. We searched the Transportation Safety Board Marine Safety Information System (MARSIS) database between 2006 and 2023 (http://www.bst-tsb.gc.ca/eng/stats/marine/data-2.html) to identify any other collisions in our study area, but no additional collisions were reported during that period. Ship-iceberg collisions occurred throughout eastern Canada and are shown in Figure 4-1. Table 4-1 describes the vessel type, damage, and severity of each collision. Over 1/3 of all collisions resulted in the sinking of a vessel and four incidents resulted in confirmed fatalities, most recently in 1975 with the sinking of the *Aigle d'Ocean* in the Labrador Sea. A total of 8 collisions have occurred since 1990, four of which were located north of 72°N.

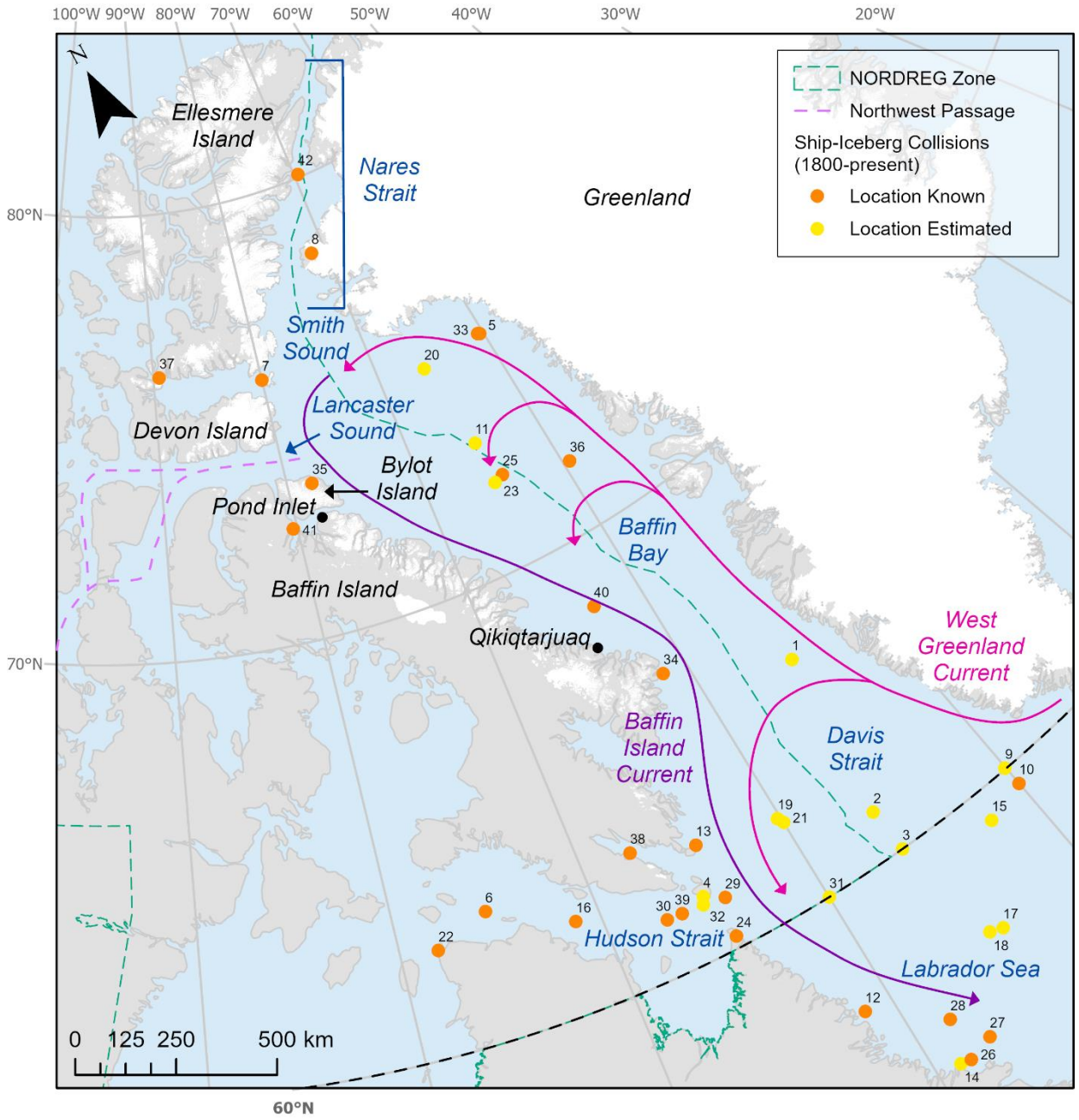

Figure 4-1: Map of study area, including location of main ocean currents and historical ship-iceberg collisions from 1800 to 2023 (Hill, 2010) throughout eastern Canada. Black dotted line shows the iceberg chart limit of 60°N. Canadian Coast Guard NORDREG Zone (Justice Laws, 2010). Glacier outlines: Randolph Glacier Inventory (RGI) 6.0 (RGI Consortium, 2017).

Table 4-1: List of historical ship-iceberg collisions from 1800-2023 (Hill, 2010; MARSIS, 2023) throughout eastern Canada. * Location estimated.

#	Vessel Name	Vessel Type	Date	Latitude (°N)	Longitude (°W)	Damage	Fatalities
1	Thomas*	Whaling Vessel	01/01/1812	65.00	55.00	No damage	No
2	Royalist*	Whaling Ship	05/04/1814	61.07	56.13	Sinking	Yes
3	London*	Whaling Vessel	01/01/1817	60.00	56.00	Sinking	Yes
4	Prince of Wales*	Sailing Ship	24/07/1821	61.42	65.12	Hole	Unknown
5	Progress	Whaling Brig	02/07/1830	75.10	60.30	Sinking	Unknown
6	Terror, HMS	Sailing Bomb Vessel	13/07/1837	63.00	75.30	Puncture	No
7	Intrepid, HMS	Steam Discovery Sloop	27/08/1851	76.00	80.00	Denting	Unknown
8	Advance	USS Brigantine	21/08/1853	78.36	71.50	Unknown	No
9	Fluorine*	Bark	01/10/1882	60.02	50.04	Denting	Unknown
10	Alumina	Bark	01/05/1884	59.55	50.00	Sinking	Unknown
11	Alert*	HMS Sloop (powered)	01/08/1884	73.00	65.00	No damage	No
12	Ethel	Sailing Vessel	25/07/1908	57.34	61.23	Sinking	Unknown
13	Snowdrop	Whaling Vessel	18/09/1908	62.54	64.30	Sinking	Unknown
14	Erik*	Wooden Steamer	21/09/1908	55.20	59.00	Denting	Unknown
15	Hugo*	Steam Schooner	05/05/1927	59.30	52.00	Sinking	Yes
16	Bright Fan	SS Cargo	01/10/1932	62.09	71.23	Sinking	No
17	Maia*	Schooner	11/10/1933	57.20	54.45	Sinking	Unknown
18	Saint Coulomb*	Fishing Schooner	11/04/1935	57.30	55.00	Sinking	Unknown
19	Maria Preciosa*	M/V Fishing Vessel	14/06/1944	62.15	60.15	Sinking	Unknown
20	Sappa Creek*	M/V Tanker	01/08/1951	75.00	66.00	Crushed	Unknown
21	Rio Caima*	M/V Fishing Schooner	01/09/1952	62.00	60.00	Sinking	Unknown
22	Kastela	SS Cargo	03/08/1963	62.45	78.10	Sinking	No
23	Westwind, USCG*	Cutter	01/07/1970	72.00	65.00	Unknown	No
24	Aigle d'Ocean	M/V Cargo	20/08/1975	60.27	64.59	Sinking	Yes
25	Arctic	M/V Bulk Carrier	17/10/1978	72.08	64.25	Hole	Unknown
26	Escort Protector	M/V Tug	10/06/1979	55.15	58.56	Unknown	Unknown
27	Pacnorse I	Drillship	25/07/1982	55.35	57.45	Cracks	Unknown
28	Kristina Logos	M/V Stern Trawler	22/06/1983	56.17	58.40	Hole	No
29	Mesange	M/V Cargo	21/07/1983	61.17	64.22	Hole	No
30	Evangelia C	M/V Bulk Carrier	31/07/1984	61.30	67.15	Unknown	Unknown
31	Ocean Prawns*	M/V Stern Trawler	16/08/1984	60.00	60.00	Sinking	No
32	Lucien Paquin*	M/V Cargo	20/07/1985	61.25	65.30	Denting	No
33	Terra Nova	M/V Cargo	31/07/1989	75.12	60.46	Unknown	Unknown
34	Des Groseilliers	CCGS Icebreaker	29/08/1989	66.34	61.40	Unknown	No
35	Terra Nova	M/V Cargo	03/10/1990	73.48	78.04	Puncture	No
36	Finnpolaris	M/V Cargo	11/08/1991	71.59	59.52	Sinking	No
37	Hubert Gaucher	M/V Product Tanker	31/08/1991	76.42	89.44	Cracks	Unknown
38	Alla Tarasova	Cruise/ Passenger	19/07/1995	63.05	67.42	Small puncture	No
39	Reduta Ordona	M/V Bulk Carrier	21/07/1996	61.28	66.38	Large hole	No
40	Lucien Paquin	M/V Cargo	20/08/1998	68.46	63.03	Unknown	Unknown
41	Arctic Viking	M/V Cargo	01/10/1998	72.59	80.32	Denting	Unknown
42	Louis S. St-Laurent, CCGS	Icebreaker	17/08/2001	80.07	69.53	No damage	No

4.3.2 Iceberg Climatology

Data from a combination of in-situ drift locations collected through the deployment of satellite tracking beacons, and the Canadian Ice Island Drift, Deterioration, and Detection (CI2D3) database, were compiled to create a climatology of known iceberg locations in the ECA between 2008 and 2019. For analysis in subsequent sections, each dataset is plotted on a 50 x 50 km grid to provide an overview of patterns across the ECA. Both datasets are described further below.

4.3.2.1 Iceberg drift track database

This study uses a dataset from the Canadian Ice Service (CIS) of in situ iceberg drift locations to characterize iceberg drift on a regional scale throughout Baffin Bay, including Nares Strait, Lancaster Sound, and Davis Strait. Of the 40 beacons used in this study, we deployed 25 between July and September each year from 2016 and 2019 onto icebergs throughout the ECA (Chapter 2). Beacons were deployed by helicopter from the *CCGS Amundsen* onto icebergs and ice island fragments and transmitted their position using the Iridium satellite network. Iceberg drift tracks from the CIS database were identified for use from 2012 to 2019, selected based on the following criteria:

i) observations were located between 50°N & 80.5°N and 85°W & 50°W;
ii) observations occurred during the shipping season (July-October);
iii) start of iceberg track was north of 60°N;
iv) observation transmission interval did not exceed six hours; and
v) drift track duration was ≥ 10 days.

Drift tracks were limited to a geographical area that extends approximately from Nares Strait to the Labrador Sea. Beacons that were deployed north of 60°N and drifted south of this boundary were also included. Beacons which transmitted data for fewer than 10 days, or which had a transmission interval exceeding six hours, were excluded due to their limited coverage. Due to lack of ship navigation within Talbot Inlet, SE Ellesmere Island, we have omitted the within-inlet tracks for the purposes of this study. Observations were plotted based on the number of times a unique iceberg tracking beacon was present within each 50 x 50 km grid cell.

4.3.2.2 Canadian Ice Island Drift, Deterioration, and Detection Database (CI2D3)

The flux of ice island fragments from ice tongues on northwestern Greenland was quantified by Crawford et al. (2018) using synthetic aperture radar (SAR) imagery from the CIS archive of Radarsat-1 and 2 scenes between July 2008 and December 2013. This dataset is publicly available at the Polar Data Catalogue (PDC) (https://www.polardata.ca/pdcsearch/PDCSearch.jsp?doi_id=12678). Ice islands were manually digitized as polygons between northwestern Greenland (Peterman, Ryder, Steensby, and C.H. Ostenfeld glaciers) and Newfoundland. The use of repeat imagery at minimum 14-day observation interval allowed for ice island lineage (linking of parent to child ice island fragments) to be tracked for all ice islands. The CI2D3 dataset contains >25000 observations of >900 individual ice islands, including where the fragments drifted and fractured. For the purpose of this study, we limit the ice island fragment observations to the NORDREG zone north of 60°N.

To analyze the spatial distribution of ice islands and the hazard they represent to ship traffic, we isolated repeat observations of all the unique ice islands and their fragments. Ice islands that were first observed calving from ice tongues or were found in the open ocean were given a unique identifier which was retained during subsequent observations of that same ice island. As smaller fragments broke away from them, they too were given an identifier, and so on. Since the time between repeat observations of ice island fragments throughout the dataset is determined to a large extent by the availability of SAR imagery, we resampled the database on a bi-weekly interval to account for sampling bias. We then took the first observation of each unique ice island within each bi-weekly interval (Crawford et al., 2018) and counted the number of unique ice islands within a grid of 50 x 50 km cells, to create an iceberg climatology of known ice island locations throughout the ECA from 2008-2013 (Figure 4-2). These results from the CI2D3 database were then added to the database of known iceberg drift tracks described in the previous section to characterize the distribution of known iceberg drift locations throughout the ECA.

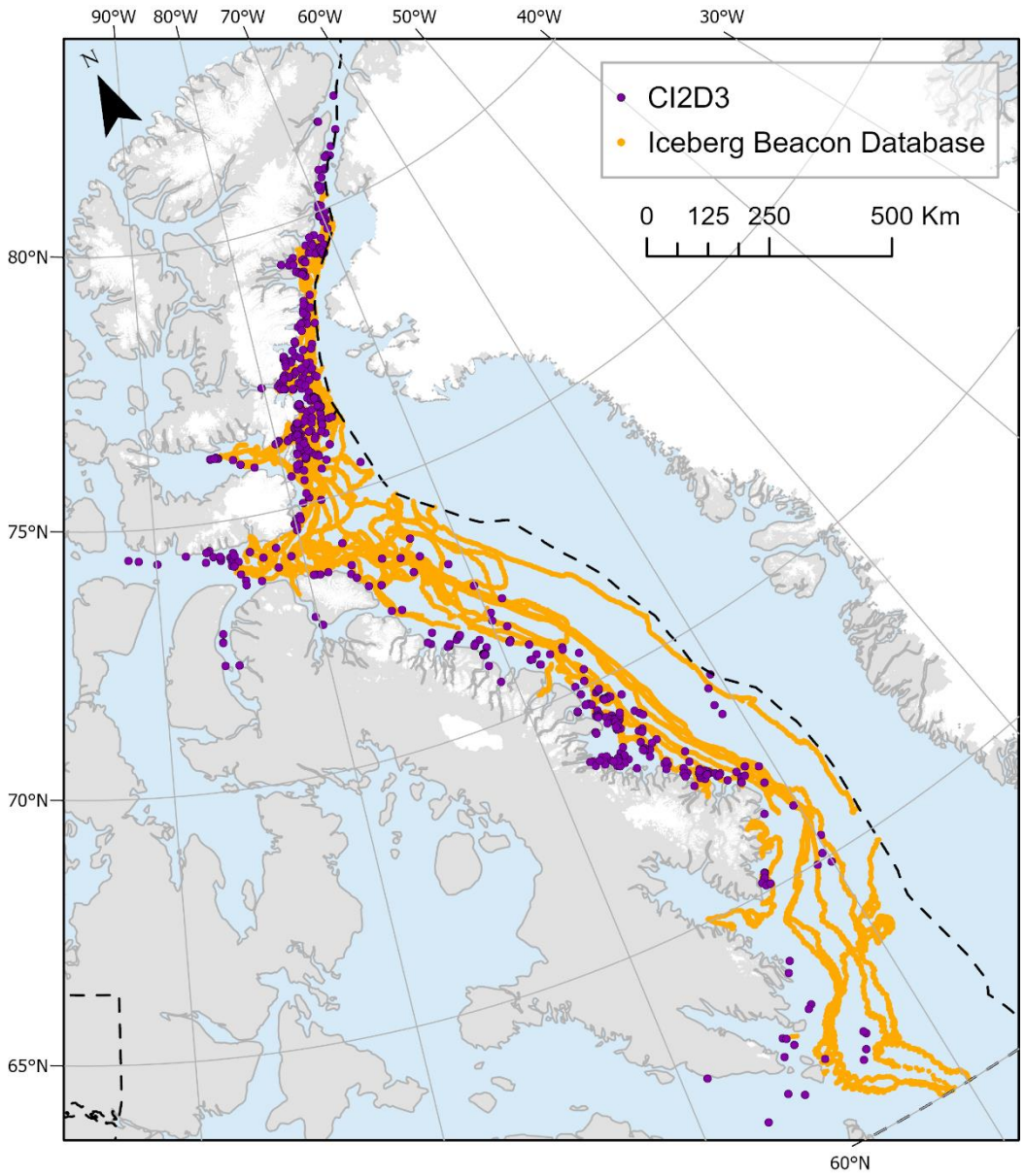

Figure 4-2: Location of raw iceberg beacon (2012-2019) and CI2D3 (2008-2013) ice island fragment observations across the ECA used in this study.

4.3.3 AIS ship data

Most vessels operating in Canadian waters are equipped with AIS transponders, which send messages to terrestrial (land-based) (T-AIS) and satellite (S-AIS) receivers (Nicoll, 2023). These messages provide voyage information, including position, speed, course, vessel name, size, and destination. There are two types of AIS transponders, Class A and Class B. Class A transponders broadcast messages more frequently and at a stronger transmission power than Class B transponders, resulting in Class A messages being more easily received. As per regulation 19 of the International Convention for the Safety of Life at Sea (SOLAS) Chapter V (December 31, 2004), the following vessels are required to carry Class A transponders internationally:

i) vessel is 150 gross tons or more, is carrying more than 12 passengers, and is engaged on an international voyage;
ii) vessel is 300 gross tons or more and is engaged on an international voyage (excluding fishing vessels);
iii) vessel is 500 gross tons or more and is not engaged on an international voyage (excluding fishing vessels); or
iv) vessel is certified to carry more than 12 passengers, or is eight or more metres in length and is carrying passengers.

Class B transponders are voluntary and are generally equipped on smaller vessels such as pleasure craft and fishing boats. This study uses S-AIS data transmitted by Class A and B transponders provided by exactEarth Ltd. (Spire) (2023), and processed courtesy of The Marine Environmental Observation, Prediction and Response Network (MEOPAR). For this analysis, positional AIS messages from the NORDREG zone (i.e., north of 60°N) were converted into spatial points using a custom Python script and stored in a geodatabase by year, following the methodology of Nicoll (2023). Points with invalid Maritime Mobile Service Identity (MMSI; unique nine-digit identifier outside the range of 201000000 to 775999999) were removed. Known ship location points were then converted into track lines using NOAA's Track Builder tool. For each MMSI, the track lines were generated from points where the next point was within 80 km and five hours. These thresholds were chosen based on the inconsistent nature of AIS message transmission and reception within remote regions of the Arctic. Where points exceeded these values, a new vessel track line was produced, creating independent vessel transits over time.

There are ten types of vessels operating in the ECA that were used in this report (Table 4-2). Additional corresponding static vessel information (e.g. MMSI, ship name, ship type) was collected from a combination of online sources (e.g., MarineTraffic.com, MyShipTracking.com, and Industry Canada). Unique number of vessels (MMSI) per 50 x 50 km grid cell was plotted to display the spatial and temporal distribution of vessel traffic throughout the ECA during the shipping season (July-October) between 2012 and 2019.

4.4 Results

4.4.1 Known Iceberg Locations: 2008-2019

4.4.1.1 Iceberg Beacon Database

A total of 40 beacons transmitted their position during the shipping season throughout the ECA (Figure 4-3a). The highest concentration of tracked icebergs occurred in the area north of 65°N along the east coast of Baffin Island and into Nares Strait. Observations south of this point are limited, with the exception of the area on SE Baffin Island near Qikiqtarjuaq and into Davis Strait (Figure 4-1), where icebergs commonly become grounded and remain in a single location for long periods of time. The greatest concentration of beacons was throughout Nares Strait and in eastern Lancaster Sound, with the maximum number of nine beacons per 50 x 50 km grid cell transmitting in Kane Basin and in Smith Sound near Coburg Island.

4.4.1.2 CI2D3

In total, 444 unique CI2D3 ice island fragment branches were detected during the shipping season (July-October) from 2008 to 2013 (Figure 4-3b). During the observation period, the distribution of fragments extended throughout the ECA from northern Nares Strait, and into the entrance of Hudson Strait. Fragments also drifted into the entrance of Lancaster Sound. The highest concentration of observations reached a maximum of 56 per 50 x 50 km grid cell in Smith Sound near Coburg Island. Over the entire period, ice island fragments drifted south along the east coast of Baffin Island, often times entering into narrow inlets and fiords.

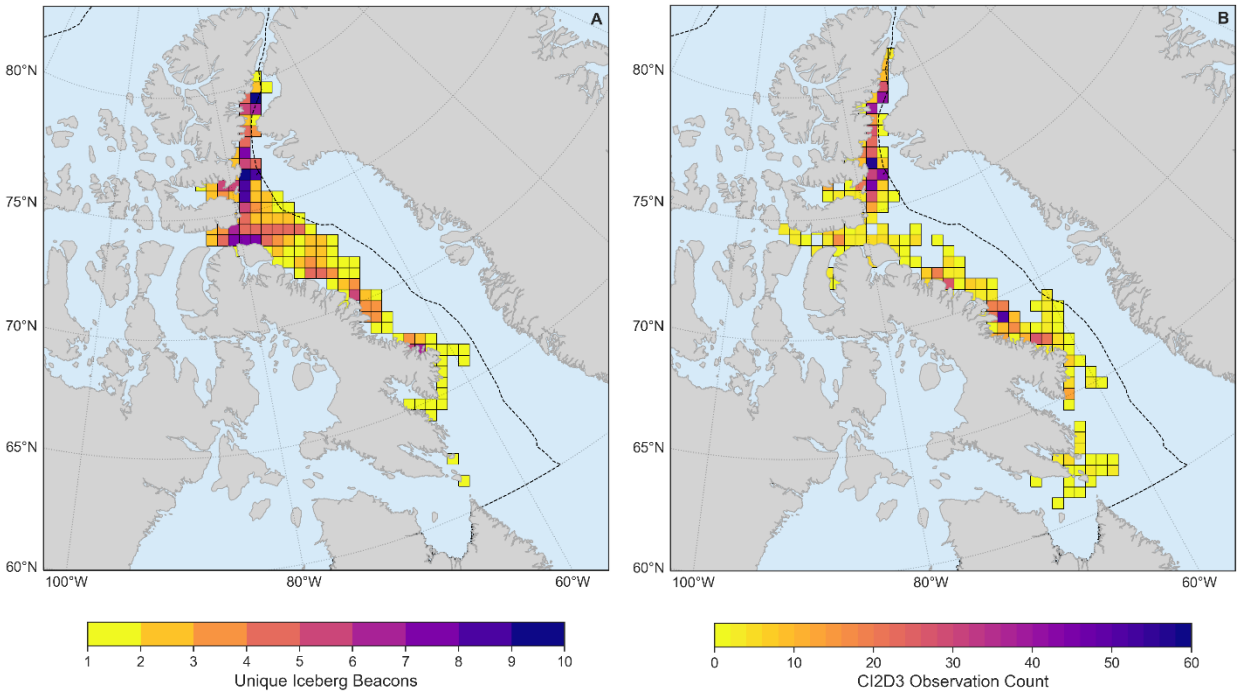

Figure 4-3: a) Unique number of icebergs tracked between 2012 and 2019 and b) total number of CI2D3 ice island fragment observations between 2008 and 2013, per 50 x 50 km grid cell.

Table 4-2: Description of vessel types analyzed in this study. Source: Dawson et al. (2017) and van Luijk et al. (2021).

Vessel Type	Description	Examples
Cargo	• Ships that carry various types and forms of cargo	Cargo, container ship, community resupply, heavy load carrier
Container	• Cargo ships that carry their load in truck-size containers	Cargo transport vessels
Dry Bulk	• Bulk carriage of ore	Bulk carrier
Passenger	• Ships that carry passengers for a fee • Roll-on/roll-off (Ro-Ro) ships designed for wheeled cargo to be driven on or off	Cruise ships passenger, Ro-Ro, ferry
Fishing	• Vessels used in commercial fishing activity and small vessels (30 –100 m long) used for fishing	Small fishing boats, trawler
Government/Research	• Vessels with a strengthened hull designed to move and navigate in ice-covered waters	Icebreaker, fishery patrol, research, military operations, pilot ship, search and rescue
Others/Special Ships	• Vessels that fall outside other categories and are mostly related to oil and gas exploration	Diving support vessel, drill ship, exploration survey vessel
Pleasure	• Recreational vessels	Cruiser, pleasure craft, sailing vessel, sloop, yacht
Tanker	• Vessels that carry bulk liquids or compressed gas	Chemical carrier, oil/chemical tanker
Tugs/Port	• Designed for towing or pushing, and general work duties (e.g. push or pull barges)	Anchor handling vessel, port tender, tug

4.4.2 Shipping Traffic: 2012-2019

4.4.2.1 Temporal Patterns

Between 2012 and 2019, the total annual number of unique ships operating in the ECA more than doubled from 108 to 271 (Table 4-3; Figure 4-4). While increases were observed in nearly every type of vessel, the greatest changes were seen in dry bulk, pleasure crafts, passenger vessels, and other/special ships while container, government/research, and tanker vessel types remained largely consistent from 2012 to 2019 with inter-annual fluctuations. The number of dry bulk vessels nearly tripled from 13 in 2012 to 46 in 2019, an increase of 354% while the number of other/special ships and pleasure vessels increased by 307% and 571%, respectively.

There has also been a clear increase in the number of vessels operating in the ECA since 2016 (Figure 4-5). From 2012 to 2015, the total number of unique ships increased from 108 to 134, while from 2016 to 2019 the total number of unique ships increased from 134 to 271, indicating a recent influx of new traffic to the ECA.

4.4.2.2 Spatial Patterns

All Vessel Types

There has been a clear shift in spatial distribution of vessel traffic between 2012 and 2019. The total number of trips by all vessels increased from 6570 between 2012-2015 (Figure 4-5a) to 10966 between 2016-2019 (Figure 4-5b). The area with the greatest observed increase in traffic occurred along the east coast of Baffin Island and into Pond Inlet towards the entrance of Lancaster Sound, where many vessels are travelling to Pond Inlet for community resupply and cruise ship visits, and to adjacent Milne Inlet to load iron ore produced from the Mary River mine. Traffic from Davis Strait through Hudson Strait remained largely consistent from 2012-2019.

Table 4-3: Total number of unique MMSI operating in the ECA by vessel type from 2012 to 2019.

Vessel Type	2012	2013	2014	2015	2016	2017	2018	2019	Total
Cargo	13	11	13	12	12	15	20	28	124
Container	0	2	4	0	0	2	0	0	8
Dry Bulk	13	16	13	19	20	24	37	46	188
Passenger	7	10	8	11	11	12	21	17	97
Fishing	18	26	27	27	31	40	38	43	250
Government/Research	16	15	16	20	16	27	19	18	147
Others/Special Ships	7	5	5	10	5	23	41	40	136
Pleasure Vessels	14	12	22	15	23	20	20	43	169
Tanker	11	13	11	12	10	13	15	14	99
Tugs/Port	9	10	6	8	6	13	19	22	93
Total	108	120	125	134	134	189	230	271	

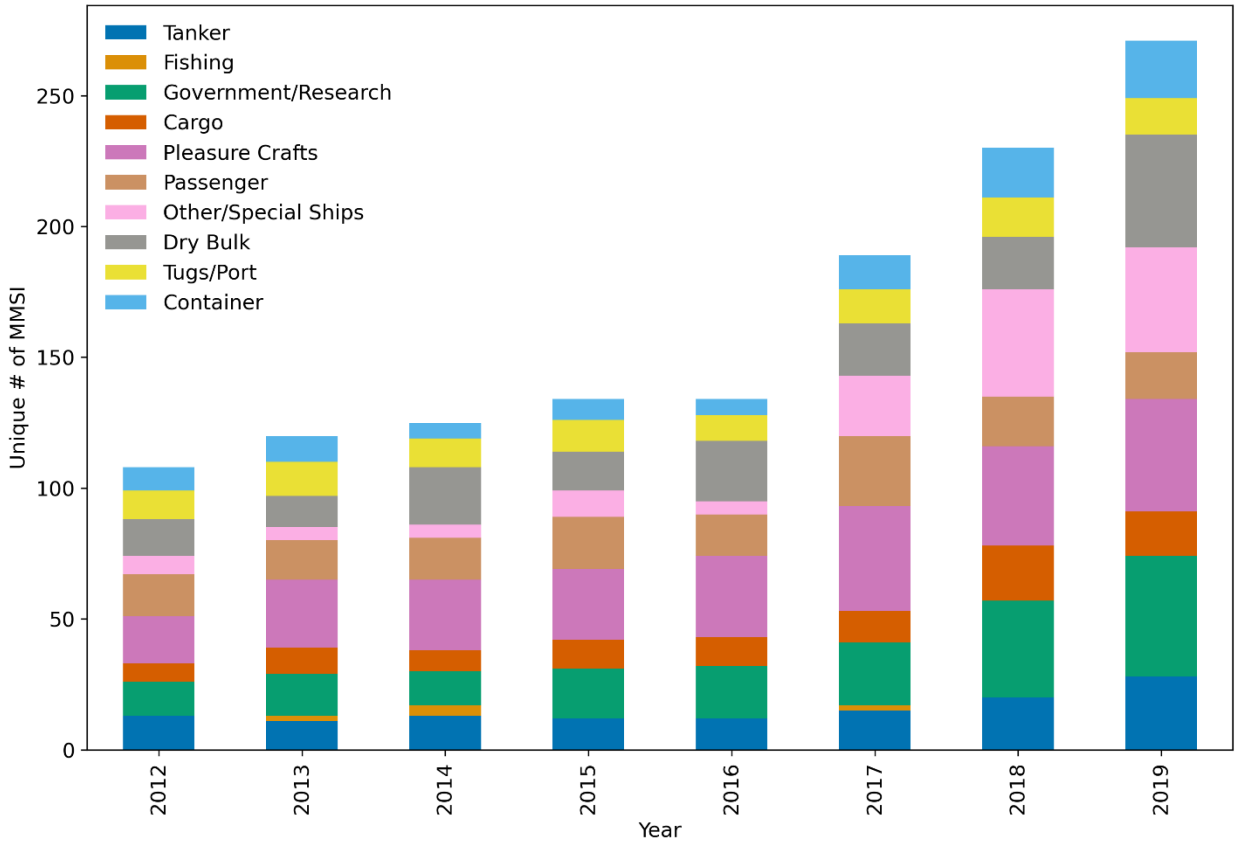

Figure 4-4: Unique number of MMSI operating in the ECA by all vessel types from 2012 to 2019.

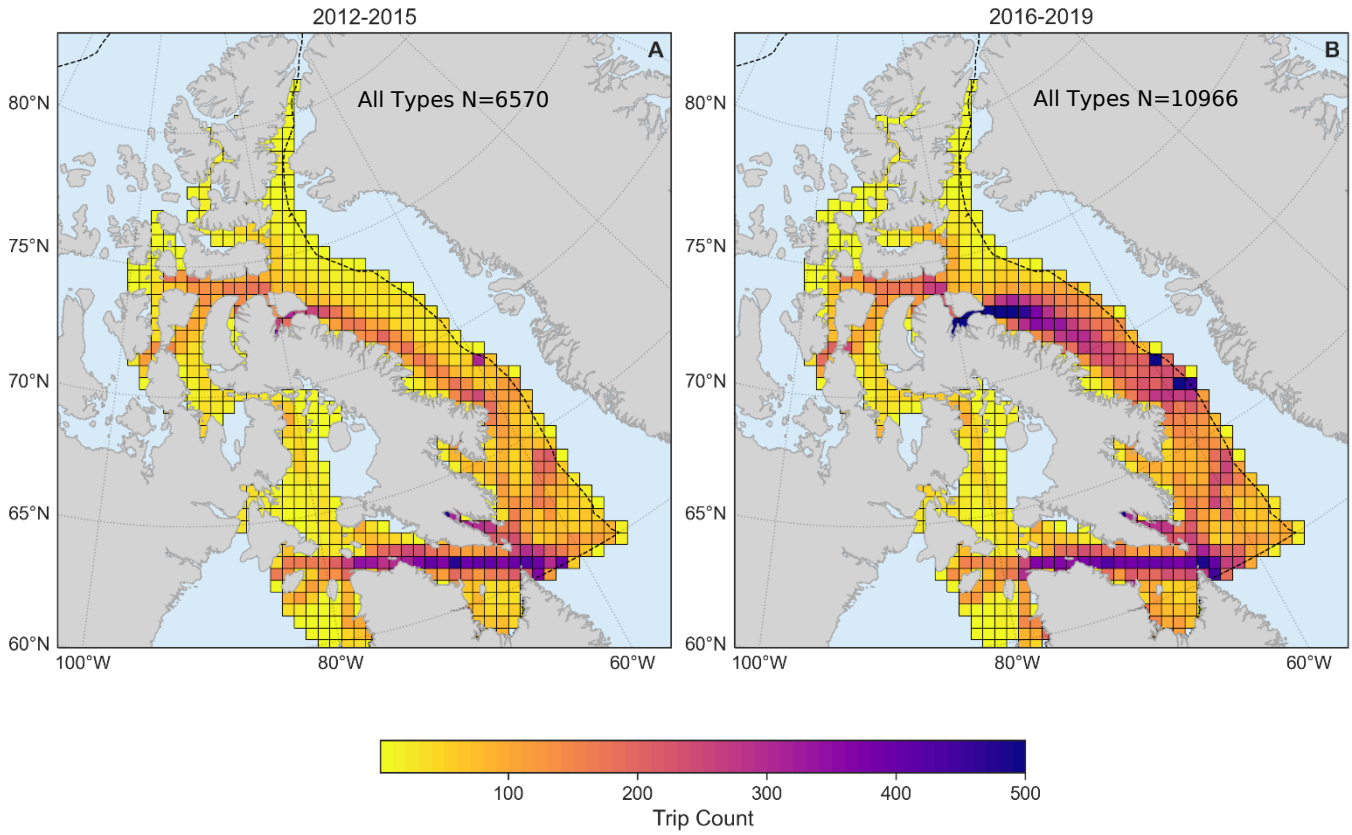

Figure 4-5: Total number of vessel trips per 50 x 50 km grid cell for: a) 2012-2015, and b) 2016-2019 throughout the shipping season (July-October).

Dry Bulk

From 2012 to 2019, there was a marked shift in navigation of dry bulk vessels throughout the ECA. In 2012, a total of 13 unique dry bulk vessels operated in the ECA, compared to 46 by 2019 (Table 4-2). From 2012-2015, the number of trips taken by dry bulk vessels reached a maximum of 326, concentrated mainly throughout Hudson Strait (Figure 4-6a). From 2016-2019, dry bulk traffic through Hudson Strait decreased and 1438 trips were recorded, predominantly along the east coast of Baffin Island into Pond Inlet, with a particularly large increase since 2018 when Mary River Mine reached full production (Figure 4-6b).

Cargo

Since 1980, cargo vessels were involved in 7 of the 16 historical collisions between ships and icebergs (Table 4-1; Figure 4-1). The number of unique cargo vessels operating in the ECA more than doubled from 13 in 2012 to 28 in 2019. Between 2012 and 2015, cargo vessel traffic totalled 1107 trips and was distributed across the ECA, with the highest number of trips occurring through Hudson Strait (Figure 4-6c). Between 2016 and 2019, the number of trips increased to 1487, with a greater concentration of trips occurring along the east coast of Baffin Island, and into Pond Inlet and the entrance to Lancaster Sound (Figure 4-6d).

Pleasure Vessels

From 2012 to 2019, the unique number of pleasure vessels operating in the ECA more than tripled from 14 to 43 per year (Table 4-2). Between 2012 and 2015, pleasure vessel traffic was dispersed throughout the ECA, with 816 trips operating throughout Baffin Bay, Lancaster Sound, and into Hudson Strait (Figure 4-6e). By 2016-2019 the total number of trips had only increased to 864, with a decrease in traffic through Hudson Strait and instead a concentration throughout the entrance to the Northwest Passage, reaching between 50 and 100 trips over the same period near Pond Inlet and Lancaster Sound (Figure 4-6f).

Passenger Vessels

The unique number of passenger vessels increased from 7 to 17 between 2012 and 2019 (Table 4-2; Figure 4-4). During the earlier time period, 2012-2015, these vessels accounted for 441 trips which, similar to pleasure vessels, were distributed throughout the ECA. This included navigation

through Hudson Strait, along the east coast of Baffin Island, and into Lancaster Sound and the Northwest Passage (Figure 4-6g). From 2016-2019 the total number of trips decreased slightly to 406, but traffic became more concentrated in the area around Bylot Island and the Northwest Passage.

4.4.3 Iceberg Ship Coexistence Index

All Vessel Types

To quantify the overlap between known iceberg and ice island drift locations and vessel traffic throughout the ECA, we computed an Iceberg Ship Coexistence Index (ISCI). The complete iceberg beacon and CI2D3 databases were first summed (2008-2019) for all months of the shipping season (July-October) to create a climatology of known iceberg and ice island locations throughout the ECA. The ISCI was then determined by multiplying the iceberg climatology (i.e., unique number of iceberg tracking beacon and CI2D3 observations per 50 x 50 km grid cell for 2008-2019) by the number of vessel trips within that grid cell for the periods 2012-2015 and 2016-2019. The ISCI was normalized on a scale of 1-100 based on the minimum and maximum values for all grid cells over each study period.

It should be noted that the ISCI provides a conservative estimate of iceberg-ship coexistence as we only have a partial measure of the number of icebergs in our study area; however, we believe that the spatial patterns in our iceberg climatology provide a realistic measure of their relative distribution as they are based on a large number of observations. Iceberg and ice island observations are used in this study as a climatology which we assume describes average conditions and locations of icebergs throughout the shipping season. In our analysis, observations from the iceberg climatology are fixed, resulting in any changes in ISCI being solely due to changes in the number and distribution of ships throughout the ECA.

For all vessel types over the periods 2012-2015 and 2016-2019, ISCI showed similar spatial patterns, with maximum values along the east coast of Baffin Island (Figure 4-7). Moderate values occurred in the entrance to Lancaster Sound and Jones Sound, and around Bylot Island, with values decreasing further east into Baffin Bay and north into Nares Strait.

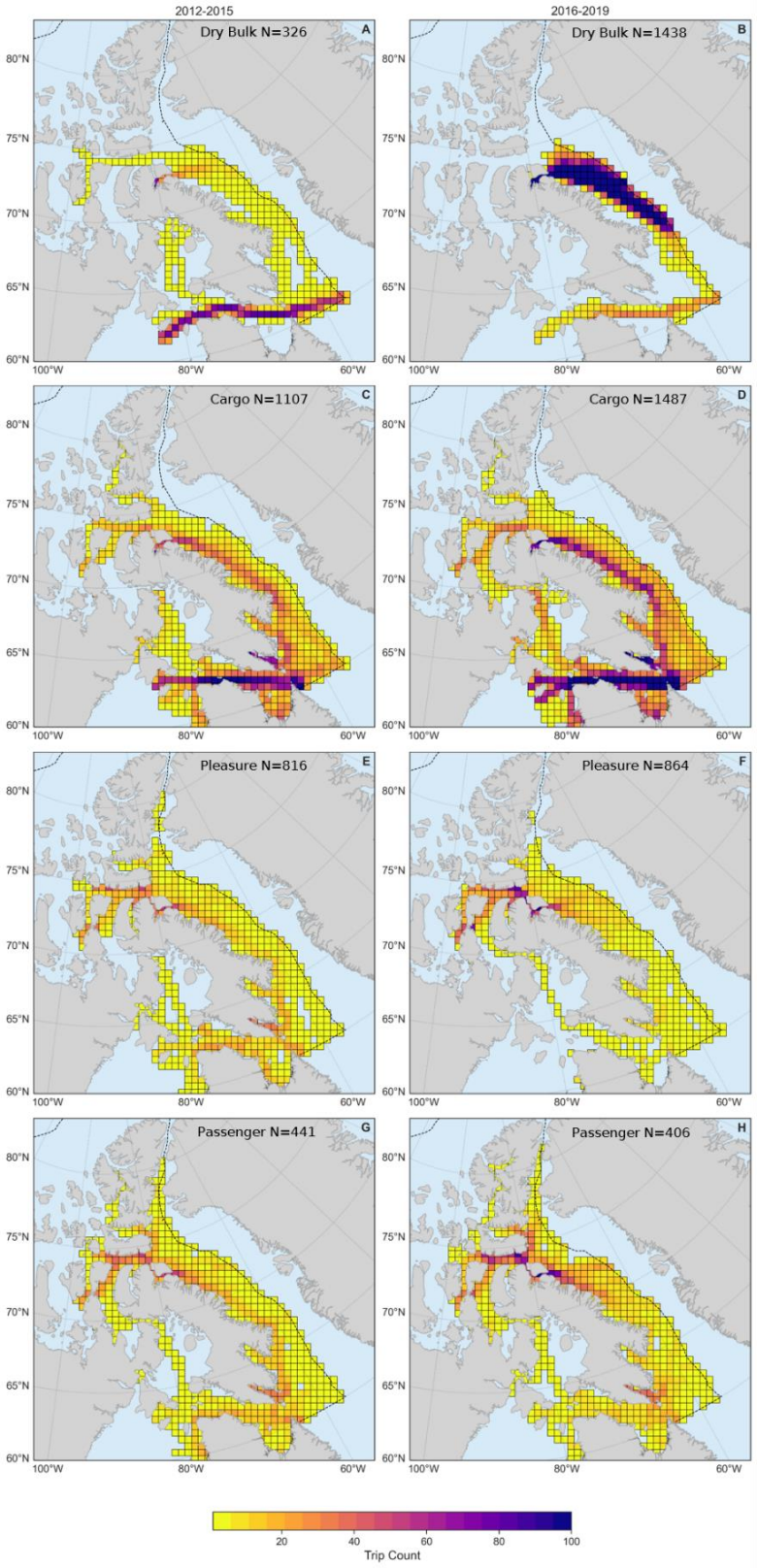

Figure 4-6: Total number of vessel trips per 50 x 50 km grid cell for: (a, b) dry bulk, (c, d) cargo, (e, f) pleasure, (g, h) passenger vessels for 2012-2015 and 2016-2019, respectively.

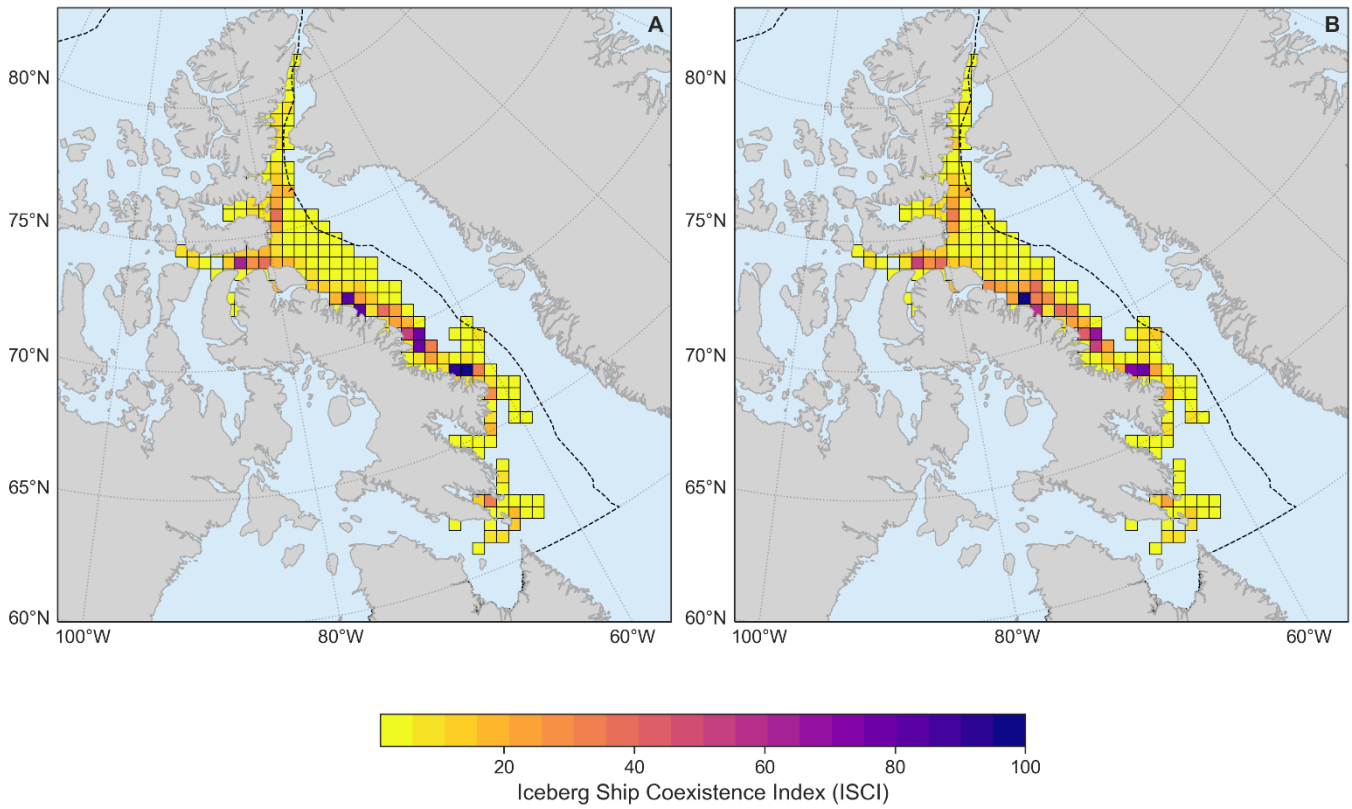

Figure 4-7: Iceberg Ship Coexistence Index (ISCI) for: a) 2012-2015 and b) 2016-2019.

Individual Vessel Types

Given the increase in the unique number of vessels operating in the ECA from 2012-2019 and historical precedent for collisions (Figure 4-1; Table 4-1), we focus our analysis on dry bulk, cargo, pleasure crafts, and passenger vessels. For each individual vessel type, we calculated the percent difference in ISCI between the earlier, 2012-2015, and later 2016-2019, time periods (Figure 4-8). For dry bulk vessels (Figure 4-8a), coexistence between icebergs and vessels was limited to the east coast of Baffin Island and the entrance of Hudson Strait. The greatest difference in ISCI was observed along the east coast of Baffin Island and east of Bylot Island and ranged from 200-775%.

For cargo vessels (Figure 4-8b), coexistence of icebergs and vessels extended from southern Ellesmere Island to Hudson Strait. ISCI increased by a maximum of 225% near Qikiqtarjuaq, while the area east of Bylot Island and in the entrance of Lancaster Sound increased by approximately 30-90%.

The coexistence of icebergs and pleasure vessels was observed from southern Kane Basin to Hudson Strait (Figure 4-8c). Overall, ISCI decreased from 2012-2015 to 2016-2019 in Davis Strait and along the east coast of Baffin Island. In northern Baffin Bay, Smith Sound, and Lancaster Sound, ISCI increased with highest values ranging from 100-150%.

Coexistence between icebergs and passenger vessels was observed between northern Nares Strait and Hudson Strait from 2012-2019 (Figure 4-8d). Overall, ISCI increased along the coast of Baffin Island. However, there were marked regional differences: in southern Baffin Bay and Davis Strait, ISCI decreased by up to 83%. In contrast, in areas to the north of Bylot Island and in Smith Sound and east of Ellesmere Island, increases in ISCI from 199-240% were observed.

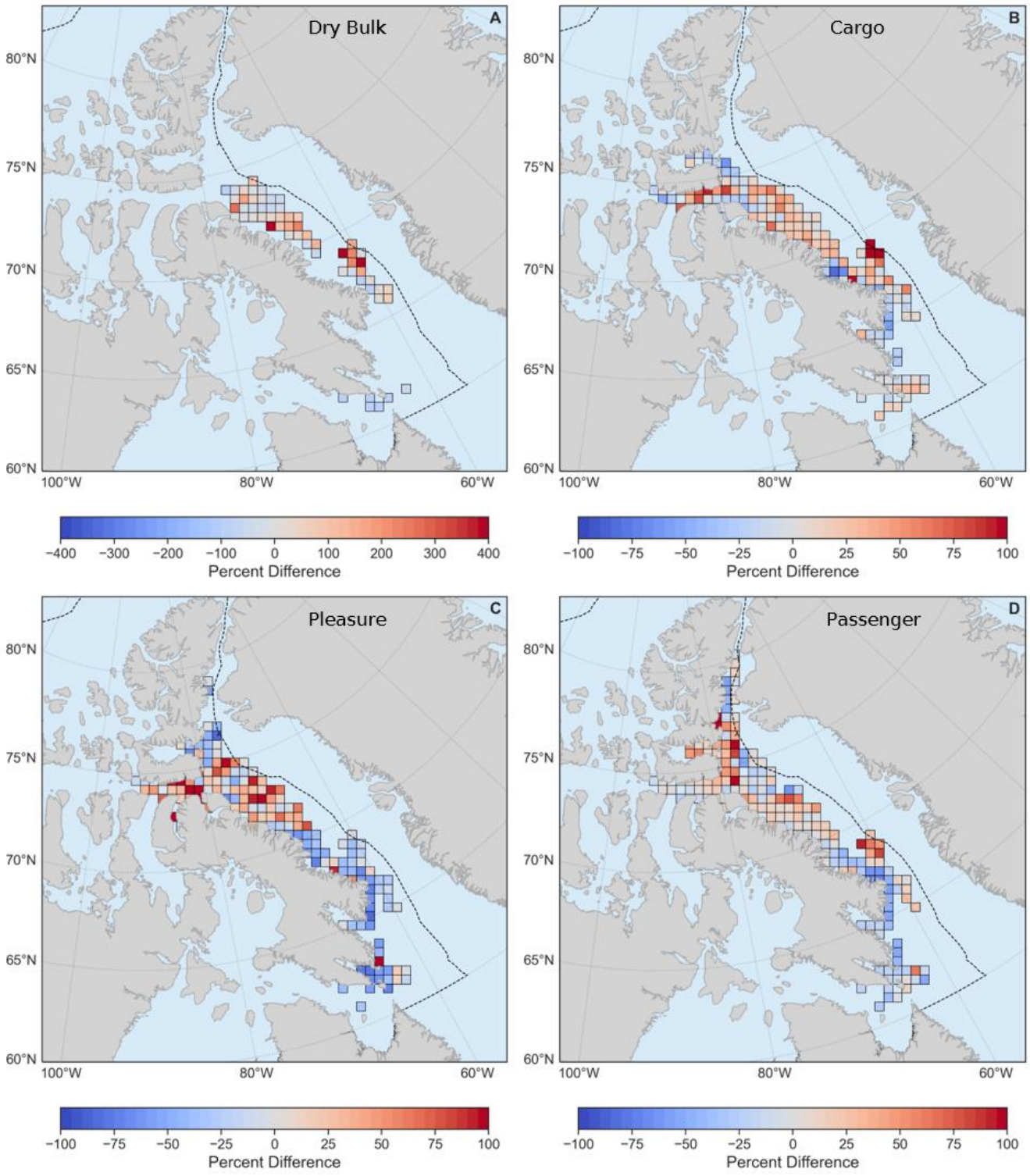

Figure 4-8: Percent difference in iceberg ship coexistence index from 2012-2015 to 2016-2019 for: a) dry bulk, b) cargo, c) pleasure, and d) passenger vessels. Note the difference in scale between dry bulk (a) and the other vessel types (b-d).

4.5 Discussion

Historically, interactions between ships and icebergs in the ECA have resulted in incidents ranging from no damage to sinking and resulting loss of life (Table 4-1). Iceberg ship collisions since 1800 have occurred in most regions of the ECA, from Nares Strait to Davis Strait (Figure 4-1; Hill, 2010). In this study, we combined the two most comprehensive datasets available of iceberg and ice island locations throughout the ECA to produce a climatology of known iceberg presence between 2008 and 2019. While the iceberg climatology presented here is limited both spatially and temporally given the challenges involved in tracking icebergs using in-situ and remote sensing methods, it provides the first assessment of iceberg distribution throughout the ECA. From these results, it is clear that ships have consistently been navigating through areas of known iceberg and ice island locations between 2012 and 2019. Here, we provide the first estimation of the coexistence of icebergs and ships throughout the ECA, quantify how coexistence has changed during 2012-2019, and present considerations for future navigation.

4.5.1 Presence of icebergs throughout the ECA

Production of icebergs from glaciers in the CAA has remained relatively consistent in the recent past, with frontal ablation (i.e., primarily iceberg production, as well as subaerial frontal melting and sublimation, and subaqueous frontal melting) accounting for ~4.28 ± 1.18 Gt a^{-1} of mass loss over the period 2010 to 2020, compared to ~4.14 ± 1.11 Gt a^{-1} from 2000-2010 (Kochtitzky et al., 2022). In western Greenland, ice discharge from tidewater glaciers into Baffin Bay and surrounding waters has increased recently, totalling ~76 Gt a^{-1} from 2010-2018 compared to ~47 Gt a^{-1} from 2000-2010 (Mouginot et al., 2019, Mankoff et al., 2020).

Ice islands are discharged at an inconsistent rate through the disintegration of ice shelves. For example, Petermann Glacier in NW Greenland underwent five major calving events from the floating glacial ice tongue at its terminus between 1959 and 2012, producing large ice islands on the order of 100 km^2 (Johannessen et al., 2013). Given the frequency of major events like these over the last several decades, the presence of ice islands and ice island fragments throughout the ECA is episodic. These events are likely to diminish given the significant loss of ice shelves in northern Greenland since the 1990s (Higgins, 1991; Falkner et al., 2011) and from the CAA since the early 20th century (Mueller et al., 2017; White & Copland, 2019). When ice islands are present in the ECA they are considered hazards for navigation, as well as a potential long term source of

additional icebergs as fragments calve from the main pieces (Scambos et al., 2005; 2008; Wagner et al., 2014; Crawford et al., 2016). For example, ice island PII-B which calved from Petermann Glacier in 2010, produced 3.8 Gt of ice island fragments over 22 months during periods of drift and grounding (Crawford et al., 2016). Ice islands are capable of providing a source of icebergs to areas where few tidewater glaciers exist that would regularly produce icebergs, such as eastern Baffin Island (Van Wychen et al., 2015; Crawford & Mueller, 2022).

Icebergs and ice islands identified in this study using satellite tracking beacons and remote sensing methods were observed to consistently drift south from Nares Strait along the east coast of Baffin Island, with frequent intrusions into eastern Lancaster Sound (Marko et al., 1982). The greatest concentration of ice island fragments was located within Nares Strait and Smith Sound, as their drift is restricted by topographic constraints between Ellesmere Island and Greenland (Figure 4-4).

4.5.2 Navigation of vessels throughout the ECA: 2012-2019

Shipping throughout the CAA is dependent on environmental factors such as sea ice conditions and the length of the open water season. It is also controlled by demand, as shipping in the CAA is primarily destinational and vessels which navigate this region are there for a purpose such as resource extraction, community resupply, or tourism (Stephenson et al., 2015). Many ships navigating within the Arctic are equipped with varying classifications of hull strengthening which allows them to operate in a range of ice conditions. Highly ice strengthened vessels such as icebreakers can operate in year-round sea ice conditions, including multiyear sea ice inclusions. Medium strength vessels, commonly cargo vessels, bulk carriers and some passenger ships, operate in summer and autumn conditions including thin first-year sea ice with some multiyear ice inclusions, whereas minimally ice strengthened vessels such as pleasure crafts are designed for operation in mostly open water conditions with little to no ice presence (Dawson et al., 2022).

Overall, shipping traffic throughout the ECA increased both in number of unique vessels operating and the total number of trips taken by vessels between 2012-2015 and 2016-2019. Of the four specific vessel types highlighted in this study, the greatest overall increases in unique numbers were observed for dry bulk vessels, which nearly tripled between 2012 and 2019, and pleasure craft, which more than tripled over the same period. While there was little increase in the number of trips taken by pleasure craft from 2012-2019, trips by dry bulk vessels more than tripled with

operations concentrated along the east coast of Baffin Island and towards Pond Inlet. Increases in unique number of ships was also observed in both cargo ships and passenger vessels. Consistent with the results of previous studies (Johnston et al., 2017; Dawson et al., 2018; 2022), while the number of trips taken by pleasure and passenger vessels throughout the ECA remained relatively stable over time, the unique number of vessels more than doubled, with vessels beginning to operate more northward than before. Our results indicate that not only did existing ships operating in the ECA take more trips from 2016-2019 compared to 2012-2015, but that new vessels have begun operating in these areas and extending their range northward into Nares Strait and westward into the Northwest Passage.

While icebergs are considered potential hazards for all vessels navigating in the Arctic, they are of particular concern for vessels with minimal or no ice strengthening. Overall, the average annual voyage count of ships with no ice strengthening operating in the NORDREG zone increased by 3300% between 1990 and 2019 (Dawson et al., 2022). Dawson et al. (2022) also found that in addition to the influx of new passenger, dry bulk, and cargo vessels operating in more northern regions of the ECA, the ice strengthening of these vessels had decreased between 1990 and 2019. Spatially, traffic of dry bulk vessels shifted out of Hudson Strait from 2012-2015 to almost exclusively along the east coast of Baffin Island in 2016-2019, where icebergs and ice islands are known to drift, resulting in an increase in the ISCI in the same region from 2012-2015 to 2016-2019. Due to cargo and passenger vessel traffic (with generally medium to minimal ice strengthening; Dawson et al., 2022) increasing in northern Baffin Bay and the entrance to the Northwest Passage, the ISCI also increased in these regions as icebergs are known to drift within eastern Lancaster Sound (Marko et al., 1982; Chapter 3) before continuing south along Baffin Island. Icebergs and ice islands which calve from NW Greenland (e.g. Petermann Glacier) and the QEI typically drift south through Smith Sound, often times becoming temporarily grounded near Coburg Island. The greatest increase in ISCI in Smith Sound was observed for passenger vessels, which, as of 2016-2019, have begun operating in higher rates in more northern regions compared to 2012-2015.

4.5.3 Considerations for coexistence of icebergs and ships in the ECA

Glaciers from Greenland and the CAA remain a continuous source of icebergs for Baffin Bay (Kochtitzky et al., 2022), while vessels operating throughout the region over the past decade have

changed both in quantity and the total number of trips taken, during which their level of ice strengthening has been reducing (Dawson et al., 2022). According to the Ice Navigation in Canadian Waters Manual, which is published by the Canadian Coast Guard and the CIS, and provides operational requirements and guidelines for vessels operating within Canadian waters, icebergs, especially growlers and bergy bits, represent extreme local hazards to vessels operating in ice-covered waters. Glacial ice is very hard and severe damage can result from collision with a ship (CCG, 2022). While the use of AIS transponders has become useful for differentiating between ships and icebergs (ABS, 2016), ship radar cannot be solely relied upon for iceberg detection due to variable iceberg geometry and environmental conditions such as heavy snow, fog, and high waves (CCG, 2022). Additionally, icebergs drifting or frozen within a sea ice pack can result in the formation of leads (open water areas) downstream of the iceberg due to sea ice ridging (Hunke & Comeau, 2011). While sea ice leads can offer a navigable passage for surface vessels, they can end suddenly at an iceberg, bergy bit, or growler (CCG, 2022).

Although icebergs have been widely identified as posing a significant hazard to ships operating in the Arctic (ABS, 2016; CCG, 2022), few formal recommendations exist about navigation in iceberg-infested waters with the exception of planning routes through polar waters that take into account the current extent and type of icebergs in the vicinity of the planned route. However, ice charts produced for the CAA tend to broadly classify the limit of icebergs as “bergy waters”, with little to no information on size, shape, or specific location. Presently, iceberg charts produced by CIS and the IIP only provide detailed information on iceberg conditions through shipping lanes south of 60°N.

The ISCI presented here indicates that the coexistence of icebergs and ships is true for nearly all regions of the ECA north of 60°N. For dry bulk vessels from 2012-2015 to 2016-2019, which typically have medium to minimal ice strengthening (Dawson et al., 2018), ISCI increased by up to 700% in areas along the east coast of Baffin and Bylot Islands. For passenger vessels, ISCI has increased not only along the east coast of Baffin Island, but also in Smith Sound, as traffic from these vessel types moves northward. As shipping traffic increases through the ECA, the findings of this study clearly indicate the need for additional monitoring and reporting of iceberg and ice island locations for shipping lanes in the ECA.

4.6 Conclusion

Using a climatology of known iceberg drift locations in combination with AIS ship location data, we provide the first quantification of the coexistence between ships and icebergs throughout the ECA. While we cannot conclude from this study that iceberg presence has increased throughout the ECA from 2012-2019, it is clear from our results that number of unique ships and voyages has increased over this time period. We are therefore able to use the ISCI to assess the changing likelihood of iceberg and ship coexistence throughout the ECA. This climatology indicates that icebergs and ice islands are consistently present throughout Nares Strait, eastern Lancaster Sound, and within Baffin Bay following the east coast of Baffin Island. When we look at the coexistence of ships and icebergs throughout the ECA between 2012 and 2019, our findings show that the greatest increases occurred along the east coast of Baffin Island, eastern Lancaster Sound, and Smith Sound. In particular, the coexistence of dry bulk vessels and icebergs has increased along the east coast of Baffin Island and east of Bylot Island. For passenger vessels, the greatest increases in coexistence were observed in Smith Sound, as operation by these types of vessels moves northward.

Icebergs present a known hazard to navigation in the Arctic around which ship operators are recommended to take caution. Operators are encouraged when planning to mark areas known to have significant concentrations of icebergs on charts, such as off the coast of Greenland (CCG, 2022). The results of this study could be used in the planning stage to expand areas of known iceberg drift and grounding in the ECA. The hazards posed by icebergs to ships is likely increasing over time due to the observed recent increases in the number of vessels operating in the ECA, with the seriousness of any potential collision also increasing due to the recent reduction in mean ice strengthening observed in vessel types such as dry bulk, passenger, and pleasure vessels (Dawson et al., 2022). For vessels such as passenger ships, icebergs are also presented as an attraction or feature during navigation, so these vessels sometimes purposely navigate close to them.

Considering these increases in shipping navigation through areas of known iceberg presence, it is important to address issues that may arise with potential future increases in vessel traffic. Given the existing framework for iceberg analysis off the Newfoundland and Labrador coasts, it is recommended that daily iceberg charts be expanded to cover primary shipping lanes in the ECA during the shipping season. By including detailed analysis of iceberg location and size, icebergs

could then be included in the ice numeral calculation for POLARIS, further refining the estimate of risk to ships navigating in the ECA.

The results of this study highlight the need for improved iceberg monitoring, both in-situ for validation of iceberg drift forecast models, and through remote sensing, to allow for greater spatial and temporal coverage of their distribution. Collection of data on environmental variables through known iceberg areas will help us to better understand the forces controlling their drift and deterioration, especially through shipping lanes in the ECA. This study will provide foundational information for policy decisions surrounding vessel navigation through known iceberg locations.

Data Availability

The Ship Iceberg Collision Database compiled by Hill (2010) can be accessed online (https://newicedata.com/the-ship-iceberg-collision-database/). The Transportation Safety Board Marine Safety Information System (MARSIS) is accessible online (http://www.bst-tsb.gc.ca/eng/stats/marine/data-2.html). The CI2D3 database of ice island locations from 2008-2013 is available for download through the Polar Data Catalogue (https://www.polardata.ca/pdcsearch/PDCSearch.jsp?doi_id=12678). Iceberg beacon data can be made available by contacting the lead author. Access to Satellite AIS data was given through a joint project agreement with MEOPAR processed ship data provided by Ltd. (Spire) (2023).

References

ABS (American Bureau of Shipping). (2016) IMO Polar Code advisory. Houston, Texas: ABS. https://ww2.eagle.org/content/dam/eagle/advisories-and-debriefs/ABS_Polar_Code_Advisory_15239.pdf

AC (Arctic Council). (2009) Arctic marine shipping assessment 2009 report. Tromso, Norway: AC. https://pame.is/images/03_Projects/AMSA/AMSA_2009_report/AMSA_2009_Report_2nd_print.pdf

AMAP (Arctic Monitoring and Assessment Programme). (2017) Adaptation actions for a changing Arctic: Perspectives from the Barents area. Oslo, Norway: AMAP. https://www.amap.no/documents/doc/adaptation-actions-for-a-changing-arctic-perspectives-from-the-barents-area/1604

Barber, D. G., Babb, D. G., Ehn, J. K., Chan, W., Matthes, L., Dalman, L. A., Campbell, Y., Harasyn, M. L., Firoozy, N., Theriault, N., Lukovich, J. V., Zagon, T., Papakyriakou, T., Capelle, D. W., Forest, A., & Gariepy, A. (2018). Increasing Mobility of High Arctic Sea Ice Increases Marine Hazards Off the East Coast of Newfoundland. *Geophysical Research Letters*, 45(5), 2370–2379. https://doi.org/10.1002/2017GL076587

Bigg, G.R., Wadley, M., Stevens, D., and Johnson, A.J. (1996) Prediction of iceberg trajectories for the North Atlantic and Arctic Oceans. *Geophysical Research Letters*. 23. https://doi.org/10.1029/96GL03369

Canadian Coast Guard (CCG) (6th Ed.). (2022). Ice navigation in Canadian waters (Rev. ed). Fisheries and Oceans Canada.

Canadian Ice Service (CIS). (2005) MANICE. Online. https://www.canada.ca/en/environment-climate-change/services/weather-manuals-documentation/manice-manual-of-ice.html

Chénier, R., Abado, L., Sabourin, O. and Tardif, L. (2017) Northern marine transportation corridors: Creation and analysis of northern marine traffic routes in Canadian waters. *Transactions in GIS*. 21. https://doi.org/10.1111/tgis.12295

Copland, L., Dawson, J., Tivy, A., Delaney, F., & Cook, A. (2021). Changes in shipping navigability in the Canadian Arctic between 1972 and 2016. *Facets*, 6, 1069–1087. https://doi.org/10.1139/facets-2020-0096

Crawford, A., Wadhams, P., Wagner, T., Stern, A., Abrahamsen, P., Church, I., Bates, R., & Nicholls, K. (2016). Journey of an Arctic Ice Island. *Oceanography*, 29(2). https://doi.org/10.5670/oceanog.2016.30

Crawford, A. J., Mueller, D., Desjardins, L., & Myers, P. G. (2018). The Aftermath of Petermann Glacier Calving Events (2008–2012): Ice Island Size Distributions and Meltwater Dispersal. *Journal of Geophysical Research: Oceans*, 123(12), 8812–8827. https://doi.org/10.1029/2018JC014388

Crawford, A., & Mueller, D. (2022). Assessing Ice Island Drift Patterns, Ice Island Grounding Locations, and Gridded Bathymetry Products between Nares Strait and the North Atlantic. *Arctic*. https://doi.org/10.14430/arctic76227

White, A., & Copland, L. (2019). Loss of floating glacier tongues from the Yelverton Bay region, Ellesmere Island, Canada. *Journal of Glaciology*, 65(251), 376–394. https://doi.org/10.1017/jog.2019.15

Dawson, J., Pizzolato, L., Howell, S. E. L., Copland, L., & Johnston, M. E. (2018). Temporal and Spatial Patterns of Ship Traffic in the Canadian Arctic from 1990 to 2015 + Supplementary Appendix 1: Figs. S1–S7 (See Article Tools). *Arctic*, 71(1). https://doi.org/10.14430/arctic4698

Dawson, J., Cook, A., Holloway, J. and Copland, L. (2022). Analysis of changing levels of ice strengthening (ice class) among vessels operating in the Canadian Arctic over the past 30 years. *Arctic*, 75(4), 413-430.

Eguíluz, V. M., Fernández-Gracia, J., Irigoien, X., & Duarte, C. M. (2016). A quantitative assessment of Arctic shipping in 2010–2014. *Scientific Reports*, 6(1), 30682. https://doi.org/10.1038/srep30682

Falkner, K. K., Melling, H., Münchow, A. M., Box, J. E., Wohlleben, T., Johnson, H. L., Gudmandsen, P., Samelson, R., Copland, L., Steffen, K., Rignot, E., & Higgins, A. K. (2011). Context for the Recent Massive Petermann Glacier Calving Event. Eos, *Transactions American Geophysical Union*, 92(14), 117–118. https://doi.org/10.1029/2011EO140001

Ford, J., & Clark, D. (2019). Preparing for the impacts of climate change along Canada's Arctic coast: The importance of search and rescue. *Marine Policy*, 108, 103662. https://doi.org/10.1016/j.marpol.2019.103662

Garbo, A. (2022) Validation of the North American Ice Service Iceberg Drift Model. *MSc thesis, University of Ottawa*. http://dx.doi.org/10.20381/ruor-27682.

Haas, C., & Howell, S. E. L. (2015). Ice thickness in the Northwest Passage. *Geophysical Research Letters*, 42(18), 7673–7680. https://doi.org/10.1002/2015GL065704

Higgins, A. K. (1991). North Greenland glacier velocities and calf ice production. Polarforschung, 60(1), 1-23.

Hill, Brian. (2010). Ship Collision with Iceberg Database. ICETECH06-117-RF

Johnston, M., Dawson, J., De Souza, E., & Stewart, E. J. (2017). Management challenges for the fastest growing marine shipping sector in Arctic Canada: Pleasure crafts. *Polar Record*, 53(1), 67–78. https://doi.org/10.1017/S0032247416000565

Johannessen, O.M.,Babiker, M. & Miles, M.W. (2013) Unprecedented Retreat in a 50-Year Observational Record for Petermann Glacier, North Greenland, *Atmospheric and Oceanic Science Letters*, 6:5, 259-265, DOI: 10.3878/j.issn.1674-2834.13.0021

Justice Laws. 2010. Northern Canada vessel traffic services zone regulations. SOR/2010-127. Ottawa: Government of Canada. https://laws-lois.justice.gc.ca/eng/regulations/SOR-2010-127/FullText.html

Kochtitzky, W., Copland, L., Van Wychen, W., Hugonnet, R., Hock, R., Dowdeswell, J. A., Benham, T., Strozzi, T., Glazovsky, A., Lavrentiev, I., Rounce, D. R., Millan, R., Cook, A., Dalton, A., Jiskoot, H., Cooley, J., Jania, J., & Navarro, F. (2022). The unquantified mass loss of Northern Hemisphere marine-terminating glaciers from 2000–2020. *Nature Communications*, 13(1), 5835. https://doi.org/10.1038/s41467-022-33231-x

Kujala, P., Goerlandt, F., Way, B., Smith, D., Yang, M., Khan, F., & Veitch, B. (2019). Review of risk-based design for ice-class ships. *Marine Structures*, 63, 181–195. https://doi.org/10.1016/j.marstruc.2018.09.008

Mankoff, K. D., Solgaard, A., Colgan, W., Ahlstrøm, A. P., Khan, S. A., & Fausto, R. S. (2020). Greenland Ice Sheet solid ice discharge from 1986 through March 2020. *Earth System Science Data*, 12(2), 1367–1383. https://doi.org/10.5194/essd-12-1367-2020

Marko, J., Birch, J., and Wilson, M. (1982). A Study of Long-Term Satellite-Tracked Iceberg Drifts in Baffin Bay and Davis Strait. *Arctic*, 35(1), 234-240. Retrieved from http://www.jstor.org/stable/40509318

Melling, H., Gratton, Y. and Ingram, G. (2001). Ocean circulation within the North Water polynya of Baffin Bay, *Atmosphere-Ocean*, 39:3, 301-325, DOI:10.1080/07055900.2001.9649683

Mouginot, J., Rignot, E., Bjørk, A. A., Van Den Broeke, M., Millan, R., Morlighem, M., ... and Wood, M. (2019). Forty-six years of Greenland Ice Sheet mass balance from 1972 to 2018. *Proceedings of the National Academy of Sciences*, 116(19), 9239-9244.

Mudryk, L. R., Dawson, J., Howell, S. E. L., Derksen, C., Zagon, T. A., & Brady, M. (2021). Impact of 1, 2 and 4 °C of global warming on ship navigation in the Canadian Arctic. *Nature Climate Change*, 11(8), 673–679. https://doi.org/10.1038/s41558-021-01087-6

Mueller, D., Copland, L. & Jeffries, M.O. (2017). Changes in Canadian Arctic ice shelf extent since 1906. In: Copland, L. and Mueller, D. (eds.). Arctic Ice Shelves and Ice Islands, Ch. 5, p.109-140. Springer Nature, Dordrecht.

Münchow, A., Falkner, K. K., & Melling, H. (2015). Baffin Island and West Greenland Current Systems in northern Baffin Bay. *Progress in Oceanography*, 132, 305–317. https://doi.org/10.1016/j.pocean.2014.04.001

Nicoll, A. 2023. Analysis of Ship Traffic and Ship Accidents in the Canadian and Global Arctic. MSc thesis, University of Ottawa. http://dx.doi.org/10.20381/ruor-28981

Pizzolato, L., Howell, S. E. L., Derksen, C., Dawson, J., & Copland, L. (2014). Changing sea ice conditions and marine transportation activity in Canadian Arctic waters between 1990 and 2012. *Climatic Change*, 123(2), 161–173. https://doi.org/10.1007/s10584-013-1038-3

Pizzolato, L., Howell, S. E. L., Dawson, J., Laliberté, F., & Copland, L. (2016). The influence of declining sea ice on shipping activity in the Canadian Arctic: Sea Ice and Shipping, Canadian Arctic. *Geophysical Research Letters*, 43(23), 12,146-12,154. https://doi.org/10.1002/2016GL071489

Rompkey, W. and Cochrane, E. (2008). The Coast Guard in Canada's Arctic: Interim Report. Senate of Canada, Standing Senate and Committee on Fisheries and Oceans. Fourth Report.

Scambos, T., Sergienko, O., Sargent, A., MacAyeal, D., & Fastook, J. (2005). ICESat profiles of tabular iceberg margins and iceberg breakup at low latitudes. *Geophysical Research Letters*, 32(23), L23S09. https://doi.org/10.1029/2005GL023802

Scambos, T., Ross, R., Bauer, R., Yermolin, Y., Skvarca, P., Long, D., Bohlander, J., & Haran, T. (2008). Calving and ice-shelf break-up processes investigated by proxy: Antarctic tabular iceberg evolution during northward drift. *Journal of Glaciology*, 54(187), 579–591. https://doi.org/10.3189/002214308786570836

Stephenson, S. R., Smith, L. C., Brigham, L. W., & Agnew, J. A. (2013). Projected 21st-century changes to Arctic marine access. *Climatic Change*, 118(3–4), 885–899. https://doi.org/10.1007/s10584-012-0685-0

Stephenson, S. R., & Smith, L. C. (2015). Influence of climate model variability on projected Arctic shipping futures. *Earth's Future*, 3(11), 331–343. https://doi.org/10.1002/2015EF000317

Sudom, D., Timco, G., & Tivy, A. (2014). Iceberg sightings, shapes and management techniques for offshore Newfoundland and Labrador: Historical data and future applications. 2014 Oceans - St. John's, 1–8. https://doi.org/10.1109/OCEANS.2014.7003298

Tang, C. C. L., Ross, C. K., Yao, T., Petrie, B., DeTracey, B. M., & Dunlap, E. (2004). The circulation, water masses and sea-ice of Baffin Bay. *Progress in Oceanography*, 63(4), 183–228. https://doi.org/10.1016/j.pocean.2004.09.005

Valeur, H. H., Hansen, C., Hansen, K. Q., Rasmussen, L., & Thingvad, N. (1996). Weather, sea and ice conditions in eastern Baffin Bay, offshore northwest Greenland: A review. Mineral Resources Administration for Greenland, 96–12 (December), 37 pp.

van Luijk, N., Holloway, J., Carter, N. A, Dawson, J., & Orawiec, A. (2021). Gap Analysis: Shipping and Coastal Management in Inuit Nunangat. A report prepared for Inuit Tapiriit Kanatami. Ottawa, Canada.

Van Wychen, W., Copland, L., Burgess, D. O., Gray, L., & Schaffer, N. (2015). Glacier velocities and dynamic discharge from the ice masses of Baffin Island and Bylot Island, Nunavut, Canada. *Canadian Journal of Earth Sciences*, 52(11), 980–989. https://doi.org/10.1139/cjes-2015-0087

Wagner, T. J. W., Wadhams, P., Bates, R., Elosegui, P., Stern, A., Vella, D., Abrahamsen, E. P., Crawford, A., & Nicholls, K. W. (2014). The "footloose" mechanism: Iceberg decay from hydrostatic stresses. *Geophysical Research Letters*, 41(15), 5522–5529. https://doi.org/10.1002/2014GL060832

Chapter 5: Conclusion

5.1 Summary

The primary goal of this thesis was to characterize icebergs from source to sink in the ECA and identify regional drift patterns of icebergs including how they overlap spatially with ships. The thesis had three main research objectives:

1. Determine the processes controlling glacier flow from the four primary sources of iceberg flux from the POW Icefield to Baffin Bay from 2009-2019. Winter surface velocities combined with terminus retreat rates, ice thickness, surface elevation, and terminus buoyancy are used determine whether glacier geometry is contributing to destabilizing changes in the largest glacier basin (Trinity and Wykeham) in the CAA.
2. Provide a survey of iceberg characteristics and drift through Canadian waters using a combination of field and remote sensing methods. A 9-year record of iceberg drift tracks through Baffin Bay is combined with bathymetry, ocean current, wind current, and sea ice conditions to characterize iceberg behaviour in Baffin Bay and describe the forces driving iceberg drift patterns.
3. Identify density of icebergs along primary shipping routes in the eastern Canadian Arctic. Known ship tracks derived from AIS data and a multi-year dataset of known iceberg drift tracks are used to establish areas of overlap between icebergs and ships throughout the eastern Canadian Arctic. This is used to identify patterns in iceberg-ship proximity based on vessel type and along primary shipping routes.

The first research objective was addressed in chapter 2. Through a combination of speckle-tracking derived winter surface velocities, ice thickness measurements, and bed elevation data, Ekblaw Glacier was confirmed as “pulse type”, indicated by periods of variable velocities confined to the area of the glacier grounded below sea level. Based on these criteria, Cadogan Glacier was also classified as “pulse type”, which was not previously identified as such by Van Wychen et al. (2016). For both glaciers, winter velocities were consistently lower than average annual velocities, indicating that the primary control of seasonal velocity dynamics are likely controlled by changes in basal hydrology resulting from surface mass balance. Consistent with the results of previous studies (Millan et al., 2017; Harcourt et al., 2020; Van Wychen et al., 2016, 2021), overall acceleration and retreat of Trinity and Wykeham glaciers was observed. Contrary to previous

work, results showed that acceleration of both glaciers was not consistent and instead underwent multi-year repeating periods of acceleration, including increased velocities propagating up-glacier. Using Cryosat-2 altimetry data, thinning rates were calculated in low elevation areas (0-300 m a.s.l.) from 2010-2020 on Trinity and Wykeham glaciers of 2.2 m a^{-1} and 2.1 m a^{-1}, respectively. Given the combination of acceleration, retreat, and thinning, it is proposed that flow of Trinity and Wykeham glaciers is now dominated by dynamic thinning. As a result, it is likely that a portion of the termini of both glaciers is now floating or very near flotation. As both glaciers are grounded below sea level ~40 km up-glacier from their termini, continued acceleration, retreat, and buoyancy will likely lead to instability of their termini, which can result periods of dramatic retreat paused periodically by subglacial topography (e.g. pinning points).

Chapter 3 addressed the second research objective. From 2016-2019, 50 satellite tracking beacons were deployed onto icebergs and ice island fragments throughout the ECA. Data from these deployments were complied into a database which extended the iceberg record to 2011-2019. Through analysis of the iceberg drift set and auxiliary environmental data, patterns of drift were identified including high speeds and acceleration, intrusion of icebergs into Lancaster Sound, and tidal influence on icebergs in Davis Strait. Overall, icebergs drifted south/southeast along the east coast of Baffin Island and Labrador. Icebergs commonly became grounded in Nares Strait, and near Coburg Island and the SE coast of Baffin Island. The highest drift speeds observed in this study were 2.3 m s^{-1}, markedly higher than previously reported observations (Robe et al., 1980; Marko et al., 1982; Tang et al., 2004). Consistent with the results of other studies (Fissel et al., 1982; Melling et al., 2001), many icebergs in this study were carried southward by strong surface currents of the BIC from SE Devon Island into the entrance of Lancaster Sound, before returning them eastward of Bylot Island. Oscillations in iceberg speed that were consistent with semi-diurnal tides in western Davis Strait were observed. Finally, the assumption that icebergs drift at 2% of the wind speed was evaluated and it was determined that this rule did not apply for the majority of icebergs in this study, particularly at low wind speeds, which had an overall median ratio of 3.04%. Evident from these results is the apparent influence of local environmental conditions such as wind speed, surface ocean currents, and tidal currents on iceberg drift speed and direction.

The final research objective was addressed in chapter 4 using a database of ship tracks derived from AIS (automatic identification system) data, in combination with iceberg drift locations

derived from in-situ satellite trackers and the CI2D3 database. The coexistence of icebergs and ships was quantified throughout the ECA from 2012-2019. AIS data showed an increase of unique ships operating in the ECA from 108 to 271 between 2012 and 2019, and a near doubling of the number of trips taken by those vessels over the same time period. Analysis of known iceberg drift location data showed icebergs were consistently present throughout Nares Strait, eastern Lancaster Sound, and along the east coast of Baffin Island. A coexistence index was calculated to determine where icebergs and ships likely coincided between 2012 and 2019. The largest increases in coexistence between dry bulk vessels and icebergs were found along the east coast of Baffin Island and east of Bylot Island, and northward into Smith Sound for passenger vessels. Given the recent reductions in ice strengthening of ships such as pleasure crafts and passenger vessels (Dawson et al., 2022), this motivates the need for increased monitoring of iceberg presence throughout the ECA for vessel navigation and offshore industry.

The research objectives of this thesis are firmly interconnected, with the first research objective providing concrete knowledge of the processes that control iceberg production into Baffin Bay. Although Chapter 2 focuses on Trinity and Wykeham glaciers, the processes identified here are insightful for other large tidewater glaciers located in Greenland that are the sources of the majority of icebergs in Baffin Bay (such as Jakobshavn Isbrae). Research objectives two and three are connected by providing fundamental knowledge of iceberg drift locations to establish areas of coexistence between ships and icebergs in the ECA. Holistically, this thesis provides an overall assessment of icebergs in the ECA, collectively describing the genesis and drift processes as well as their consequences (i.e. impacts to shipping).

5.2 Key Contributions

This thesis provides key contributions to the field of Canadian glaciology and Arctic oceanography. Previous work on glacier processes across the CAA has focused primarily on inter-annual flow regimes (Williamson et al., 2008; Van Wychen et al., 2014; Van Wychen et al., 2016; Millan et al., 2017; Van Wychen et al., 2021). This study uses a dense record of speckle-tracking derived winter velocities, annual velocity composites, basal topography, and surface elevation changes from 2009 to 2019 to provide an overview of the processes driving ice discharge from the four major tidewater glaciers on the POW Icefield. For the first time, findings suggest that Trinity

and Wykeham glaciers are responding to external forcing by switching between seasonal flow and flow dominated by dynamic thinning. These flow regimes have previously been observed on large Greenlandic glaciers (Joughin et al., 2004; 2008; Williams et al., 2021), which currently account for ~95% of ice discharge into Baffin Bay (Mouginot et al., 2019; Kochtitzky et al., 2022) and therefore dominate iceberg production into Canadian waters, but have not been previously reported in such detail for the Canadian Arctic. Dynamic processes identified in this study, and the rate at which they are changing, can thus provide insights into the processes and stability of major iceberg producing glaciers in Greenland which ultimately dictates how many icebergs are present in the eastern Canadian Arctic.

While previous studies exist examining iceberg drift tracks in the ECA, little research had been conducted since the 1980s (Robe et al., 1980; Marko et al., 1982) and data was limited both spatially and temporally. Through deployment via helicopter from the *CCGS Amundsen* from 2016-2019, 50 beacons were contributed to the CIS iceberg beacon database to bring the total number of iceberg tracks to 161 for 1997-2021. Given the challenges associated with tracking icebergs using remote sensing methods, this approach has produced a collection of iceberg tracks that fills significant gaps in our knowledge of the patterns of iceberg drift in Baffin Bay. The CIS relies upon both iceberg observations and predictions through operational models to provide information on iceberg distribution in Canadian waters (Kubat et al., 2005; Turnbull et al., 2022). This dataset is therefore crucial for understanding the lifecycle and drift patterns of icebergs to identify long-term trends in their distribution and deterioration. It will contribute to ongoing validation of iceberg drift models for the purpose of improving safety in navigation and can be used to inform future work such as infrastructure planning and routing.

Finally, this work provides the first estimate of iceberg and ship coexistence in the ECA for 2012-2019. Previous research has focused mainly on compilation of past collisions between ships and icebergs (Hill, 2010). Using AIS data, estimates of vessel traffic were produced throughout the ECA. When compared to areas of known iceberg and ice island drift, the ISCI was calculated to quantify the coexistence of icebergs and ships throughout the ECA and show how it has increased in nearly all regions. Icebergs have been identified as a significant hazard to ships operating in the Arctic (ABS, 2016; CCG, 2022), yet they are not included in existing risk assessment frameworks such as POLARIS to manage operational limitations of vessels in icy waters. Future work should

therefore focus on including icebergs in POLARIS during the shipping season and expanding current risk assessments of life-safety and environmental consequences to Arctic shipping north of 60°N (Browne et al., 2020; Bergström et al., 2022).

5.3 Future Work

This research has demonstrated the importance of long term monitoring of tidewater glaciers and icebergs throughout the Canadian Arctic. While a dense record of glacier surface velocities and regional patterns of iceberg drift and coexistence with ships throughout the ECA was produced, there are limitations in the datasets used for this research which can be improved for future work.

For studies of glacier dynamics and the processes controlling glacier flow and ice discharge, there is a lack of in situ observations of glaciers on the POW Icefield. While this study has demonstrated the benefits of combining multiple sources of remote sensing data to measure surface velocity, bed topography, and surface elevation, in-situ observations at the glacier level would validate and improve work quantifying seasonal and inter-annual changes in glacier flow. The potential future destabilization of Trinity and Wykeham glaciers described in Chapter 2 is largely based on a qualitative assessment of the results. Future work should focus on providing a quantitative assessment of destabilization for Trinity and Wykeham glaciers, focusing on driving stress calculations, flow regime mapping, and further ice thickness and flotation calculations. Monitoring other glaciers around the CAA to determine whether similar patterns in flow also exist will be crucial for understanding the mechanisms controlling iceberg production. In addition, few climatological observations exist for Trinity and Wykeham glaciers. Given their current suspected instability and contributions to ice discharge from the CAA, collection of data on external factors such as fiord geometry and ocean and air temperature will be essential to develop in-depth datasets to enable improved investigations of the dynamic processes of Canadian Arctic glaciers.

Future efforts to quantify the processes controlling iceberg drift would benefit from additional deployments of iceberg tracking beacons throughout Canadian and Greenlandic waters. Temporally, beacon deployments within the ECA have been limited to the summer months (approximately July-September) when sea ice is near its minimum, allowing for easier navigation. Spatially, deployments are limited to areas within helicopter flying distance and along the

navigation route of ships such as the *CCGS Amundsen*. Due to the techniques used for safe deployment, beacons are preferentially deployed onto larger tabular icebergs which introduces bias into the resulting datasets. Additionally, few tracking beacons have been deployed onto icebergs within fiords and inlets throughout the CAA and Greenland, creating a gap in knowledge of the local controls on iceberg drift in these regions. While it is possible to monitor iceberg and ice island movement using remote sensing (e.g. CI2D3; Crawford et al., 2018), in-situ measurements of iceberg drift are important inputs for validating remote detection and improving model reliability. For all iceberg drift tracks, there is a scarcity of bathymetric and ocean and wind current data throughout the ECA which would be useful for quantifying the influence of environmental variables on local drift patterns. Modelled data from ERA5 and GLORYS were unable to fully capture the influence of these variables, likely due to their relatively low spatial and temporal resolution. Future work should focus on the collection of local environmental data alongside additional beacon deployment to create a more robust dataset. By expanding deployments to all regions of Baffin Bay, future work can include an integrated assessment of icebergs in both Greenland and the CAA to better understand and the lifespan of icebergs from source to sink.

To improve our understanding of the relationship between icebergs and ships in the ECA, continued monitoring of icebergs both via remote sensing and in-situ deployment of tracking beacons is necessary. The introduction of AIS data has provided comprehensive data concerning the location of ships operating in the ECA, but we do not presently have the iceberg or environmental data to match this, either spatially or temporally. Monitoring by the IIP and CIS for iceberg presence and movement through shipping lanes and areas of offshore industry does not generally extend beyond 60°N. Given the recent increase in shipping traffic throughout the ECA, particularly along the coast of Baffin Island and in eastern Lancaster Sound, it will be important to extend monitoring of icebergs north of the current limit. Formal recommendation for navigation through iceberg infested waters relies on the knowledge of both an iceberg climatology and near real-time monitoring of icebergs. It is therefore crucial for collection of iceberg data and the monitoring of coexistence between icebergs and ships to continue in the ECA, and to extend to other regions of the CAA.

Despite these limitations, the results of this research provide a significant improvement in our knowledge of the lifecycle of icebergs in the ECA. Remote sensing methods were used to provide

a comprehensive investigation of the processes controlling glacier terminus dynamics and stability on SE Ellesmere Island. Field measurements were used to spatially and temporally characterize the drift paths of icebergs once calved and, in combination with AIS data, quantify for the first time the coexistence of icebergs and ships throughout the ECA. Continued monitoring of glaciers and icebergs throughout this region will be essential for furthering our knowledge of the dynamic processes of Canadian Arctic glaciers in a warming climate.

References

ABS (American Bureau of Shipping). (2016) IMO Polar Code advisory. Houston, Texas: ABS. https://ww2.eagle.org/content/dam/eagle/advisories-and-debriefs/ABS_Polar_Code_Advisory_15239.pdf

Bergström, M., Browne, T., Ehlers, S., Helle, I., Herrnring, H., Khan, F., Kubiczek, J., Kujala, P., Kõrgesaar, M., Leira, B. J., Parviainen, T., Polojärvi, A., Suominen, M., Taylor, R., Tuhkuri, J., Vanhatalo, J., & Veitch, B. (2022). A comprehensive approach to scenario-based risk management for Arctic waters. Ship Technology Research, 69(3), 129–157. https://doi.org/10.1080/09377255.2022.2049967

Browne, T., Taylor, R., Veitch, B., Kujala, P., Khan, F., & Smith, D. (2020). A Framework for Integrating Life-Safety and Environmental Consequences into Conventional Arctic Shipping Risk Models. Applied Sciences, 10(8), 2937. https://doi.org/10.3390/app10082937

Canadian Coast Guard (CCG) (6th Ed.). (2022). Ice navigation in Canadian waters (Rev. ed). Fisheries and Oceans Canada.

Crawford, A., Crocker, G., Mueller, D., Desjardins, L., Saper, R., & Carrieres, T. (2018). The Canadian Ice Island Drift, Deterioration and Detection (CI2D3) Database. *Journal of Glaciology*, 64(245), 517–521. https://doi.org/10.1017/jog.2018.36

Dawson, J., Cook, A., Holloway, J., & Copland, L. (2022). Analysis of Changing Levels of Ice Strengthening (Ice Class) among Vessels Operating in the Canadian Arctic over the Past 30 Years. *Arctic*. https://doi.org/10.14430/arctic75553

Fissel, D. B. (1982). Tidal Currents and Inertial Oscillations in Northwestern Baffin Bay. *Arctic*, 35(1), 201–210. https://doi.org/10.14430/arctic2319

Harcourt, W. D., Palmer, S. J., Mansell, D. T., Le Brocq, A., Bartlett, O., Gourmelen, N., Tepes, P., Dowdeswell, J. A., Blankenship, D. D., & Young, D. A. (2020). Subglacial controls on dynamic thinning at Trinity-Wykeham Glacier, Prince of Wales Ice Field, Canadian Arctic. *International Journal of Remote Sensing*, 41(3), 1191–1213. https://doi.org/10.1080/01431161.2019.1658238

Hill, Brian. (2010). Ship Collision with Iceberg Database. ICETECH06-117-RF

Marko, J. R., Birch, J. R., & Wilson, M. A. (1982). A Study of Long-Term Satellite-Tracked Iceberg Drifts in Baffin Bay and Davis Strait. *Arctic*, 35(1), 234–240. https://doi.org/10.14430/arctic2322

Melling, H., Gratton, Y., & Ingram, G. (2001). Ocean circulation within the North Water polynya of Baffin Bay. *Atmosphere-Ocean*, 39(3), 301–325. https://doi.org/10.1080/07055900.2001.9649683

Millan, R., Mouginot, J., & Rignot, E. (2017). Mass budget of the glaciers and ice caps of the Queen Elizabeth Islands, Canada, from 1991 to 2015. *Environmental Research Letters*, 12(2), 024016. https://doi.org/10.1088/1748-9326/aa5b04

Robe, R. Q., Maier, D. C., & Russell, W. E. (1980). Long-term drift of icebergs in Baffin Bay and the Labrador Sea. *Cold Regions Science and Technology*, 1(3–4), 183–193. https://doi.org/10.1016/0165-232X(80)90047-6

Tang, C. C. L., Ross, C. K., Yao, T., Petrie, B., DeTracey, B. M., & Dunlap, E. (2004). The circulation, water masses and sea-ice of Baffin Bay. *Progress in Oceanography*, 63(4), 183–228. https://doi.org/10.1016/j.pocean.2004.09.005

Turnbull, I. D., King, T., & Ralph, F. (2022). Iceberg Drift Simulations Using Inferred, Measured, and Ocean Model Currents. International Journal of Offshore and Polar Engineering, 32(2), 176–185. https://doi.org/10.17736/ijope.2022.jc856

Van Wychen, W., Burgess, D. O., Gray, L., Copland, L., Sharp, M., Dowdeswell, J. A., & Benham, T. J. (2014). Glacier velocities and dynamic ice discharge from the Queen Elizabeth Islands, Nunavut, Canada. *Geophysical Research Letters*, 41(2), 484–490. https://doi.org/10.1002/2013GL058558

Van Wychen, W., Davis, J., Burgess, D. O., Copland, L., Gray, L., Sharp, M., & Mortimer, C. (2016). Characterizing interannual variability of glacier dynamics and dynamic discharge (1999-2015) for the ice masses of Ellesmere and Axel Heiberg Islands, Nunavut, Canada: Glacier Dynamics of the Canadian Arctic. *Journal of Geophysical Research: Earth Surface*, 121(1), 39–63. https://doi.org/10.1002/2015JF003708

Van Wychen, W., Burgess, D., Kochtitzky, W., Nikolic, N., Copland, L., & Gray, L. (2021). RADARSAT-2 Derived Glacier Velocities and Dynamic Discharge Estimates for the Canadian High Arctic: 2015–2020. *Canadian Journal of Remote Sensing*, 46(6), 695–714. https://doi.org/10.1080/07038992.2020.1859359

Williamson, S., Sharp, M., Dowdeswell, J., & Benham, T. (2008). Iceberg calving rates from northern Ellesmere Island ice caps, Canadian Arctic, 1999–2003. *Journal of Glaciology*, 54(186), 391–400. https://doi.org/10.3189/002214308785837048

Appendix A: NASA 3D tomography derived bed elevation (black line) and ArcticDEM derived surface elevation (blue line) profiles for a) Ekblaw Glacier, b) Cadogan Glacier, c) Wykeham Glacier, and d) Trinity Glacier.